NOAA OAR Special Report

PMEL Tsunami Forecast Series: Vol. NNNN
Development of a Tsunami Forecast Model for Elfin Cove, Alaska

Michael C. Spillane [1,2]

[1]Joint Institute for the Study of the Atmosphere and Ocean (JISAO), University of Washington, Seattle, WA
[2]NOAA/Pacific Marine Environmental Laboratory (PMEL), Seattle, WA

October 2012

NOTICE from NOAA

Mention of a commercial company or product does not constitute an endorsement by NOAA/OAR. Use of information from this publication concerning proprietary products or the tests of such products for publicity or advertising purposes is not authorized. Any opinions, findings, and conclusions or recommendations expressed in this material are those of the authors and do not necessarily reflect the views of the National Oceanic and Atmospheric Administration.

Contribution No. XXXX from NOAA/Pacific Marine Environmental Laboratory

Also available from the National Technical Information Service (NTIS)
(http://www.ntis.gov)

Contents

List of Figures

Figure 13. Synthetic and historic event scenarios employed in inter-comparison of the Reference and Forecast versions of Elfin Cove tsunami model. Evenly-distributed slip values, are applied in ten adjacent unit sources (yellow rectangles) of the propagation database to represent mega-tsunami events; single unit sources are used for the other synthetic events. For the historic cases, a linear combination of unit sources is employed as detailed in Table 6.

Figure 14. Comparison of Reference (RM) and Forecast Model (RM) predictions for the Elfin Cove tide gage site for three "null" (very low magnitude) sources. Such runs highlight low level model instabilities that might be missed in modeling larger events. The lower panel shows the Reference Model at an early stage of development; instabilities emanating from upper Dundas Bay (see Figure 11) proved difficult to eliminate while employing reasonable time and space steps. These instabilities are essentially eliminated in the final C-grid.

Figure 15. Comparison of Reference (RM) and Forecast (RM) results for the ACSZ 40-49 mega-tsunami scenario, which is local to Elfin Cove. The left hand panels are for the C-grid domain of the Forecast Model; the right hand panel shows the entirety of the Reference Model C-grid. The lower panel contrasts the Reference (black) and Forecast (red) versions of the time series at the Elfin Cove tide gage. a) distribution of maximum amplitude during the 18-hour simulation, b) distribution of maximum speed, c) a snapshot of the current field at the time indicated by the green line in the lower panel.

Figure 16. As in Figure 15, but for a synthetic mega-tsunami source, ACSZ 56-65, representative of the Cascadia Subduction Zone.

Figure 17. As in Figure 15, but for a synthetic mega-tsunami source, CSSZ 102-111, located in southern Chile.

Figure 18. As in Figure 15, but for a synthetic mega-tsunami source, MOSZ 1-10, located in the western Pacific.

Figure 19. Comparison of Reference (RM) and Forecast Model (FM) solutions for a mild synthetic tsunami near Samoa (the single unit source NTSZ B36.) Though tracking well for 22 hours of the simulation, the time series at the tide gage diverge later and degrade the comparison of the maximum amplitude field.

Figure 20. As for Figure 15 but for a hindcast of the Honshu-2011 historic event. The model is forced by a combination of unit sources and slip values selected in real time during the event (see Table 6) using DART® observations near the tsunami source. The Reference (RM) and Forecast Model (FM) predictions are in good agreement; validation results, using data from the Elfin Cove tide gage, are presented later.

Figure 21. As for Figures 15 and 20, but for a hindcast of the Chile-2010 historic event. The model forcing is based on DART® data collected during the event, and validation results are presented later.

Figure 22. As for Figures 15 and 20 but for a hindcast of the Alaska-1964 tsunami, the largest event impacting Gulf of Alaska communities. The event pre-dated deep ocean tsunami detection capability so the representation of the source is based on post-event studies reported in the literature.

Figure 23. As for Figures 15 and 20 but for a hindcast of the Chile-1960 historic event which was widely felt through the Pacific basin. The source representation is shown later to be poor, but this does not invalidate its use for inter-comparison.

Figure 24. Propagation of the Honshu-2011 tsunami across the North Pacific from its epicenter (red star) to the Gulf of Alaska. DART® observations and model results from MOST use a common vertical and horizontal scale at all locations. The ratio of observed to model amplitude is denoted by R; Δt is the time lead of the model.

Figure 25. Model validation based on detided and low-passed observations (green) of the Honshu-2011 tsunami at locations within the Elfin Cove model grids. The Reference (RM) and Forecast Model (FM) hindcasts are shown in black and red respectively. Model time series lead the observations, as is common for tele-tsunami events. Agreement is best for Elfin Cove, in the model C-grid, Sitka, and Ketchikan (which is outside the FM grids.) The Port Alexander validation is unclear due to noise in the observations. At Juneau and Skagway, whose grid representation has low resolution, only an approximate match is found.

Figure 26. As in Figure 25 but for the Chile-2010 historic tsunami. The model results at the various sites are consistent for the upper three panels in overestimating the observed signal. For Juneau and Skagway the better resolution of the RM A-grid results in improved agreement with the data.

Figure 27. Model validation based on the Alaska-1964 historic tsunami. An observed time series is only available for Sitka, based on a digitized marigram in the WCATWC archives. At Elfin Cove, Port Alexander, and Skagway the agreement between the Reference (RM) and Forecast Model (FM) hindcasts is good, throughout the event. Juneau is less satisfactory but, consistent with the Honshu-2011 and Chile-2010 results, FM exceeds RM.

Figure 28. Attempted model validation based on digitized marigrams for Sitka associated with the Unimak-1946, Kamchatka-1952 and Chile-1960 tsunamis.

Figure 29. Comparison of Forecast Model (FM) hindcasts at the Elfin Cove tide gage with observations for selection of historic events since one-minute data became available. Owing to the weak response of the Gulf of Alaska region, and poor signal to noise ratios, none of these events were of use in model validation.

Figure 30. Forecast Model hindcasts for Elfin Cove during various earlier tsunamis for which tide gage records are unavailable. Some Sitka runup reports are indicated.

Figure 31. Chart summarizing predicted maximum amplitudes at the Elfin Cove tide gage associated with the full suite of mega-tsunami events listed in Table 5. Numerical values are shown on the chart, together with great circle distances to Elfin Cove as an indication of the likely main beam direction near the source.

Figure 32. Complete time series of Forecast Model predictions at the Elfin Cove tide gage site for each of the mega-tsunami scenarios. Time is in hours from the event and, although each simulation is limited to 18 hours after the wave enters the model domain, some events extend into a second day after the event.

Figure 33. Current meter sites instrumented by NOAA's EcoFOCI Program (Stabeno, personal communication) for which mega-event speed maxima from the Elfin Cove model were extracted and listed in Table 10. The inset panel shows the 10 knot contour for the local (ACSZ 40-49) scenario which produces the strongest currents.

List of Tables

North and South Inian Passes. Observed maxima (and water depths) are based on NOAA EcoFOCI current meter data from 2010 and 2011.

PMEL Tsunami Forecast Series: Vol. NNNN
Development of a Tsunami Forecast Model for Elfin Cove, Alaska

Michael C. Spillane [1,2]

Foreword

Tsunamis have been recognized as a potential hazard to United States coastal communities since the mid-twentieth century, when multiple destructive tsunamis caused damage to the states of Hawaii, Alaska, California, Oregon, and Washington. In response to these events, the United States, under the auspices of the National Oceanic and Atmospheric Administration (NOAA), established the Pacific and Alaska Tsunami Warning Centers, dedicated to protecting United States interests from the threat posed by tsunamis. NOAA also created a tsunami research program at the Pacific Marine Environmental Laboratory (PMEL) to develop improved warning products.

The scale of destruction and unprecedented loss of life following the December 2004 Sumatra tsunami served as the catalyst to refocus efforts in the United States on reducing tsunami vulnerability of coastal communities, and on 20 December 2006, the United States Congress passed the "Tsunami Warning and Education Act" under which education and warning activities were thereafter specified and mandated. A "tsunami forecasting capability based on models and measurements, including tsunami inundation models and maps." is a central component for the protection of United States coastlines from the threat posed by tsunamis. The forecasting capability for each community described in the PMEL Tsunami Forecast Series is the result of collaboration between the National Oceanic and Atmospheric Administration office of Oceanic and Atmospheric Research, National Weather Service, National Ocean Service, National Environmental Satellite Data and Information Service, the University of Washington's Joint Institute for the Study of the Atmosphere and Ocean, National Science Foundation, and United States Geological Survey.

Abstract. Operational tsunami forecasting by NOAA's Tsunami Warning Centers relies on the detection of tsunami wave trains in the open ocean, inversion of these data (transmitted via satellite) to quantify their source characteristics, and real-time modeling of the impact on threatened coastal communities. The latter phase of the process involves, for each such community, a pre-tested Forecast Model capable of predicting the impact, in terms of inundation and dangerous inshore currents, with sufficient resolution and within the time constraints appropriate to an emergency response.

In order to achieve this goal, considerable advance effort is required to tune each forecast model to the specific bathymetry and topography, both natural and manmade, of the impact area, and to validate its performance with a broad set of tsunami sources. Where possible the validation runs should replicate observed responses to historical events, but the sparse instrumental record of these rare but occasionally devastating occurrences

dictates that comprehensive testing should include a suite of scenarios that represent extreme events.

During the forecast model design phase, and in research mode outside the pressures of an emergency situation, more detailed and slower-running models can be investigated. Such a model, referred to as a Reference Model, represents the most credible numerical representation of tsunami response for the study region, using the most detailed bathymetry available and without the run-time constraint of operational use. Once a reference model has been developed, the process of forecast model design is to determine where efficiencies can be gained, through reducing the grid resolution and increasing the model time step, while still adequately representing the salient features of the full solution.

This report documents the reference and forecast model development for Elfin Cove and vicinity, comprising much of the Alexander Archipelago. Elfin Cove is a small inlet on the north coast of Chichagof Island, and is exposed to the Pacific Ocean via Cross Sound. Icy Strait provides a connection eastward to Glacier Bay, which extends deep into the Alaska Panhandle mainland, and Chatham Strait. The latter forms the eastern boundary of Chichagof and Baranof Islands and is another deep-water connection to the Pacific. Chatham Strait continues northward as Lynn Canal, leading to Skagway; other branches connect to Juneau and other communities. The vicinity of Elfin Cove is sparsely populated but has important marine resources, commercial and recreational fishing, and is traversed by several segments of the Alaska Marine Highway. Glacier Bay is a popular venue for cruise ships and other tourist activity. This report addresses the tsunami aspects of the natural hazard spectrum.

[1] Joint Institute for the Study of the Atmosphere and Ocean (JISAO), University of Washington, Seattle, WA
[2]NOAA/Pacific Marine Environmental Laboratory (PMEL), Seattle, WA

1.0 Background and Objectives

1.1. The Setting

The "Panhandle" of Southeast Alaska (see Figures 1-3) extends from Yakutat to the U.S./Canada border and is a region incised with deep channels and complex topography. The mainland is exposed to the open ocean north of Cross Sound while to the south the islands of the Alexander Archipelago provide a screen. The deep waters of Chatham Strait provide a passage for tsunami waves deep into the interior: to Skagway and Haines via Lynn Canal, to the state capital Juneau, and to several of the larger communities. Cross Sound is linked to Chatham Strait via Icy Strait along which Glacier Bay and its associated National Park is a major tourist destination.

Tsunami models are being developed for several communities of southeastern Alaska in recognition of the threat they face from both local and remote sources. Tide gages are in place that can serve to validate these models permitting their use to provide real-time warning capability to emergency managers. One such tide gage is located in Elfin Cove, approximately midway between Sitka and Yakutat and the subject of this report and tsunami modeling effort. The small community (2000 population 30 and accessible only by water or seaplane) is a census-designated place on the Inian Peninsula of Chichagof Island. Although the fifth largest island in the U.S. its entire population in 2000 was only 1,342. The Inian Peninsula, and a cluster of islands of the same name, partially block Icy Strait while to the west several islands screen Elfin Cove from the open Pacific Ocean. The Alaska Marine Highway passes between Elfin Cove and the Inian Islands with ferry service to Hoonah (2000 population 560) at the mouth of Port Frederic inlet, Pelican (2000 population 163) on Lisianski Inlet and northward to Yakutat and Anchorage. During the summer months there is a significant though transient population increase. Commercial fishing vessels transiting to the Bering Sea or engaged in local recreational fishing swell the population of Elfin Cove to 170 or so and the community is occasionally visited by tour vessels with up to 100 passengers that can tax its limited infrastructure. Power is generated locally, potable water comes from a spring and there are no regularly scheduled modes of transportation. Elfin Cove has no roads but is served by a network of boardwalks. Medical services are volunteer-provided; all in all the community is self-sustaining but at risk if an emergency were to arise.

As the most northerly access to the Inland Passage, Cross Sound and Icy Strait are heavily traversed year-round by ferry, cargo, and cruise ship traffic. In summer cruise ship traffic is particularly intense with two vessels, each carrying up to 3,000 passengers and crew, visiting Glacier Bay each day. Tidal currents through the narrow North and South Inian Passes and other navigational channels are very strong and it is important that the tsunami model being designed here should address the impact of tsunami-driven currents in addition to the potential for inundation. While the forecast model is named for Elfin Cove, its choice is largely dictated by the presence of a tide gage for use in model validation and in operations; the scope of the model must be more regional than is usual. By contrast, models created for the closest communities to the north and south (Yakutat

and Sitka respectively with greater population and infrastructure) have a more local focus.

Lisianski Strait separates Chichagof Island from the smaller Yakobi Island to the west. Further south Peril Strait provides another, albeit far more constricted, connection between the Pacific and Chatham Strait, allowing ferry service to Sitka (2000 population 8,881) on Baranof Island. At the south end of Baranof Island, just inside the entrance to Chatham Strait, is Port Alexander (2000 population 81) whose selection for as a forecast model site also reflects it strategically located tide gage.

Though far from the open ocean, Skagway and Juneau have reported substantial tsunami waves, particularly from the major Alaskan earthquake of 1964 but also from more remote events such as Chile 1960 and Honshu 2011. The domain of the Elfin Cove model, which must allow for the possibility of waves arriving from the east via Chatham and Icy Straits, will be large enough to permit estimates for Juneau, Skagway and other communities in its vicinity.

1.2. Natural Hazards

Lander (1996), in an extensive compilation of tsunami knowledge for Alaska since the earliest records in the 1700s, distinguishes between the several categories of tsunami to which the region is prone. Together with the National Geophysical Data Center's (NGDC) online hazard database (Dunbar, 2007; see www.ngdc.noaa.gov/hazard/), a wide set of historical cases are available with which to exercise a forecast model. Observations suited to model validation are however quite limited. Tide gage records from Elfin Cove itself are only available after August 2005, and reports and observations from other sites in the vicinity (primarily Sitka) will be employed to validate the model for earlier events.

The instrumental record is too short, in the geologic context, to provide samples of the range of tsunami events that may occur at future times within the Pacific basin. Thus, once developed and validated, the model will be exercised with a comprehensive suite of synthetic scenarios. The benefits of this are twofold: to check that the model is robust, unlikely to fail in an operational setting and, as a byproduct, identify tsunami source regions to which southeast Alaska is particularly susceptible. It should be noted that the model currently is applicable only to tsunamis generated by direct seismic forcing. Lander (1996) discusses other mechanisms: related to volcanic activity, or landslides perhaps triggered by seismic action, that are manifested in the observational record. Notorious among the latter is the 1958 event in Lituya Bay, just north of Cross Sound, where the collapse of a steep mountainside caused a surge of over 500 meters at the other side of the bay. Though dramatic, such events are generally quite localized, but it should be stressed that in its current form the tsunami model employed in the forecast system does not cover landslide-generated tsunamis.

Earthquake, landslide, and flooding damage can result even without the medium of tsunami waves. Nonetheless history has shown that death, injury, and property damage associated with tsunamis both local and remote have been significant so that the

modeling effort and operational forecast capability provides important benefits to the State of Alaska. Equally, since tsunamis generated off southeast Alaska can potentially impact the entire Pacific basin, the degree of success of the Elfin Cove model in a local event can lend credence to the forecast systems projections for more remote and larger communities, of the United States and other nations.

An inset to Figure 6, taken from the USGS seismic hazard analysis for Alaska (Wesson et al., 2007), shows the major fault ruptures that have occurred in the region since the 1930s. Several are local to the Alaska Panhandle region, though none have caused major tsunami impacts since 1964. The main panel of Figure 6 shows (in green) several of the faults, together with the unit source rectangles employed to represent them in the NCTR propagation database. The Fairweather Fault, extending northward from Haida Gwaii generated the Queen Charlotte event of 1949, the 1958 earthquake associated with the Lituya Bay tsunami and one near Sitka in 1972 (Doser and Lomas, 2000). It is primarily a strike slip fault, as is the Transition Zone Fault which angles off to the northwest. The junction near Cross Sound was the site of a series of a cluster of small earthquakes in 1973. Between these faults is the Yakutat Terrane (Worthington, 2012) or Yakutat Block (whose submarine portion is cross-hatched in Figure 6).

The rectangular outlines of the 100x50km unit sources of the NCTR propagation database are shown in Figure 6. Those drawn in black are combined for the ACSZ 40-49 mega-tsunami source described later in this report. Representing an Mw 9.3 event this synthetic source is likely far in excess of any probable occurrence but should serve as an extreme test of model stability. At the northern end of the Yakutat Block the potential for a larger event becomes more realistic as it subducts beneath the North American Plate in the vicinity of the Chugach-St Elias Mountains. Major earthquakes occurred near Yakutat in 1899 for which the 1979 event shown in Figure 6 is considered an aftershock. The rupture zone of the 1964 Alaska earthquake did not extend into the region (Shennan et al., 2009). Often referred to as the "Yakataga Gap" this is a potential site for future large earthquakes in Alaska seismic hazard mapping (Wesson et al., 2007), and Alaska Earthquake Information Center (AEIC) charts (www.aeic.alaska.edu).

1.3. Tsunami Warning and Risk Assessment

The forecast model development, described here, will permit Elfin Cove, AK, to be incorporated into the tsunami forecasting system SIFT, developed at NCTR (NOAA Center for Tsunami Research) and now in use at the U.S. Tsunami Warning Centers (TWC's). The system has had considerable success in accurately forecasting the impact of both moderate and severe tsunami events in recent years and in the following section the methodology that permits such forecasts is discussed as prelude to a description of development of the forecast model for Elfin Cove. With the model in hand, validated with historical events and with its stability verified by extensive testing against extreme scenarios, real-time forecasts will be available to inform local emergency response. Additionally, the synthetic scenarios investigated during model development, and reported here, provide an initial tsunami risk assessment as described in the Results and Discussion section.

2.0 Forecast Methodology

2.1 The Tsunami Model

A tsunami forecast model is used to extend a pre-computed deep-water solution into the shallows, and onshore as inundation if appropriate. The model consists of a set of three nested grids, of increasingly fine resolution that, in a real-time application of the MOST model (Method of Splitting Tsunami: Titov and Synolakis, 1998; Titov and González, 1997), permits forecasts at spatial scales (as little a few tens of meters) relevant to local emergency management. The validity of the MOST model applied in this manner, and the operational effectiveness of the forecast system built around it, has been demonstrated during unplanned tests triggered by several mild to moderate tsunami events in the years since the 2004 Indian Ocean disaster (Wei et al., 2008). Successful hindcasting of observed historic events, even mild ones, during forecast model development lends credence to the ability to accurately forecasting the impact of future events. Such validation of tsunami modeling procedures is documented in other volumes of the series of which this report is but one. Before proceeding to a description of the forecast model development for Elfin Cove, it is useful to describe the steps in the overall forecast process.

2.2 The SIFT Forecast System

Tsunami forecasts are generated at Tsunami Warning Centers, staffed 24/7 in Alaska and Hawaii, using the SIFT (Short-term Inundation Forecasting for Tsunamis) tool, developed at NCTR. The semi-automated process facilitates the steps by which TWC operators assimilate data from an appropriate subset of the DART® tsunami sensors, "invert" the data to determine the linear combination of pre-computed propagation solutions that best match the observations, then initiate a set of forecast model runs if coastal communities are threatened or, if warranted, cancel the warning.

Steps in the process are as follows:

- When a submarine earthquake occurs the global network of seismometers registers it. Based on the epicenter, the unit sources in the Propagation Database (Gica et al., 2008) that are most likely to be involved in the event, and the DART® array elements (Spillane et al., 2008) best placed to detect the waves passage are identified. TWC watch-standers can trigger DART®s into rapid sampling mode in the event that this did not occur automatically in response to the seismic signal.
- There is now an unavoidable delay while the tsunami waves are in transit to the DART®s; at least a quarter of a cycle of the first wave in the train must be sampled before moving to the "inversion" step.
- When sufficient data have accumulated, at one or more DART®s, the observed time series are compared with the model series from the candidate unit sources. Since the latter are pre-computed (using the MOST code), and the dynamics of tsunami waves in deep water is linear, a least squares approach taking very little time can identify the unit sources, (and the appropriate scale factors for each), that

best fit the observations. The "inversion" methodology is described by Percival et. al., (2009).

- Drawing again on the Propagation Database, the scale factors are applied to produce a composite basin-wide solution with which to identify the coastal regions most threatened by the radiating waves.
- It is at this point that one or more forecast models are run. The composite propagation solution is employed as the boundary condition to the outermost (A-grid) domain of a nested set of three real-time MOST grids that telescope with increasingly fine scale to the community of concern. A-grid results provide boundary conditions to the B-grid, which in turn forces the innermost C-grid. Non-linear processes including inundation are modeled so that, relying on the validation procedures during model development, credible forecasts of the current event are available.
- Each forecast model provides quantitative and graphic forecast products with which to inform the emergency response, or to serve as the basis for canceling or reducing the warnings. Unless the tsunami source is local, the forecast is generally available before the waves arrive but, even when lead-time cannot be provided, the several hour duration of a significant event (in which the first wave may not be the most damaging) give added value to the multi-hour forecasts provided.

Because multiple communities may be potentially at risk, it may be necessary to run simultaneously, or in a prioritized manner, multiple forecast models. Each must be optimized to run efficiently in as little time as possible; the current standard is that an operational forecast model should be capable of simulating 4 hours of real time within about 10 minutes of CPU time on a fast workstation computer.

3.0 Model Development

3.1 Digital Elevation Models

Water depth determines local tsunami wave speed and sub-aerial topography determines the extent to which tsunami waves may inundate the land. Thus a prerequisite for credible tsunami modeling is the availability of accurate gridded bathymetric and topographic datasets, termed Digital Elevation Models (DEM). Given their expertise in this area, and the number of coastal communities needing tsunami forecast capability, NCTR relies heavily on the National Geophysical Data Center (NGDC) to provide the DEMs needed. An extract from the South Alaska DEM was used as background in Figure 1 and the outlines of the more finely resolved Southeast Alaska and Elfin Cove DEMs are indicated. In the case of Elfin Cove a customized high resolution DEM, a composite of multiple data sources for the region between Cross Sound and the mouth of Glacier Bay was provided by NGDC. To create this various datasets were merged and converted to a common datum of Mean High Water (MHW). The main features of the Elfin Cove DEM are summarized in Table 1 and documented by Love et al. (2011). Oblique views of these DEMs, produced by NGDC, are reproduced in Figure 3 and assist in visualizing the complexity of the terrain and its multiple waterways. All of the DEMs employed were verified for consistency with charts, satellite imagery, and other datasets during the course of MOST grid development.

Table 1. The main features of the Elfin Cove, Alaska Digital Elevation Model (DEM), whose development is described by Love et al., (2011).

Grid Area	**Elfin Cove, Alaska**
Coverage Area	137.27º to 135.97º W; 57.53º to 58.67º N
Coordinate System	Geographic decimal degrees
Horizontal Datum	World Geodetic System 1984 (WGS84)
Vertical Datum	**Mean High Water (MHW)**
Vertical Units	Meters
Cell Size	**1/3 arc-second**
Grid Format	ESRI Arc ASCII grid
Version Employed	Update of March 31, 2011

The use of MHW as the "zero level" for forecast results is standard. The MOST model does not include tidal fluctuations and, since a tsunami may arrive at any stage of the tide, it is generally best to employ a "worst-case" approach by assuming high tide when forecasting inundation. For some Forecast Models grounding of vessels and the strong and rapidly varying currents often associated with even mild tsunamis are of concern. Even under normal circumstances the tidal currents in North and South Inian Passes are very strong. NOAA Chart 17302, a portion of which is shown in Figure 4a, alerts mariners to currents of 8 to 10 knots. In light of the importance of cruise ship and ferry traffic, the extent to which these might be accentuated during a tsunami will be assessed. For Elfin Cove itself, there are piers floating docks and refueling facilities associated with seaplane and both commercial and recreational fishing activity as shown in the NOAA

chart reproduced as Figure 4b. Figure 5, a photograph by Rick Sood, shows the character of the inner cove of this small community: in particular the reliance on piers and floating docks that do not substantially impede the circulation.

Two different resolutions are available for the Southeast Alaska DEM: eight thirds of an arc-second, and 8 arc-second. The coverage encompasses the region from Skagway to the north to the Haida Gwaii (Queen Charlotte) Islands in British Columbia, Canada. These DEM datasets, together with the Elfin Cove DEM, are employed in the construction of the three nested grids for the Elfin Cove model. As noted earlier, the scope of the outer Elfin Cove grid was chosen to permit estimates of tsunami signals at Skagway and Juneau but, with the relatively coarse grid spacing needed to attain acceptable operational run times, the estimates are of lower quality than would be possible in dedicated models for these communities.

3.2 Tides and Sea Level Variation

The history of tidal observation at Elfin Cove dates back to 1938 though the earlier records are not readily available. Some marigrams are stored in microfiche format at NGDC and a project to digitize the full collection is underway. The present installation of NOAA's National Ocean Service tide gage (NOS 9452634) at Elfin Cove was in August 2005 with quality controlled 6-minute, and preliminary 1-minute records available online.

Table 2. Characteristics of the Elfin Cove, AK Tide Gage (NOS[1] 9452634).

<table>
<tr><th colspan="4">Elfin Cove, AK Station#9452634 58^0 11.6'N, 136^0 20.8'W
Present Installation Aug 11, 2005</th></tr>
<tr><th colspan="4">Tidal Datum and Range Values (Epoch 1983-2001)</th></tr>
<tr><td>MHHW (Mean Higher High)</td><td>6.250m</td><td rowspan="5">Great Diurnal Range
3.367m</td><td></td></tr>
<tr><td>MHW (Mean High Water)</td><td>5.977m</td><td rowspan="3">Mean Range
2.648m</td></tr>
<tr><td>MSL (Mean Sea Level)</td><td>4.637m</td></tr>
<tr><td>MLW (Mean Low Water)</td><td>3.329m</td></tr>
<tr><td>MLLW (Mean Lower Low)</td><td>2.883m</td><td></td></tr>
<tr><th colspan="4">Sea Level Trend (1924-2006) and Cycles (from Sitka[2] AK, NOS 9451600)</th></tr>
<tr><td>Long Term SL Trend</td><td colspan="3">Decreasing 2.05±0.32mm/year</td></tr>
<tr><td>Seasonal Cycle Range</td><td colspan="3">Minimum -106mm(Jul); Maximum 131mm(Dec)</td></tr>
<tr><td>Interannual Variation
(from1980)</td><td colspan="3">Minimum -20mm(1989); Maximum +21mm(1998)</td></tr>
<tr><th colspan="4">Extremes to date (Jun 2012)</th></tr>
<tr><td>Maximum</td><td colspan="3">7.435m on 31 Dec, 1985</td></tr>
<tr><td>Minimum</td><td colspan="3">1.449 on 14 Dec, 2008</td></tr>
</table>

[1]NOAA's National Ocean Service, whose CO-OPS Program Office disseminates tide gage information and data.
[2]At Yakutat AK (NOS 9453220), the long-term trend is -11.54 ± 1.39mm/year.

The tide gage if located off the seaplane-fueling pier in the outer cove (see Figure 4b). The outer cove is screened by an unnamed nearby island; several other islands to the west (George and Three Hill Islands) and north (the Inian Islands) further limit its exposure. A narrow channel leads to an inner cove in a steep-sided valley where the remainder of the sea level infrastructure of the community is located (see Figure 5). There are no roads; a network of boardwalks links the various structures and facilities.

Station characteristics for NOS 9452634 are provided in Table 2, based on the wealth of online tidal information available at NOAA's CO-OPS (Center for Operational Oceanographic Products and Services) website (tidesandcurrents.noaa.gov). Note the sizeable mean diurnal range of over 2.6 meters and that (based on the records at Sitka and Yakutat) there is a significant long-term sea level trend as expected for this tectonically active area of glacial rebound. Seasonal and inter-annual variability is also substantial as are episodic short-term changes associated with meteorology that are reflected in the extremes listed.

Another feature of the local tidal regime, noted earlier, is the strength of the tidal currents, particularly in the North and South Inian Passes that lie between Chichagof Island and the mainland. There is the potential for tidal power generation in these passes, and in Icy Strait to the east. If it comes to fruition, electricity generation could positively impact the local economy and supply both southeast Alaska and nearby British Columbia (Polagye and Bedard, 2006). From the perspective of tsunami hazard however, the bathymetric features that accentuate tidal currents and their spatial variability may pose a significant risk to commercial and recreational marine traffic in the area, including the large cruise vessels that ply the region during the summer months. An unrelated NOAA project, investigating the Cross Sound and Icy Strait region, includes current meter observations from recent years. These have been made available (Stabeno, personal communication) but do not, unfortunately, cover the recent tsunami events. They do, however, provide a baseline for a discussion of the strength of the additional rapidly varying currents that might arise in a major tsunami event.

3.3 Signal to Noise Considerations for the Elfin Cove Tide Gage

Unlike the U.S. West Coast, where the Kuril event of November 2006 is a useful test case for model validation, run-up reports in the NGDC catalog for the Gulf of Alaska are much weaker (~ 12 cm for Sitka and Yakutat and unreported for Elfin Cove). Other events, among the mild tsunamis of recent years, were only weakly felt in the region. The number of test cases for model validation at Elfin Cove is further reduced by weather and wave-related noise background at the tide gages, particularly during the winter months. In addition to sea level itself, the validated 6-minute tide data from CO-OPS provides the standard deviation of the 1-second subsamples used to form each reported value. In the upper panel of Figure 7 the standard deviation is plotted for the month (March 2011) during which the Honshu event occurred. The increased high-frequency activity (periods less than 6 minutes) at the gage associated with the tsunamis arrival on March 11 is evident in the sharp rise in subsample variability as well as in the detided 1-minute gage record (highlighted in red). There is however another period of high variability

(highlighted in blue), of similar duration though of smaller amplitude which we refer to as a "noise burst". Such bursts are not rare; referring to Figure 8 where an entire year of the subsample standard deviation is employed as a measure of high-frequency variability, the sole tsunami event does not stand out from the numerous bursts that occur particularly during the winter months.

The detided 1-minute record for one day extracts are contrasted in Figure 7, both in the time domain and through a spectral analysis. The spectrum is presented in "energy-preserving" format in the lower panel. Here the area beneath the curves indicates the partition of energy with wave period. With the exception of a broad peak near 100 minutes and another near 8 minutes, the energy of the noise burst is concentrated near the shortest periods detectable. By contrast during the Honshu event the bulk of the energy is in a tsunami band with periods between 10 and 60 minutes. The 100 minute and 8 minute peaks are present together with some other "lines" that may represent resonances associated with the topography.

A similar analysis to that shown in Figure 7 was performed for the month of February 2010 when the Chile-2010 tsunami occurred. One-day subsamples, representing the tsunami (red) and a noise burst (blue), are extracted from the Kalman-filtered, 1-minute record. Longer-period energy again dominates the tsunami subset while the noise burst is dominated by high-frequency energy. There is however more energy in the "tsunami band" than was the case during March 2011. Figure 10 exposes the limitations of the Elfin Cove tide gage in discriminating weak tsunami signals in the presence of noise. The first wave peak of the Kuril-2006 event is barely visible and later waves are lost in the high-frequency noise. In the energy-preserving spectra, in the lower panel of Figure 10, the tsunami band is barely visible.

The detiding, referred to above and used throughout this report, was achieved using the same procedure applied to tide removal in the DART® records (Percival et al., 2011) with an R-code script (Percival, personal communication). Based on the spectra presented in Figures 7, 9, and 10, subsequent smoothing of the residuals seems best achieved with a low-pass filter with a cutoff near 10 minutes. This is applied with a Butterworth filter implemented in Matlab and provided by Elena Tolkova (personal communication) .

3.4 The CFL Condition and other considerations for grid design

Water depth dependent wave speed, in conjunction with the spacing of the spatial grid representation, place an upper limit on the time step permissible for stable numerical solutions employing an explicit scheme. This is the CFL limit (Courant-Friedrichs-Levy), which requires careful consideration when the grids employed for a reference or forecast model are being designed. Finer-scale spatial grids, or greater water depths, require shorter time steps thereby increasing the amount of computation required to simulate a specific real time interval.

Another feature of the application of gridded numerical solutions to the tsunami wave problem is the shortening that the wave train encounters in moving from deep water onto

the shelf. In deep water a grid spacing of 4 arc-seconds (of latitude and longitude, corresponding to ~7km) is normally used to represent propagating wave trains whose wavelength is typically of the order of a few hundred kilometers. The stored results of such propagation model runs are typically decimated by a factor of 4, resulting in a database of ~ 30km spacing (and 1 minute temporal sampling) with which to generate the boundary conditions for the outermost of the nested grids in a model solution. The extraction of the boundary conditions (of wave height and the two horizontal velocity components) is achieved by linear interpolation in space and time. To provide realistic interpolated values the stored fields for these variables must be smoothly varying, and have adequate sampling in space and time to resolve their structure. This necessitates the placement of the offshore boundary of the forecast model domain well offshore.

3.5 Specifics of the model grids

After several rounds of experimentation, the extents and resolutions of the nested grids were chosen, and are illustrated in Figures 11 and 12; details are provided in Table 3.

Table 3. Specifics of the Reference (RM) and Forecast model (FM) grids employed for Elfin Cove, AK. For the paired values in the resolution and grid point columns, the zonal (East to West) value is listed first, followed by the meridional (North to South).

Elfin Cove, AK Reference Model (RM)						
Grid	**Zonal Extent**		**Meridional Extent**		**Resolution**	**Grid Points**
A	138.203ºW	129.750ºW	54.190ºN	59.610ºN	48”x24”	635 x 814
B	137.310ºW	135.409ºW	57.830ºN	59.110ºN	5.333”x2.667”	1284 x 1729
C	136.430ºW	136.260ºW	58.090ºN	58.330ºN	$^4/_3$” x $^2/_3$”	460 x 1297

Elfin Cove, AK Forecast Model (FM)						
Grid	**Zonal Extent**		**Meridional Extent**		**Resolution**	**Grid Points**
A	138.210ºW	132.210ºW	56.010ºN	59.610ºN	120”x72”	181 x 181
B	136.630ºW	136.050ºW	57.840ºN	58.390ºN	8” x 4”	262 x 496
C	136.410ºW	136.337ºW	58.18ºN	58.210ºN	$^4/_3$” x $^2/_3$”	199 x 163

The outermost A-grid encompasses the same northern and western limits in both the Reference Model (RM) and Forecast Model (FM) versions. The RM A-grid extents about two degrees further east and south to permit confirmation that the multiple passages there can be safely excluded from the operational model. The expanded domain includes the Canadian tide gage sites of Prince Rupert and Henslung Cove (on Haida Gwaii, see Figure 1) for validation purposes. For the B-grid the FM domain was somewhat curtailed from its FM equivalent in order to improve operational run times while retaining sufficient resolution to reasonably represent the Inian Passes. The initial choice for the RM B-grid (Figure 11) included more of Dundas Bay to the north but the broad tidal flats, barely submerged with the MHW datum, caused numerous minor local instabilities that, in longer runs, impacted areas further afield. Finally, for the innermost C-grid domains, the same resolution was employed for both the RM and FM versions in order to reasonably represent inner Elfin Cove and its entrance. The RM version is far more

extensive, as seen in Figure 10, extending south into the Port Althorp inlet (see Figure 4a) where a strong response to tsunami waves is felt. For all of the grids, both in the RM and FM versions, the convergence of the meridians at this northerly latitude allows a reduction of a factor of about two in the east-west direction, achieving almost square grid cells in distance units and a considerable saving in computational effort.

Both C-grids lie entirely within the NGDC-provided DEM for Elfin Cove; A and B-grids incorporate bathymetry and topography from other DEM datasets available at NCTR. Some smoothing and editing were necessary to eliminate features that tend to cause model instability. For example, "point" islands where an isolated grid cell stands above water are eliminated, as are narrow channels or inlets one grid unit wide; these tend to resonate in the numerical solution. Large depth changes between adjacent grid cells can also cause numerical problems; customized tools (such as "bathcorr") are available to correct many of these grid defects. An additional constraint on the bathymetry is the SSL (Elena Tolkova, personal communication), which identifies excessive depth changes in the discrete representation.

Table 4. Grid file names and grid-related parameters for the Elfin Cove model. The time steps for the A and B-grids must be integer multiples of the basic time C-grid time as indicated in parentheses.

Grid	Filename	Maximum Depth (m)	Minimum CFL (s)	Model Time Step (s)	Water Cells
A	ElfinCoveAK_RM_A	3445	4.031	3.0 (12x)	225,975
	ElfinCoveAK_FM_A	2949	11.661	5.0 (12x)	13,142
B	ElfinCoveAK_RM_B	469.6	1.215	1.0 (4x)	743,650
	ElfinCoveAK_FM_B	347.8	2.119	1.667 (4x)	50,619
C	ElfinCoveAK_RM_C	295.1	0.383	0.25	323,566
	ElfinCoveAK_FM_C	204.2	0.461	0.41667	22,301

Table 4 lists the maximum depth, the CFL time step requirement that must not be exceeded, and the actual time steps chosen for the reference and forecast model runs. Since in the current version of MOST, employed by SIFT, the numerical solutions in the three grids proceed simultaneously, there is a requirement that the A and B-grid time steps be integer multiples of the (innermost) C-grid time step in addition to satisfying the appropriate CFL requirement. For both reference and forecast models the CFL requirement for the C-grid was the most stringent. The time step chosen are shown in the fifth column of Table 4 and are such that an integer multiple of each time step is exactly 30 seconds, the chosen output time interval for both models. When run on an Intel® Xeon® E5670 2.93GHz processor the Elfin Cove, AK forecast model simulates four hours in 13.57 minutes, exceeding the 10-minute target for this metric. This is somewhat compensated for by the narrow continental shelf, which reduces the overall simulation time requirement, but the wide range of communities included in the model domain is the main argument against curtailment of the grids to achieve shorter run times.

3.6 Model Run Input and Output Files

In addition to providing the bathymetry file names and the appropriate time step and A, B grid multiples as provided in the tables above, the designer must provide a number of additional parameters in an input file. These include the Manning Friction Coefficient, a depth threshold to determine when a grid point becomes inundated, and the threshold amplitude at the A-grid boundary that will start the model. An upper limit is specified in order to terminate the run if the wave amplitude grows beyond reasonable expectation. Standard values are used: 0.0009 for the friction coefficient and 0.1m for the inundation threshold. The latter causes the inundation calculation to be avoided for insignificant water encroachments that are probably below the uncertainty in the topographic data. Inundation can, optionally, be ignored in the A and B-grids, as is the norm in the (non-nested) MOST model runs that generate the propagation database. When A and/or B-grid inundation is excluded, water depths less than a specified "minimum offshore depth" are treated as land; in effect a "wall" is placed at the corresponding isobath. When invoked, a value of 5m is applied as the threshold, though A and B inundation is normally permitted as a way to gain some knowledge of tsunami impact beyond the scope of the C-grid domain. Other parameter settings allow decimation of the output in space and/or time. As noted earlier, 30-second output has been the target and output at every spatial node is preferred. These choices avoid aliasing in the output fields that may be suggestive of instability (particularly in graphical output), when none in fact exists.

Finally the input files (supplied in Appendix A) provide options that control the output produced. Output of the three variables: wave amplitude, and the zonal (positive to the east) and meridional (positive to the north) velocity components can be written (in netCDF format) for any combination of the A, B, and C-grids. These files can be very large! A separate file, referred to as a "SIFT" file, contains the time series of wave amplitude at discrete cells of a selected grid. Normally the time series at a "reference" or "warning point", typically the location of a tide gage is selected to permit validation in the case of future or historical events. Also output in the SIFT file is the distribution of the overall minimum and maximum wave amplitude and speed in each grid. By contrast with the complete space-time results of a run, the SIFT file (also netCDF) is very compact and, if more than a single grid point is specified, a broader view of the response is provided.

By default several additional output files are generated: a listing file, which summarizes run specifications, progress, and performance in terms of run time and files that detail modifications to the grid files applied internally my MOST. The listing file provides information on the cause, should a run not start or terminate early. Finally a "restart" file is produced so that a run can be resumed, beginning at the time it ended, either normally or by operator intervention. During execution MOST looks for the presence of a file that signals the operators desire for a controlled termination of a run. A restart file is created allowing the run to be resumed if appropriate.

The input files described above are specific to the model itself. For an actual run, the program must be pointed toward the files that contain the boundary conditions of wave

amplitude (HA), and velocity components (UA, VA), to be imposed at the A-grid boundary. Time varying conditions are generally extracted as a subset of a basin-wide propagation solution (either a single unit source or several, individually scaled and linearly combined) that mimic a particular event. These boundary-forcing files typically consist of 24 hours of values (beginning at the time of the earthquake), sampled at 1-minute intervals and available on a 16 arc-minute grid. Occasionally, for more remote seismic sources (or when delayed arrival of secondary waves due to reflections are a concern, as has been seen at Hawaii), the time span of the propagation run available for forcing is extended beyond one day.

4.0 Results and Discussion

Before proceeding to an extensive suite of model runs, that explore the threat to Elfin Cove and Southeast Alaska from various source regions, the stability of the model is tested in both low and extreme amplitude situations. The former we refer to as "null source" testing: where the boundary forcing is at such a low level (but not precisely zero of course) that the response is expected to be negligible. These tests can be highly valuable in revealing localized instabilities that may result from undesirable features in the discretized bathymetric representation. Inlets or channels that are only one grid cell wide may "ring" or resonate in a non-physical way in the numerical solution. An instability may not grow large enough to cause the model to fail but, in a run with typical tsunami amplitudes, may be masked by actual wave variability.

Forcing by extreme events should also be tested. In addition to the need to test model stability under such circumstances, there is a parameter in the input file that truncates the run if a prescribed threshold is exceeded. For operational use, the threshold must be set high enough so that an extreme event run is not unnecessarily terminated. Both tests should be done for synthetic sources whose waves enter the model domain from different directions since, although stable for one set of incoming waves, instability may result for others. The "null" and "extreme" case testing of the forecast and reference models are reported in the following subsections; the placement of the test sources for these tests is illustrated in Figure 13. Further evidence of stability for the forecast model is provided by a more extensive set of extreme scenarios, described later in the report, and in independent testing by other members of the NCTR team before the model was released for use by the Warning Centers.

4.1 The "Null" Tests

Three null test cases (see Table 5) were run representing sources in the western Aleutians, the Philippines, and south of Japan. Based on sources from the propagation database (Gica et al., 2008), their amplitudes were scaled down by a factor of 100 so as to mimic an M_w=6.17 / Slip 0.01m source rather than the M_w=7.5 / Slip 1m standard. A number of grid cells in the B and C grids emerged as potential sources of instability. These were generally minor indentations of the coastline, barely resolved by the grids, or narrow channels. The region contains several inlets extending far inland and straits that, at a practical level of spatial resolution, proved difficult to accommodate. Minor grid corrections were made to retain features of potential importance, for example the branch of Lisianski Strait extending westward from near the community of Pelican along the south shore of Yakobi Island. Also retained was Peril Strait, between Chichagof and Baranof Islands, which though narrow in places is a route serving Sitka for the Alaska Ferry System (see Figure 2). A limited number of grid cells in the outermost (A) grid required correction. Generally these were associated with non-physical features in the topographic database, such as where a track of ship-based soundings were improperly merged with other data sources.

Table 5. Synthetic tsunami events employed in Elfin Cove testing. The Reference and Forecast model solutions of those shown in bold text were inter-compared extensively.

Scenario Name	Source Zone	Tsunami Source	α [m]
Mega-tsunami Scenario			
KISZ 1-10	Kamchatka-Yap-Mariana-Izu-Bonin	A1-A10, B1-B10	25
KISZ 22-31		A22-A31, B22-B31	25
KISZ 32-41		A32-A41, B32-B41	25
KISZ 56-65		A56-A65, B56-B65	25
ACSZ 6-15	Aleutian-Alaska-Cascadia	A6-A15, B6-B15	25
ACSZ 16-25		A16-A25, B16-B25	25
ACSZ 22-31		A22-A31, B22-B31	25
ACSZ 40-49		A40-A49, B40-B49	25
ACSZ 50-59		A50-A59, B50-B59	25
ACSZ 56-65		A56-A65, B56-B65	25
CSSZ 1-10	Central and South America	A1-A10, B1-B10	25
CSSZ 37-46		A37-A46, B37-B46	25
CSSZ 89-98		A89-B98, B89-B98	25
CSSZ 102-111		A102-A111, B102-B111	25
NTSZ 30-39	New Zealand-Kermadec-Tonga	A30-A39, B30-B39	25
NVSZ 28-37	New Britain-Solomons-Vanuatu	A28-A37, B28-B37	25
MOSZ 1-10	ManusOCB	A1-A10, B1-B10	25
NGSZ 3-12	North New Guinea	A3-A12, B3-B12	25
EPSZ 6-15	East Philippines	A6-A15, B6-B15	25
RNSZ 12-21	Ryukus-Kyushu-Nankai	A12-A21, B12-B21	25
M_w 7.5 Scenario			
NTSZ B36	New Zealand-Kermadec-Tonga	B36	1
Micro-tsunami Scenarios			
EPSZ B19	East Philippines	B19	0.01
RNSZ B14	Ryukus-Kyushu-Nankai	B14	0.01
ACSZ B6	Aleutian-Alaska-Cascadia	B6	0.01

After an iterative process of grid correction and retesting using these "null" sources, both of the reference (RM) and forecast model (FM) grids were deemed satisfactory and the testing of realistic events could begin. The lower panel of Figure 14 illustrates a step in the process where a deficiency in the RM grid generated a mild instability in the ACSZ B06 micro-tsunami scenario (see Table 5) causing the RM time series at the reference point, initially in close agreement with the FM, to develop unrealistic, high frequency oscillations. Though still generally tracking the FM result, and not growing without bound, the feature could behave erratically in simulating real events. Modification of the RM bathymetry, to exclude the upper portion of Dundas Bay, eliminated the problem, as seen in the third panel of Figure 14, and "null" tests involving other sources (RNSZ B14 and EPSZ B19) did not reveal other issues.

4.2 The Extreme Case Tests

The record of tsunami impact on the southeast Alaskan coast, included in the comprehensive report on the region by Lander (1996) and searchable in the online NGDC catalog (www.ngdc.noaa.gov/hazard/) reveals that sources around the entire periphery of the Pacific can be felt. Indeed the catastrophic Indian Ocean tsunami of 2004 was detected at nearby Sitka and Yakutat though it preceded the current installation of the Elfin Cove gage. A broad suite of 20 extreme events (so-called mega-tsunamis) whose locations are standard for testing of Pacific basin forecast models, are described in Table 5. The normal list is supplemented by one, ACSZ 40-49, which overlays the study area (see Figure 6) and is expected to generate the largest response at Elfin Cove. The locations of the full set can be seen in Figure 31, later in this report, where the impacts to Elfin Cove are presented graphically. To simulate each mega-tsunami source, ten A-B pairs of unit sources (as illustrated in Figure 13) are used, with an evenly distributed slip of 25m in each. As described by Gica et al. (2008), each unit source represents a 100x50km area of the fault surface with the long axis parallel to the plate boundary. The B-row is shallowest, sloping from a nominal depth of 5km (unless a depth estimate has been provided by the USGS based on the earthquake catalogs), row-A is deeper, followed by rows Z, Y, X, … where appropriate. Thus, the extreme case sources represent 1,000 km long ruptures with a width of 100km; the corresponding moment magnitude is M_w=9.3. Note that recent (and future) additions to the propagation database extend portions of the source domain seaward as a C row. The aim is to represent outer-rise earthquake events where they are likely to occur, such as off the Kuril Islands as evidenced by the January 2007 normal fault event.

Discussion of the entire set of mega-tsunamis in greater detail is provided later in the report, once the validity of the Forecast Model has been established by the modeling of historic events. Here we focus on a subset of four, highlighted in Figure 13 and Table 5, to contrast the Forecast Model (FM) with the more highly resolved Reference Model (RM). Results are presented in Figures 15-18, which share a common format. Part a) contrasts the RM and FM maximum amplitude fields in the sub-region of the FM C-grid. The larger C-grid of the reference model is shown at the right to broaden the scope of the result and confirm that nothing untoward happens at the smaller C-grid's boundary. The lower panel compares the time series at the reference point (the Elfin Cove tide gage);

black and red curves represent the RM and FM respectively. Part b) is similar but contrasts the maximum speed fields with the speed time series at the tide gage in the lower panel. Finally part c) for each scenario compares the speed and velocity fields for a single time step, identified by the green line in the lower panel.

It is noticeable that, in the lower panels of part a) for all four of the cases shown, the Reference (RM) and Forecast Model (FM) are in almost perfect agreement for the amplitude of the earliest waves. Phase differences appear later, though the envelope of later wave amplitude is in essential agreement. However there is a tendency for the largest peaks and troughs to appear in the RM solution. This bias is reflected in the maximum wave distributions. Though the structure of the RM and FM maximum amplitude fields is similar, the common color bar can suggest a greater disparity.

The level of agreement for speed is less for the local event ACSZ 40-49 than was seen for its amplitude. After initially close agreement, reference model speeds can be several times larger than those of the forecast model later in the event (Figure 15b). For the more remote sources tested, the level of speed mismatch is far less pronounced. The velocity comparison of Figure 15c is for an early time in the record, as the first wave ebbs. The circulation patterns of the two model results are quite similar though, away from Elfin Cove itself, the RM speeds are somewhat higher.

This larger response of the reference model version quite likely reflects a physical reality: the more highly resolved bathymetry and coastline of the RM provide greater scope for non-linear features or reflected waves to develop. This observation suggests a caveat to operational use of the FM. While accurate portrayal of the early history of an event is to be expected, the duration of the event and the amplitude of some later waves may be under-estimated. Tide gage data will be needed to verify this conjecture, which is pursued later in the report. It is worth noting too that, although the ACSZ 56-65 mega-event represents a massive Cascadia tsunami, the scale of its impact to the Elfin Cove area (~60 cm) is not substantially different from those caused by remote sources: CSSZ 102-111 off southern Chile or MOSZ 1-10 near New Guinea.

In Figure 17c the comparison time was intentionally chosen much later in the CSSZ 102-111 mega-tsunami scenario, although still at a time where the amplitudes at the tide gage are in good agreement. This agreement clearly extends to the velocity field throughout the C-grid domain of the FM. The same is true when, in the case of the MOSZ 1-10 synthetic event (Figure 18c), the comparison time is at the leading edge of the wave's arrival at the tide gage. Note that in Figure 18a the spatial structure of maximum amplitude is consistent between the RM and FM solutions though peaks in the former raise the level. In conclusion it would appear that, while the solutions may temporarily deviate from each other, overall they maintain general agreement over several hours of simulation.

One further confirmatory test of the agreement between the Reference and Forecast versions of the model is usual: a mild source of magnitude 7.5 at a remote location. A single unit source near Samoa (NTSZ-B36) was employed for this purpose and its

representations by the RM and FM are compared in Figure 19. Such an event results in a response of less than a centimeter in Elfin Cove sea level and there is excellent agreement between both model representations in the early portion of the record. Later there is an onset of a high frequency, but low-level, instability in the Reference Model result. Since the forcing fields for NTSZ B36, drawn from the propagation database terminate at 24 hours, it appears that the Forecast model more realistically represents the tapering to zero of the forcing imposed in the MOST model.

4.3 Model Inter-comparison using Historical Cases

Several historical scenarios will be employed in model validation, using observed records from tide gages within the model domain. The issue of validation is somewhat different from that of comparing the predictions of the Reference (RM) and Forecast (FM) versions of the model. Both versions are forced with the same fields, derived in recent events from a fit to DART® observations of propagation model results. No tsunami observations along the boundary of the model domain are available and so it is not possible to directly inter-compare the RM and FM response to known forcing.

Thus, and as a means to reduce the volume of graphics in the validation phase, we treat several historical cases as further scenarios (but now based on real situations) with which to inter-compare the models. Similar graphical presentations are employed to those described earlier for the mega-tsunami scenarios. In Figure 20 the maximum amplitude and speed distributions and time series at the Elfin Cove tide gage, and the vector velocity at a single time step, are contrasted for a hindcast of the Honshu-2011 event. The results are quite satisfactory though, as before, the Reference Model tends to produce greater excursions, particularly for speed at the tide gage (Figure 20b). Figure 21 illustrates the Chile-2010 event; the conclusions are similar, though an excessive speed value at low water in the southeast corner of the FM C-grid may indicate a shoal that is not well represented. Figure 22 represents the Alaska-1964 event, the largest event with observations to impact the region. The results are very satisfactory with good agreement between the Reference and Forecast Model renditions of the massive historic event. Finally, in Figure 23, the RM and FM results for a representation of the Chile-1960 event are represented. The unit source representation of this event is based solely on the reported epicenter and moment magnitude of the earthquake, rather than observations of the tsunami it generated. As seen later (Figure 28), the predicted wave amplitude at Sitka is considerably overestimated by the model, though the arrival time is reasonable. However the agreement between the solutions, reflected in Figure 23, is again satisfactory, particularly in Elfin Cove.

These historical cases, together with the mega-tsunami scenarios described earlier, confirm that the Forecast (FM) version of the model captures the essential features of the more highly resolved (and slower running) Reference Model (RM). It may reduce somewhat the extreme amplitudes and speeds within the domain, but does perhaps, produce more realistic results for later waves.

4.4 Model Validation: The Honshu-2011 Tsunami

In addition to its disastrous impact on the coast of Japan, the Honshu tsunami of March 11, 2011 radiated waves throughout the Pacific Basin. Those arriving at nearby DART®s were of unprecedented amplitude and their signal/noise ratios facilitated accurate and early source characterization. Further afield, the waves were detectable at all operational DART®s in the basin (26 in all) and, while major damage was mainly confined to Japan, significant signals were obtained at multiple coastal tide gages. Prior to this event, the Kuril-2006 tsunami event was the best available for model validation. For the U.S. West Coast and Southeast Alaska at least, that role has now been taken by Honshu-2011. The adequacy of the composite propagation solution can be assessed by comparison with the BPR signal from the closest DART® 46410, some 440 km west of Elfin Cove. Located 1,140 km to the south of Elfin Cove, the northernmost West Coast DART®, 46419, was unfortunately out of action in early 2011.

In Figure 24 the eastward progression of predicted tsunami waves from the Honshu-2011 event across the North Pacific, as observed by the DART® array, is illustrated and compared with the forecasts produced in real-time using SIFT. As described earlier, the first phase in the forecast process is to ingest observations from the closest DART®(s), and determine the linear combination of unit sources from the propagation database that best matches those observations. In addition to providing the boundary conditions for the community-specific forecast models, the linearly-combined propagation solution can be directly interrogated to provide forecasts for DART®s not involved in its selection. It is this set of forecasted DART® time series that are compared with the observations in Figure 24.

There is clearly a strong agreement between the first wave of the tsunami as detected by the DART® sensors (drawn as black curves) and model predictions (drawn in red), although the observations increasingly lag the predictions and the ratio of their amplitudes varies with location Ultimately, on reaching DART® 46410, the model "waves" are seen to be about nine minutes early, a difference that is small compared to the several hours of transit time. Perhaps coincidently the amplitude ratio for the leading wave (denoted by R in Figure 24) is closest to unity for the DART® (46410) closest to Elfin Cove. Four DART®s between Oregon and southern California (46404, 46407, 46411 and 46412, not shown in Figure 24) have amplitude ratios of approximately 1.5 – 2.0 and time lags of about 8 minutes. Early arrival model is typical and is associated with the limited resolution of the basin-wide bathymetry. Finer-scale features in the actual bathymetry, such as the Emperor Seamount chain in the western Pacific (south of ACSZ B06 in Figure 13), slow down the real wave trains. As part of the ongoing testing and evaluation (OT&E) process to determine the suitability of SIFT for operational use, the forecast procedures are applied in hindsight using accuracy metrics based on the success of a set of forecast models in replicating tide gage observations. While such ongoing efforts may determine the "best" propagation solution, for the purpose of model validation in this report, we employ the real time source characterization defined in Table 6. It is one of the sources employed by Tang et al. (2012) in characterizing the energy released by the Honshu-2011 event.

Figure 25 compares Reference (RM) and Forecast (FM) predictions with observations, at several sites within the model domain (Ketchikan falls outside the FM grids though it is available to the RM.) The observed time series are 1-minute tide gage data (6-minute in the case of Skagway), detided using the Kalman Filter (Percival et al., 2011) and low pass filtered. Black and red curves represent Reference (RM) and Forecast Model (RM) predictions; the green curves are the detided and filtered observations. Runup values, from the NGDC catalog, are indicated in this and subsequent figures. At Elfin Cove itself, the focus of the innermost C-grid, the result is satisfactory: the model waves arrive early and slightly under-estimate the amplitude of the leading wave (but consistent with expectation based on Figure 24), and the later waves sustain a level consistent with the data. The other sites are in the outermost A-grid, whose reduced spatial resolution has limited ability to reflect complex topography. In particular the Gastineau Channel leading to Juneau is not resolved at all in the FM A-grid and only poorly in the RM version.

Nonetheless the results for these A-grid sites are, in most cases, quite gratifying (Skagway and Ketchikan are underestimated by the model). For Sitka, close to the open ocean, the results are best both for the leading wave and the amplitude of the later waves. At Port Alexander the match for the leading wave is acceptable but the excessive noise in the observed record obscures the later waves. For the remaining sites, which currently do not have dedicated forecast models, the degree of agreement is such as to suggest their utility as a significant improvement over a Green's Law coastal forecast. When the forecast models specific to Sitka and Port Alexander are validated the degree of agreement with the Elfin Cove A-grid results should be used to cast further light on this conjecture. The main reason that the Elfin Cove A-grids are so extensive is to ensure that tsunami waves entering Cross Sound and Icy Strait, from the east are appropriately represented. The relative success in replicating the observations from Juneau and Skagway suggest that this goal has been met.

Table 6. Source characterization for historical tsunami events employed in Elfin Cove model testing. Those in bold text were used in RM/FM inter-comparison. Sources identified as "ad hoc" may not be identically defined in other Forecast Model reports.

Earthquake / Seismic				Model		
Event	**USGS Date Time (UTC) Epicenter**	**CMT Date Time (UTC) Centroid**	**Magnitude M_w**	**Tsunami Magnitude**	**Subduction Zone**	**Tsunami Source (Reference/Derivation)**
1946 Unimak	01 Apr 12:28:56 52.75ºN 163.50ºW		8.5	8.5	ACSZ	7.5×B23 + 19.7×B24 + 3.7×B25 (López & Okal, 2006)
1952 Kamchatka	04 Nov 16:58:26.0 52.76ºN 160.06ºE		9.0	9.0	KISZ	19.71 × (A4 + Y4 + Z4 + A5 + Y5 + Z5 + A6 + Y6 + Z6) (ad hoc)
1957 Andreanof	09 Mar 14:22:31 51.56ºN 175.39ºW		8.6	8.7	ACSZ	31.4×A15 + 10.6×A16 + 12.2×A17 (Preliminary)
1960 Chile	22 May 19:11:14 38.29ºS 73.05ºW		9.5	9.5	CSSZ	125×(A93 + B93 + Z93 + A94 + B94 + Z94 + A95 + B95) Kanamori & Cipar (1974)
1964 Alaska	28 Mar 03:36:00 61.02ºN 147.65ºW		9.2	8.9	ACSZ	15.4×A34 + 18.3×B34 + 48.3×Z34 +19.4×A35 +15.1×B35 (Tang et al., 2006, 2009)
1994 East Kuril	04 Oct 13:22:58 43.73ºN 147.321ºE	04 Oct 13:23:28.5 43.60ºN 147.63ºE	8.3	8.1	KISZ	9.0×A20 (ad hoc)
1996 Andreanof	10 Jun 04:03:35 51.56ºN 175.39ºW	10 Jun 04:04:03.4 51.10ºN 177.410ºW	7.9	7.8	ACSZ	2.40×A15 + 0.80×B16 (Preliminary)
2001 Peru	23 Jun 20:33:14 16.265ºS 73.641ºW	23 Jun 20:34:23.3 17.28ºS 72.71ºW	8.4	8.2	CSSZ	5.7×A15 + 2.9×B16 + 1.98×A16 (Preliminary)
2003 Hokkaido	25 Sep 19:50:06 41.775ºN 143.904ºE	25 Sep 19:50:38.2 42.21ºN 143.84ºE	8.3	8.3	KISZ	3.95 × (A22 + B22 + A23 + B23) (ad hoc)
2003 Rat Island	17 Nov 06:43:07 51.13ºN 178.74ºE	17 Nov 06:43:31.0 51.14ºN 177.86ºE	7.7	7.8	ACSZ	2.81×B11 (Real-time)
2006 Tonga	03 May 15:26:39 20.13ºS 174.161ºW	03 May 15:27:03.7 20.39ºS 173.47ºW	8.0	8.0	NTSZ	6.6×B29 (ad hoc)
2006 Kuril	15 Nov 11:14:16 46.607ºN 153.230ºE	15 Nov 11:15:08 46.71ºN 154.33ºE	8.3	8.1	KISZ	4.0×A12 + 0.5×B12 + 2.0×A13 + 1.5×B13 (Real-time)
2007 Kuril	13 Jan 04:23:20 46.272ºN 154.455ºE	13 Jan 04:23:48.1 46.17ºN 154.80ºE	8.1	7.9	KISZ	-3.64 × B13 (Real-time)
2007 Solomon	01 Apr 20:39:56 8.481ºS 156.978ºE	01 Apr 20:40:38.9 7.76ºS 156.34ºE	8.1	8.2	NVSZ	12.0×B10 (Preliminary)
2007 Peru	15 Aug 23:40:57 13.354ºS 76.509ºW	15 Aug 23:41:57.9 13.73ºS 77.04ºW	8.0	8.1	CSSZ	0.9×A61 + 1.25× B61 + 5.6×A62 + 6.97×B62 + 3.5×Z62 (Preliminary)
2007 Chile	14 Nov 15:40:50 22.204ºS 69.869ºW	14 Nov 15:41:11.2 22.64ºS 70.62ºW	7.7	7.6	CSSZ	1.65×Z73 (Real-time)
2009 Samoa	29 Sep 17:48:10 15.509ºS 172.034ºW	29 Sep 17:48:26.8 15.13ºS 171.97ºW	8.1	8.1	NTSZ	3.96×A34 + 3.96×B34 (Real-time)
2010 Chile	27 Feb 06:34:14 35.909ºS 72.733ºW	27 Feb 06:35:15.4 35.95ºS 73.15ºW	8.8	8.8	CSSZ	17.24×A88 + 8.82×A90 + 11.84×B88 + 18.39×B89 + 16.75×B90 + 20.78×Z88 + 7.06×Z90 (Real-time)
2011 Honshu	11 Mar 05:46:24 38.297^{0}N 142.372^{0}E	11 Mar 05:47:47.2 38.486^{0}N 142.597^{0}E	9.0	9.0	KISZ	4.66 × B24 + 12.23×B25 + 26.31×A26 + 21.27×B26 + 22.75×A27 + 4.98×B27 (Real-time; Tang et al., 2012)

4.5 Further Historical Simulations

Before proceeding with the discussion of the historical simulations, the contents of Table 6 should be defined. Two specifications of source location and time are given: one based on the epicenter and reported early in the event, the other coming later as seismic waveforms from a more widespread set of stations are assimilated. The latter Centroid-Moment-Tensor (CMT) solution provides details of the source mechanism, moment magnitude (listed in Table 6). The right hand side of Table 6 provides the specifics of the combination of unit sources employed to represent the tsunami waves. The subduction zone in which the event occurred is given by a 4-character acronym: ACSZ for example refers to a line of unit sources extending from the western Aleutians to Cascadia. Individual unit sources are identified by a character-number combination. Further detail on each unit source can be found in Gica et al., (2008) and in Appendix B of this report.

As discussed earlier, a linear combination of unit source functions provides the time varying forcing of the model that simulates a tsunami event. The coefficient applied to each source function is a weight assigned to the 100x50km sub-fault it represents. Thus, in the final column of Table 6, the term "7.5×B23" in the characterization of the 1946 Unimak event implies a scaling by a factor of 7.5 of unit source B23 in the Aleutian to Cascadia subduction zone. Each unit source represents a moment magnitude 7.5 event; by combining the coefficients a "Tsunami Magnitude" can be produced. It should be stressed that this is not an alternate estimate of the magnitude of the seismic event. Rather it summarizes the combined effect of the unit sources in generating tsunami waves.

Since the advent of the tsunameter array, and the SIFT system to invert its observations, the "recipes" (linear combinations of unit source functions) for events are being produced in "real-time" and are classified as such in Table 6. The tsunamigenic description of earlier events have in some instances been reconstructed from tide gage observations and reported in the literature. Others in Table 6 are listed as "preliminary" in the sense that they have not been thoroughly studied but show some skill in representing an event. Included in Table 6 are several sources considered "ad hoc". Generally chosen as equally-weighted groupings of unit sources whose location and scaling are based on the epicenter and magnitude of an event, they should be considered as exploratory providing a "reality check" on the waves that might be hindcast for the model domain. Since in reality tsunami waves may be less than the magnitude of the earthquake would suggest, or exceed expectation if for example a submarine landslide were triggered, the quality of the ad hoc cases will likely be poor. The arrival time of the simulated waves may be of use for comparison with observations.

Model validation, based on a DART®-derived propagation solution, is possible for the Chile-2010 event and is illustrated in Figure 26. The source characterization given in Table 6 was derived in real-time as the waves were detected at DART® sites in the southeast Pacific and were successfully employed to forecast impacts to Hawaii and the U.S. West Coast. With regard to timing and overall amplitude the model predictions are satisfactory in the Gulf of Alaska, but neither the Reference (RM) nor Forecast (FM) versions capture the leading trough apparent in the observed time series at Elfin Cove and

Sitka. Port Alexander is again noisy but at the remaining sites the amplitude at least of the response is reasonably rendered for all of the sites shown.

For south and southeast Alaska the defining tsunami event to date has been that associated with the 1964 earthquake in Prince William Sound. Though preceding open ocean tsunami detection, the source characteristics were elucidated though a number of studies incorporating seismic and tide gage records. The unit source selection and slip assignments provided in Table 6 are discussed by Tang et al., (2006, 2009) and used successfully in modeling the impact on Hawaii. In Figure 27 the predictions of the impacts at several sites in the Elfin Cove model domain are presented. Only for Sitka is an observed time series available but several runup values are available from the NGDC catalog. The Sitka time series is based on a digitized marigram, available in the WCATWC archives and detided and filtered using the same methods employed throughout this study. The comparison with the reported runup values at Sitka, Juneau, and Ketchikan is satisfactory. At Elfin Cove itself the model results are only about 50% of the reported runup. This was derived from the tide gage but the marigram is not available. The Skagway runup (eyewitness report) is also under-predicted by the model but overall, the success in replicating the character of this huge event, together with the results from the Honshu-2011 analysis, discussed earlier, strongly support the validity of the Elfin Cove models.

Two other historical events are represented by digitized marigrams for Sitka in the WCATWC archives: Kamchatka-1952 and Chile-1960. The results for these are provided in Figure 28. Perhaps because these are remote events, so that the source characterizations (in Table 6) are less appropriate to the Gulf of Alaska, the level of success in validating the Elfin Cove model with these cases is much less than for the local Alaska-1964 tsunami. The model prediction at Sitka for the Chile-1960 event is too large by a factor of 4-5, as is that for Kamchatka-1952! Further effort is clearly needed to more appropriately define these source in terms of the propagation database when the application of the model to these historically important events should be revisited.

Next, in Figure 29, simulated historical events from Table 6 since the advent of the DART® array are presented. The results are disappointing at best, though they do confirm a feature of the region noted earlier: Elfin Cove is less impacted by trans-basin tsunami sources than other U.S. interests in the Pacific. On a less positive note the frequent noise bursts in recorded sea level, associated with wind and waves and illustrated in Figure 8, limit the suitability of Elfin Cove as a monitoring site for weak tsunami signals thereby limiting the number of recent events available for model validation.

The modeling results for the remaining standard cases, those prior to the advent of the DART® array and lacking any time series in the vicinity of Elfin Cove, are presented in Figure 30. The time series represent Elfin Cove but NGDC runup values from nearby Sitka are shown when available. These model time series do little beyond demonstrating the absence of stability issues in the application of the model.

A number of other local events, not included in Table 6 but mentioned earlier in the context of seismic hazard, deserve investigation. On September 10, 1899 a major earthquake occurred in Yakutat Bay, and was one of the earliest events measured by seismograph. Several tsunami observations outside the immediate vicinity of Yakutat were reported (Lander, 1996) though some may have been associated with secondary generation through landslides. An icefall was reported in Glacier Bay but no tide gages were operational in Alaska at the time. On October 24, 1927 a magnitude 7.1 earthquake occurred that affected the Alexander Archipelago with widespread qualitative, but no quantitative reports. The Queen Charlotte earthquake of August 22, 1949 had reported observations in the Sitka area but only an unreliable 8 cm measurement on the marigram. The Fairweather earthquake of July 10, 1958 is best known for the Lituya Bay landslide and tsunami it triggered. There were reports of seiching in Cross Sound and a weak wave of about 10 cm was reported on the Sitka tide gage. A magnitude 7.6 earthquake near Sitka on July 30, 1972 was felt over a wide area but registered only 10cm at Juneau and 8cm at Sitka itself. The Cross Sound sequence of earthquakes in mid-1973 have been discussed in the seismological literature (Doser and Lomas, 2000) but no reports appear in the tsunami catalogs.

None of these local events are well enough described or observed to merit a full investigation, or inclusion in Table 6 as well-documented tsunami sources. Instead approximate (ad hoc) source definitions were adopted and run to ensure no untoward behavior of the model. The results are summarized in Table 7 and, where observations at Sitka are reported in the catalogs, they are approximately confirmed. When sources are designated as "ad hoc" in Table 6, they may not be uniformly implemented in other Forecast Model reports.

Table 7. Ad hoc unit source representation of several local events for southeast Alaska investigated using the Elfin Cove forecast model, with Sitka observations where available.

Event	M_w Estimate	Date	Location	Unit Sources Used	Maximum Amplitude (cm)		Sitka Reports (cm)
					ElfinCove	Sitka	
Yakutat Bay	8.2	10 Sep 1899	60N, 140W	40-42 A,B	17.4	30.5	n/a
Sitka Region	7.4	24 Oct 1927	57.7N, 136.1W	44 B	7.4	5.5	n/a
Queen Charlotte	8.1	22Aug 1949	53.6N, 133.3W	47-51B	4.1	16.4	8
Fairweather Fault	7.7	10 Jul 1958	58.3N, 136.5W	43A	26.8	12.2	10
Sitka Region	7.6	4 Aug 1972	56.2N, 135.3W	46B	6.1	33.4	8
Cross Sound	6.7	1 Jul 1973	57.8N, 137.3W	43B	1.2	0.9	n/a

One other event was noted in the run-up catalog statistics for Sitka: on November 29, 1975 a magnitude 7.2 earthquake on the island of Hawaii triggered the Kalapana landslide off the southeast coast, generating waves which were seen at several sites around the Pacific, Sitka AK was among them with an amplitude of about 10cm. The marigram shown in Lander (1996) was digitized. Although the MOST model in its current form does not apply to landslide-generated tsunamis and there are not unit sources near Hawaii, a similar modeling approach to ours was applied by Ma et al. (1999) to study the local impact. An ad hoc source was created (Newman, personal communication), mimicking that of Ma et al. (1999), and applied to the Elfin Cove model. The result was of the appropriate amplitude and consistent with the reported arrival time. Given the typical noise environment of the Gulf of Alaska in November, this side exercise is not conclusive but does perhaps provide indirect support to the model.

4.6 Simulation of the remaining Synthetic Mega-events

We conclude this section with a summary of other model runs that were made in order to verify its stability, but which provide useful information on the exposure of the Elfin Cove region to potentially hazardous future events within the Pacific. As noted earlier, the sparse instrumental record of actual events needs to be augmented with credible scenarios to permit risk assessment. While not pretending to be a full-blown risk assessment for the region, the full set of mega-tsunamis modeled during stability testing can provide some early estimates.

Table 8. Comparison of the response at Elfin Cove, AK to that of Point Reyes, CA (Spillane, 2011) for synthetic (M_w 9.3) mega-tsunami scenarios, The maximum amplitude at the reference point is used as the measure of response which is generally far weaker at Elfin Cove than at Point Reyes. The ratio, expressed as a percentage is tabulated below; the Elfin Cove responses are illustrated graphically in Figure 31.

Scenario Name	Source Region	Response (cm) Elfin Cove	Response (cm) Point Reyes	Ratio (%)
KISZ 1-10	Kamchatka	27.6	354	7.8
KISZ 22-31	Japan Trench	42.9	251	17.1
KISZ 32-41	Bonin Trench	31.3	318	9.8
KISZ 56-65	Mariana Trench	33.9	166	20.4
ACSZ 6-15	West Aleutians	26.3	134	19.6
ACSZ 16-25	Aleutian Trench	37.9	266	14.2
ACSZ 22-31	Aleutian Trench	59.8	239	25.0
ACSZ 40-49	Cross Sound	**495.7**	n/a	n/a
ACSZ 50-59	Cascadia-North	65.2	202	32.3
ACSZ 56-65	Cascadia-South	59.6	159	37.5
CSSZ 1-10	Mid-America Trench	11.5	99	11.6
CSSZ 37-46	Colombia-Ecuador	43.2	42	**102.9**
CSSZ 89-98	Chile Trench	11.9	140	8.5
CSSZ 102-111	South Chile	28.0	265	10.6
NTSZ 30-39	North Tonga Trench	38.9	402	9.7
NVSZ 28-37	New Hebrides Trench	**56.4**	258	21.9
MOSZ 1-10	Manus, West Melanesia	**55.3**	460	12.0
NGSZ 3-12	New Guinea	42.6	162	26.3
EPSZ 6-15	East Philippines	34.9	246	14.2
RNSZ 12-21	Ryukyu	15.8	209	7.6

Mega-tsunami sources, not highlighted in Table 5, were investigated with the Forecast Model alone; results for the entire set of twenty are provided in Table 8 and Figures 31 and 32. Each source is a composite of 20 unit sources (see Figure 13) from the A and B rows with an evenly distributed slip representing an M_w 9.3 event. A color-coded square, drawn at the geometric center of each synthetic source, is used to represent the impact at

the Elfin Cove tide gage predicted for that source. The measure of impact employed, in Table 8 and Figure 31, is the maximum amplitude of the predicted time series at the reference point. Great circle distances to Elfin Cove are provided and a vector, normal to the source line, is drawn as a crude indicator of the initial main beam orientation. The impact of the local mega-source (ACSZ 40-49) dominates all others. Moderate impacts are associated with the closer sources (AC 22-31 near the Alaskan Peninsula, and ACSZ 50-59 and 56-65 representing the northern and southern portions of Cascadia) but otherwise the impacts are only loosely related to distance. Sources in the southwest Pacific (NVSZ 28-37 near the New Hebrides, and MOSZ 1-10 near Manus) have almost as large an impact although, with one exception beyond the local source, the impact predicted for Elfin Cove is much less than that expected along the U.S. West Coast (see Table 8, where Point Reyes, CA is used for comparison).

The results provided in Table 8 and Figures 31 and 32 are specific to the reference site: the Elfin Cove tide gage. Based on the 20 mega-tsunami simulations, impact statistics were extracted for several communities in the region. The results are presented in Table 9, whose footnote identifies the site name abbreviations. Values provided for Sitka and Port Alexander would be better represented by their specific forecast models which better resolve local bathymetry, With the exception of Elfin Cove itself, the other sites are represented by A-grid cells close to their geographic coordinates. Several of the communities are marked in Figure 2. Pelican, though unlabeled in Figure 2, is at the north-western terminus of the Alaska ferry routes shown and can also be seen in Figure 4a. Bartlett Cove, north of Point Gustavus in Figure 4a, is offshore of the Visitor Center where cruise ships take on their National Park guides at the entrance to Glacier Bay. Auke Bay, also unlabeled in Figure 2, is northwest of Juneau and home to an Alaska Fisheries Science Center laboratory.

Figures produced earlier, that showed the distribution of maximum current speed in the Reference Model C-grid, confirmed the strength of tsunami-induced currents in the Inian Passes north of Elfin Cove. Since these are already well known for strong tidal currents, are traversed by ferries and cruise ships plying the Alaska Marine Highway, and have potential for tidal power generation, it seems worthwhile to extract from the model results estimates of the additional rapidly varying current speeds that might accompany a major tsunami event. A comprehensive treatment would jointly model tides and tsunami so the results provided in Table 10 are incomplete. Results are given for a selection of sites, shown in Figure 33, instrumented by NOAA's EcoFOCI program during 2010 and 2011. The sampling interval of the Acoustic Doppler current profilers is not suited to tsunami study and the instruments were not deployed during the Honshu-2011 event. The final row of Table 10 provides an estimate of the maximum current at each site, based on the 95th percentile of the depth average (only 5% of the currents exceed the tabulated value).

The strongest observed tidal currents are at the shallower locations: South Inian Pass and the mouth of Glacier Bay. Even shallower depths in the 30-40 meter range are found south of the latter marking the terminal moraine of the Glacier Bay glacier which protruded into Icy Strait in the mid-1700s at the end of the Little Ice Age. Only for the local mega-event scenario (ACSZ 40-49) do the maximum tsunami current speed

predictions exceed those associated with the tides. However, with their rapid changes in direction, tsunami-induced currents are potentially of concern. In Figure 33, the greatest currents are to be expected near the western end of South Inian Pass with predicted currents in excess of 10 knots for the ACSZ 40-49 scenario.

Table 10. Maximum speeds at various locations from Cross Sound to Icy Strait in mega-tsunami simulations using the Elfin Cove forecast model (FM/RM in the rows with bold text). Speeds are given in knots for ease of comparison with the NOAA chart warnings of tidal currents of 8-10 knots that are frequently encountered in North and South Inian Passes. Observed maxima (and water depths) are based on NOAA EcoFOCI current meter data from 2010 and 2011.

Scenario Name	Cross Sound	North Inian Pass	South Inian Pass	Glacier Bay	Icy Strait
KISZ 1-10	0.10	0.26	0.58	0.17	0.22
KISZ 22-31	0.13	0.28	0.61	0.15	0.17
KISZ 32-41	0.14	0.26	0.60	0.12	0.20
KISZ 56-65	0.11	0.34	0.80	0.13	0.26
ACSZ 6-15	0.08	0.18	0.39	0.14	0.21
ACSZ 16-25	0.12	0.34	0.78	0.23	0.30
ACSZ 22-31	0.17	0.45	0.97	0.23	0.38
ACSZ 40-49	**1.39 / 1.43**	**3.52 / 3.35**	**5.63 / 6.78**	**1.93 / 1.55**	**2.33 / 2.77**
ACSZ 50-59	0.23	0.69	1.56	0.35	0.48
ACSZ 56-65	**0.19 / 0.23**	**0.71 / 0.61**	**1.40 / 1.39**	**0.29 / 0.42**	**0.29 / 0.46**
CSSZ 1-10	0.04	0.15	0.28	0.08	0.08
CSSZ 37-46	0.07	0.19	0.34	0.08	0.09
CSSZ 89-98	0.12	0.32	0.67	0.22	0.15
CSSZ 102-111	**0.18 / 0.17**	**0.42 / 0.32**	**0.87 / 0.71**	**0.24 / 0.20**	**0.23 / 0.23**
NTSZ 30-39	0.12	0.27	0.54	0.18	0.21
NVSZ 28-37	0.15	0.39	0.83	0.17	0.27
MOSZ 1-10	**0.16 / 0.23**	**0.35 / 0.35**	**0.74 / 0.95**	**0.25 / 0.18**	**0.25 / 0.18**
NGSZ 3-12	0.16	0.36	0.91	0.26	0.48
EPSZ 6-15	0.09	0.30	0.72	0.20	0.25
RNSZ 12-21	0.06	0.16	0.38	0.06	0.14
Observed Maxima (kts)	**1.19 (318m)**	**2.21 (289m)**	**3.16 (72m)**	**3.49 (71m)**	**1.24 (132m)**

5.0 Conclusions

To conclude, good agreement between observations and model predictions for a subset of the larger historical events, including the recent Honshu-2011 tsunami, has been established and the stability of the model for numerous synthetic events has been demonstrated. In particular the reliability of the forecast model, designed to run rapidly in a real time emergency conditions, has been proven by the favorable comparison with reference model predictions, particularly during the early hours of an event. The model will be included in the SIFT system employed by the Tsunami Warning Centers, and will permit the Cross Sound - Icy Strait region of southeast Alaska and the community of Elfin Cove to be added to the coastal areas for which forecast capability is available. Additionally it will provide a tool of use in risk assessment studies.

The presence of Icy Strait, linking Cross Sound to the deep north-south channel of Chatham Strait, necessitated a more extensive outermost grid for the Elfin Cove model. While this increases model run-time somewhat, it does provide the benefit of permitting forecasts for communities not presently selected for specific forecast models: Juneau and Skagway for example. Statistics for tsunami wave amplitude were extracted during model development and testing for other communities of southeast Alaska and maximum tsunami-induced currents were extracted for the Cross Sound – Icy Strait region where tidal currents are known to be strong.

Testing of model stability using mega-tsunami (M_w=9.3) scenarios from a selection of sites around the Pacific Rim suggest that, with the exception of sources in the vicinity of Elfin Cove, the impact there is considerably less than on the U.S. West Coast. This, in conjunction with recurring episodes of noise at the tide gage, substantially reduced the number of historical events in recent years available for model validation. Tsunami waves emanating from the southwest Pacific result in proportionately greater response in the Alaska Panhandle. The report does not suggest that the mega-event scenarios represent probable tsunami sources and should not be considered a thorough risk assessment study.

In addition to the scenarios run by the author, and reported here, further tests have been made by other members of the group at NCTR, and will continue to be made by staff at the Warning Centers and others, perhaps in training situations. Among the many related tools developed at NCTR is ComMIT (Community Model Interface for Tsunami, nctr.pmel.noaa.gov/ComMIT/), which provides a highly intuitive graphical environment in which to exercise and explore forecast models for any combination of propagation database unit sources. Were any of these avenues to reveal a problem with the model, its origin (most likely in some quirk of the bathymetric files) would be located and corrected and the revised version re-installed at the Warning Centers. The development of the forecast system will be a dynamic process, with new models added (and old ones revisited) from the current list of U.S interests and globally. In the coming years it is expected that further capabilities will be added as algorithms and methodologies mature.

6. Acknowledgments

Many members of the NCTR GROUP provided valuable assistance in the production of this report. In particular Diego Arcas edited the first draft for content and style; Elena Tolkova provided scripts for filtering time series and bathymetry. The modeling could not proceed without the detailed DEMs produced at NGDC by the painstaking combination of numerous bathymetric and topographic surveys. Digitized marigrams for a number of historic events were acquired from the WCATWC archives. Figure 2 was reproduced with the permission of the Alaska Department of Transportation and Public Facilities. Current meter observations from the Cross Sound–Icy Strait region were provided by the EcoFOCI group at NOAA-PMEL. This publication is partially funded by the Joint Institute for the Study of the Atmosphere and Ocean (JISAO) under NOAA Cooperative Agreements NA17RJ1232 and NA10OAR4320148, Contribution No. XXXX. It is PMEL Contribution No. NNNN

7. References

Doser, D.I. and R. Lomas (2000): The transition from strike-slip to oblique subduction in southeastern Alaska from seismological studies. Tectonophysics, 316:45-65.

Dunbar, P. (2007): Increasing public awareness of natural hazards via the Internet. *Nat. Hazards 42(3) 529-536, DOI: 10.1007/s11069-006-9072-3*

Elfin Cove Community Plan (2007). Developed by the Elfin Cove Community NonProfit Corporation in association with Southeast Strategies and Glenn Gray and Associates.

Gica, E., M. Spillane, V.V. Titov, C.D. Chamberlin, and J.C. Newman (2008): Development of the forecast propagation database for NOAA's Short-term Inundation Forecast for Tsunamis (SIFT). NOAA Tech. Memo. OAR PMEL-139, NTIS: PB2008-109391, 89 pp.

Kanamori, H. and J.J Cipar (1974): Focal process of the great Chilean earthquake, May 22, 1960. *Phys. Earth Planet. Int., 9,128-136.*

Lander, J.F., (1996) Tsunamis Affecting Alaska 1737-1996, KGRD No. 31, National Oceanic and Atmospheric Administration, National Geophysical Data Center, Boulder, Colorado, USA, September, 155 p.

López, A.M., and E.A. Okal (2006): A seismological reassessment of the source of the 1946 Aleutian "tsunami" earthquake. *Geophys. J. Int., 165(3), 835–849*, doi: 10.1111/j.1365-246x.2006.02899.x.

Love, M.R., B.W. Eakins, L.A. Taylor, K.S. Carignan, D. Friday, P.R. Grothe (2011): Digital Elevation Model of Elfin Cove, Alaska: Procedures, Data Sources and Analysis. National Geophysical Data Center, Boulder, Colorado

Ma, K-F, H. Kanamori and K. Satake (1999) JGR 104: 13,153-13,167. Mechanism of the 1975 Kalapana, Hawaii, earthquake inferred from tsunami data.

National Geophysical Data Center / World Data Center (NGDC/WDC) Global Historical Tsunami Database, Boulder, CO, USA.
(Available at: http://www.ngdc.noaa.gov/hazard/tsu_db.shtml)

Percival, D.B., D. Arcas, D.W. Denbo, M.C. Eble, E. Gica, H.O. Mofjeld, M.C. Spillane, L. Tang, and V.V. Titov (2009): Extracting tsunami source parameters via inversion of DART® buoy data. NOAA Tech. Memo. OAR PMEL-144, 22 pp.

Percival, D.B., D.W. Denbo, M.C. Eble, E. Gica, H.O. Mofjeld, M.C. Spillane, L. Tang, and V.V. Titov (2011): Extraction of tsunami source coefficients via inversion of DART® buoy data. *Nat. Hazards*, *58*(1), doi: 10.1007/s11069-010-9688-1, 567–

590.

Polagye, B., and R Bedard (2006)" Tidal In-stream Energy Assessment for Southeast Alaska. Report EPRI-TP-003 AK to the Alaska Energy Authority. Available at: http://oceanenergy.epri.com/attachments/streamenergy/reports/003_TP_AK_011007.pdf

Spillane, M.C., E. Gica, V.V. Titov, and H.O. Mofjeld (2008): Tsunameter network design for the U.S. DART® arrays in the Pacific and Atlantic Oceans. NOAA Tech. Memo. OAR PMEL-143, 165 pp.

Spillane, M.C. (2011): Development of a Tsunami Forecast Model for Point Reyes, California. NOAA OAR Special Report, PMEL Tsunami Forecast Series. nctr.pmel.noaa.gov/forecast_reports/final_reports/PtReyesCA_DRAFT.pdf

Tang, L., C. Chamberlin, E. Tolkova, M. Spillane, V.V. Titov, E.N. Bernard, and H.O. Mofjeld (2006): Assessment of potential tsunami impact for Pearl Harbor, Hawaii. NOAA Tech. Memo. OAR PMEL-131, NTIS: PB2007-100617, 36 pp.

Tang, L., V.V. Titov, and C.D. Chamberlin (2009): Development, testing, and applications of site-specific tsunami inundation models for real-time forecasting. *J. Geophys. Res.*, *114*, C12025, doi: 10.1029/2009JC005476.

Tang, L., V.V. Titov, E.N. Bernard, Y. Wei, C.D. Chamberlin, J.C. Newman, H.O. Mofjeld, D. Arcas, M.C. Eble, C. Moore, B. Uslu, C. Pells, M. Spillane, L. Wright, and E. Gica (2012): Direct energy estimation of the 2011 Japan tsunami using deep-ocean pressure measurements. J. Geophys. Res. 117, C08008, doi:10.1029/2011JC007635, 2012.

Titov, V., and F.I. González (1997): Implementation and testing of the Method of Splitting Tsunami (MOST) model. NOAA Tech. Memo. ERL PMEL-112, NTIS: PB98-122773, NOAA/Pacific Marine Environmental Laboratory, Seattle, WA, 11 pp.

Titov, V.V., and C.E. Synolakis (1998): Numerical modeling of tidal wave run-up. *J. Waterw. Port Coast. Ocean Eng.*, *124*(4), 157–171.

Wei, Y., E. Bernard, L. Tang, R. Weiss, V. Titov, C. Moore, M. Spillane, M. Hopkins, and U. Kânoğlu (2008): Real-time experimental forecast of the Peruvian tsunami of August 2007 for U.S. coastlines. *Geophys. Res. Lett.*, *35*, L04609, doi: 10.1029/2007GL032250.

Wesson, R.L., O.S. Boyd, C.S. Mueller, C.G. Bufe, A.D. Frankel, M.D. Petersen, (2007): Revision of time-Independent probabilistic seismic hazard maps for Alaska: U.S. Geological Survey Open-File Report 2007-1043.

Worthington, L.L., H.J.A Van Avendonk, S.P.L Gulic, G.L. Christeson, and T.L. Pavlis (2012): Crustal structure of the Yakutat terrane and the evolution of subduction and collision in southern Alaska. J. Geophys. Res., 117: B01102 doi:10.1029/2011JB008493, 2012.

FIGURES

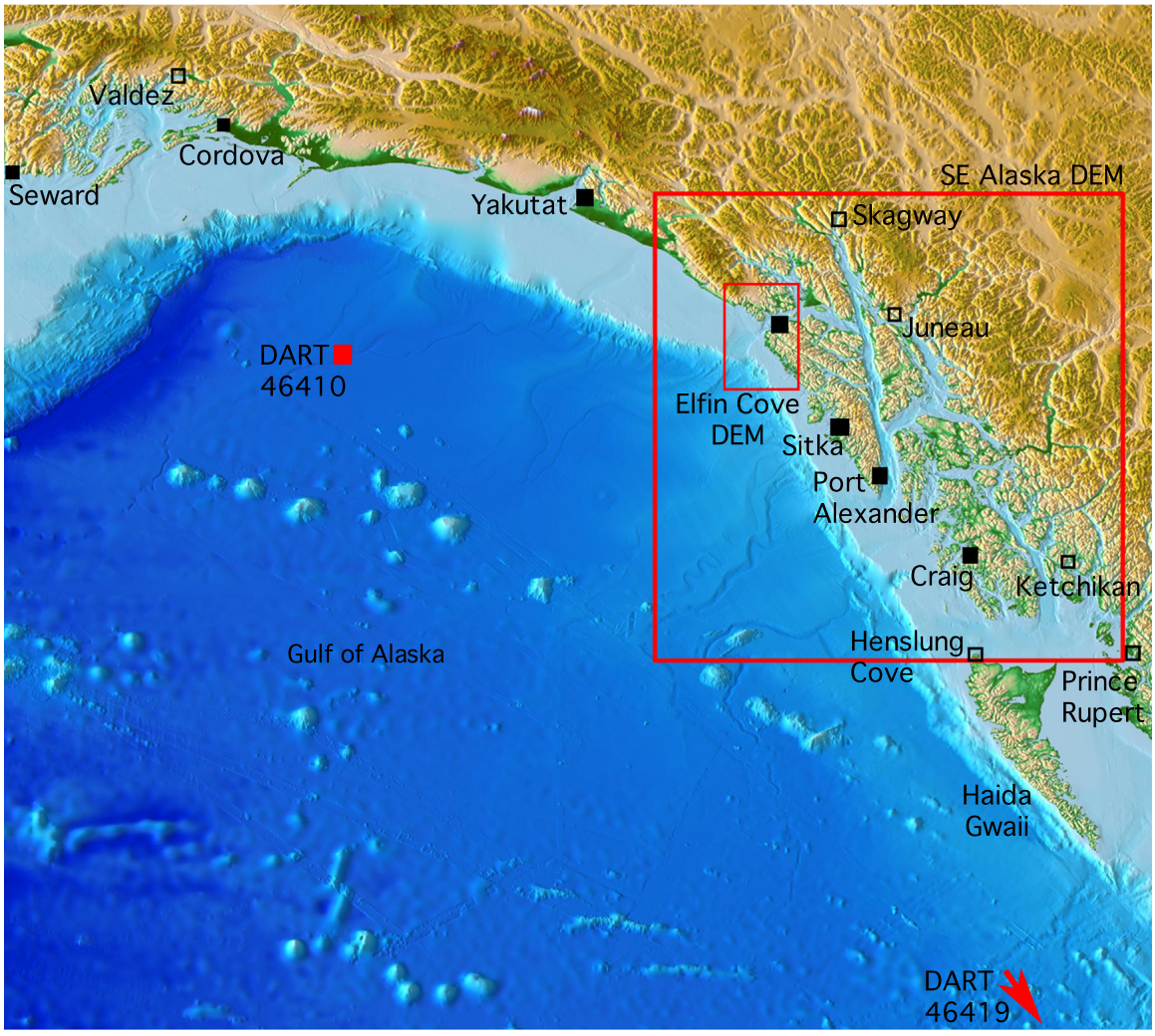

Figure 1. The northern Gulf of Alaska showing regional Digital Elevation Model (DEM) resources, tide gage, and DART® tsunami detection assets.

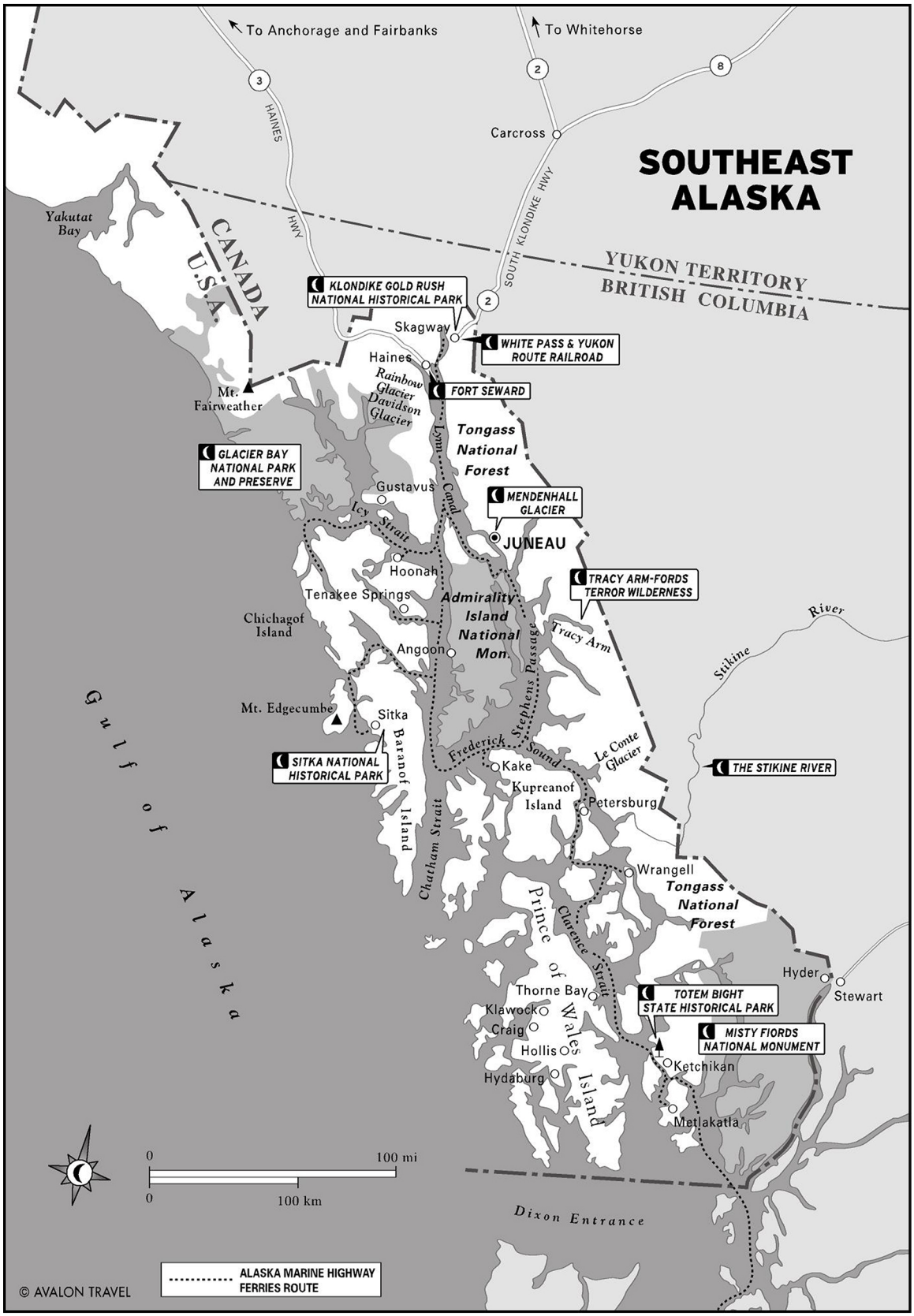

Figure 2. Southeast Alaska geographic features, communities, and the Alaska Marine Highway (reproduced with permission of the Alaska Department of Transportation and Public Facilities).

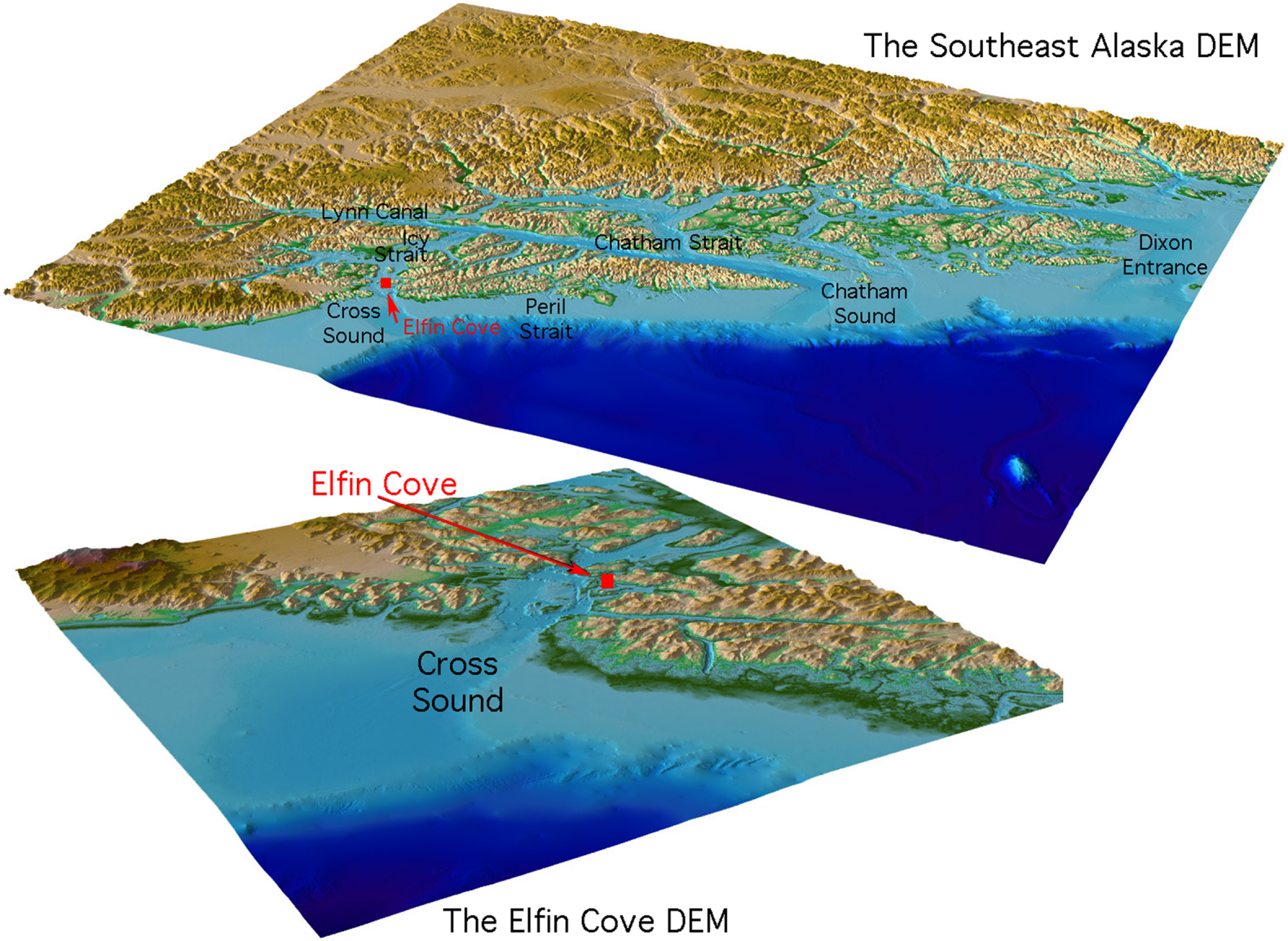

Figure 3. Oblique views of the Southeast Alaska and Elfin Cove Digital Elevation Models developed by the National Geophysical Data Center.

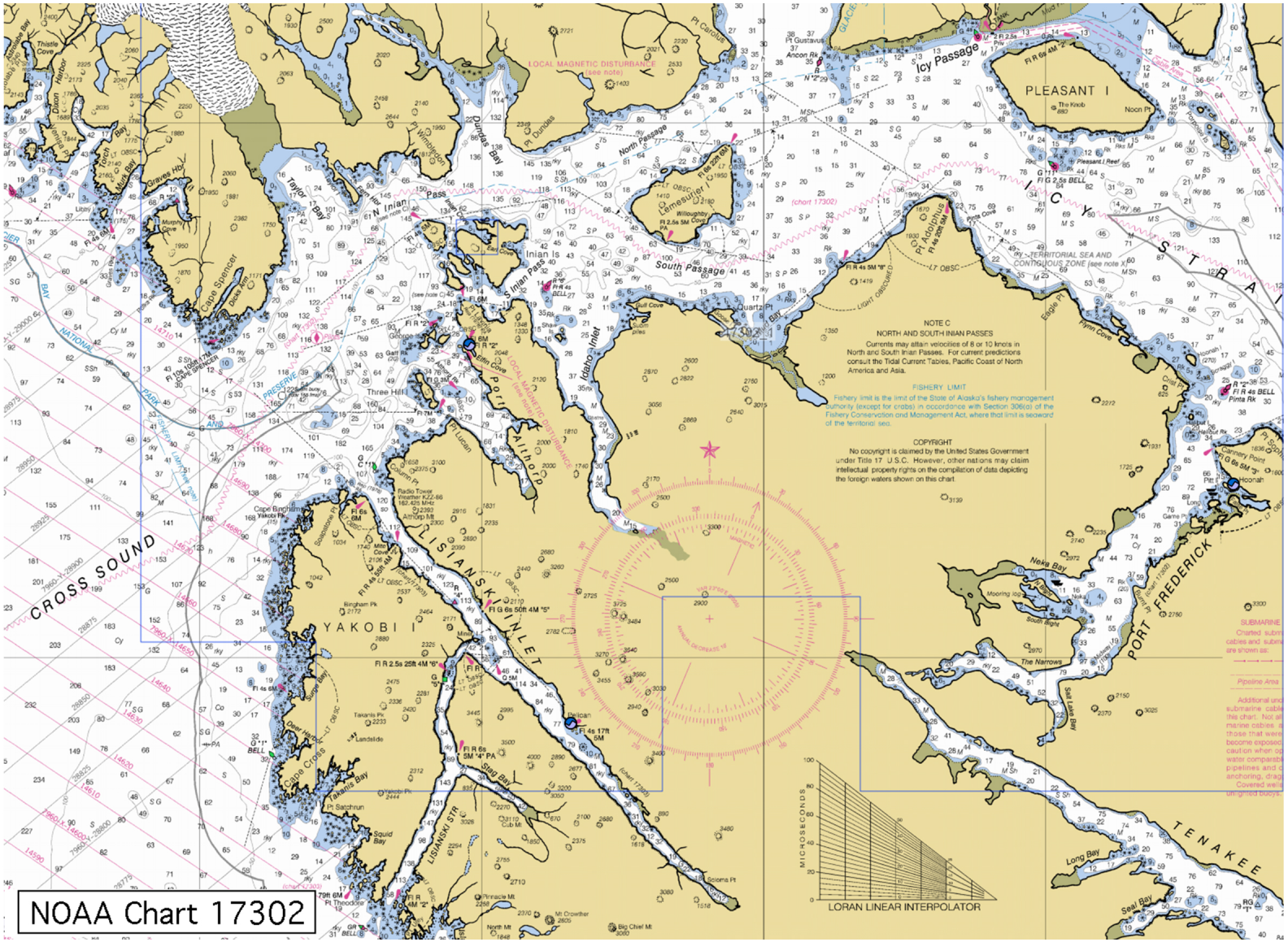

Figure 4. Extracts from NOAA Chart 17302 showing a) Cross Sound to Icy Strait.

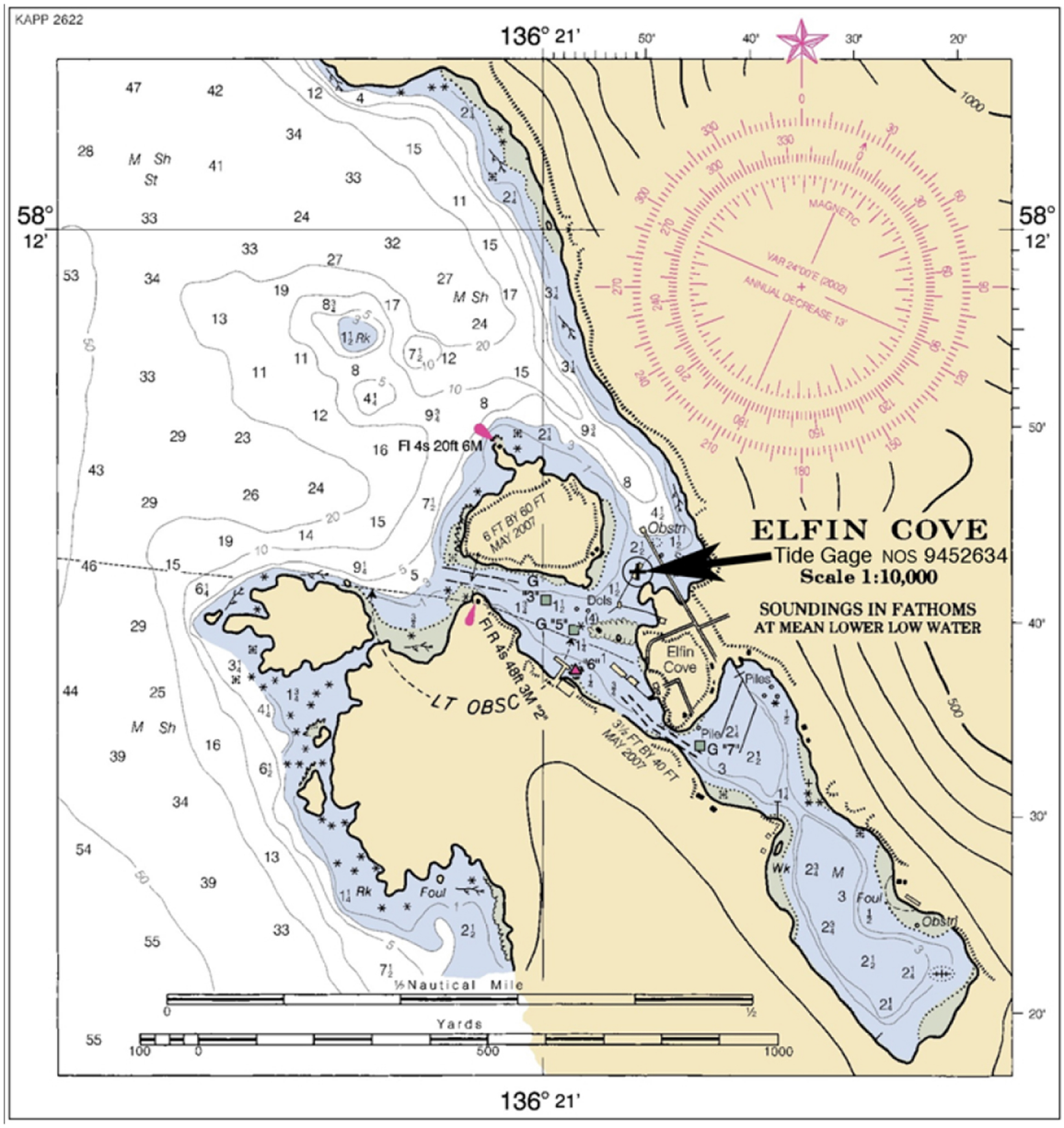

Figure 4 continued. Extract from NOAA Chart 17302
b) Elfin Cove sub-chart, annotated with the NOS tide gage location.

Figure 5. View south east into Elfin Cove's inner cove showing the boardwalks, finger docks (visible in Figure 4b) and other community facilities. (Photograph by Rick Sood http://roundezvous.com/Images/Alaska2006/ElfinCove.jpg)

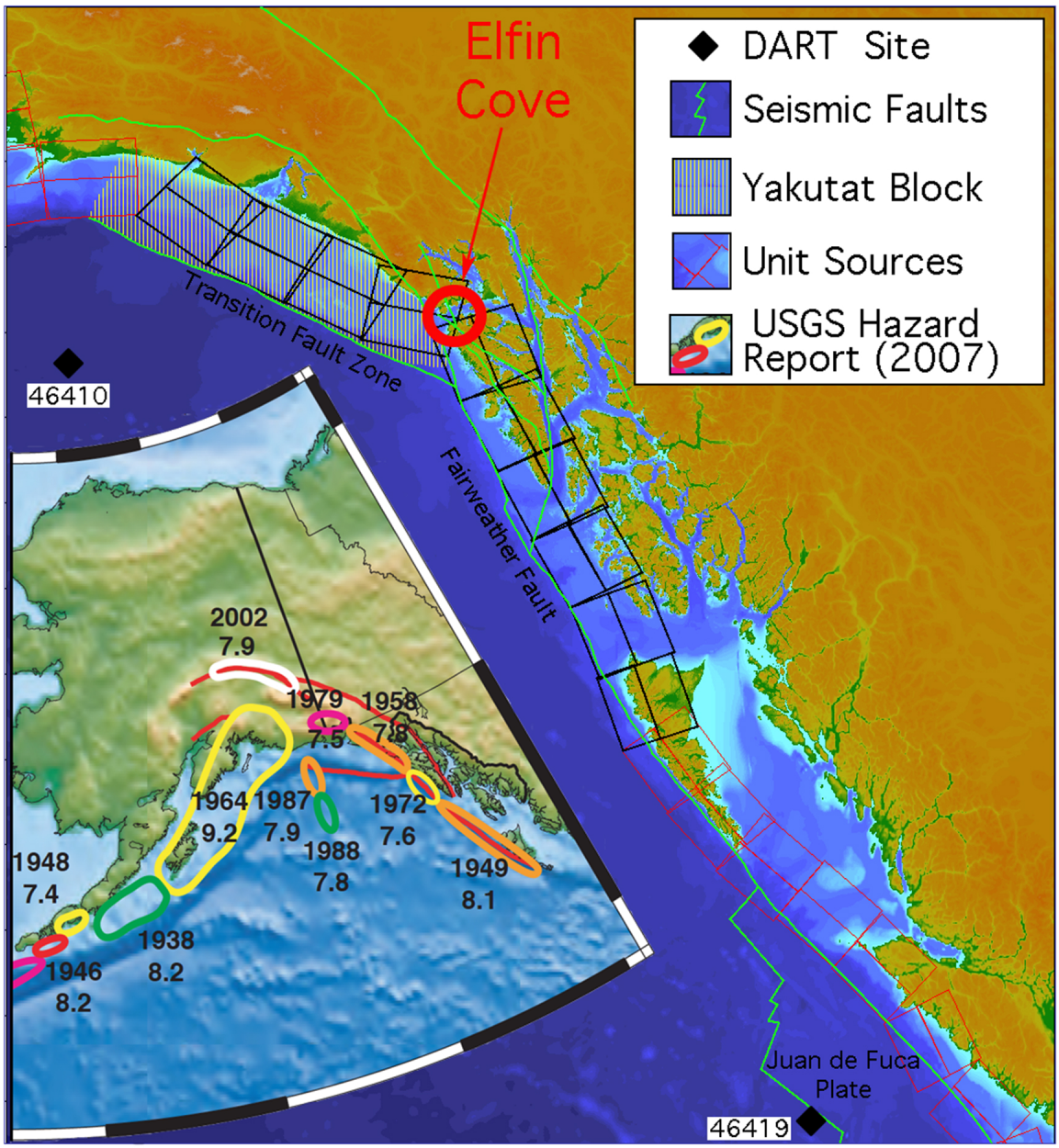

Figure 6. Regional seismic hazards and the unit sources employed to model their tsunamigenic potential. The inset panel is adapted from the USGS Seismic Hazard Maps for Alaska (Wesson et al., 2007).

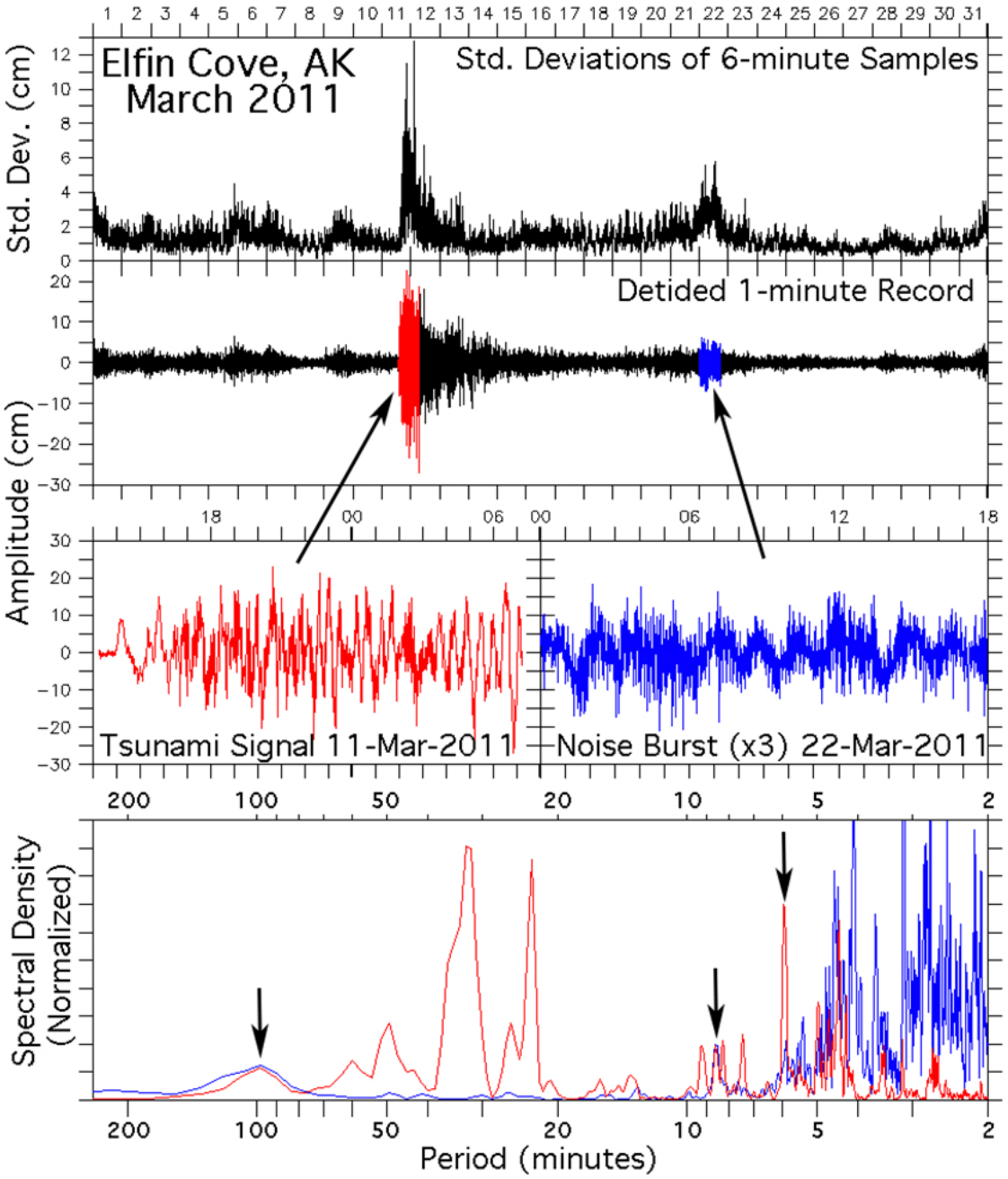

Figure 7. Elfin Cove tide gage data from March 2011 illustrating episodes of high frequency, non-tsunami related signals (blue) that can mask tsunami signals such as that associated with the Honshu-2011 event (red.) The upper panel is the standard deviation of the subsamples employed in computing the published 6-minute data record. The central panels show the 1-minute record, processed with a Kalman filter to eliminate the tidal signal. In the lower panel the spectrum (in energy-preserving form) of two highlighted one-day segments are contrasted.

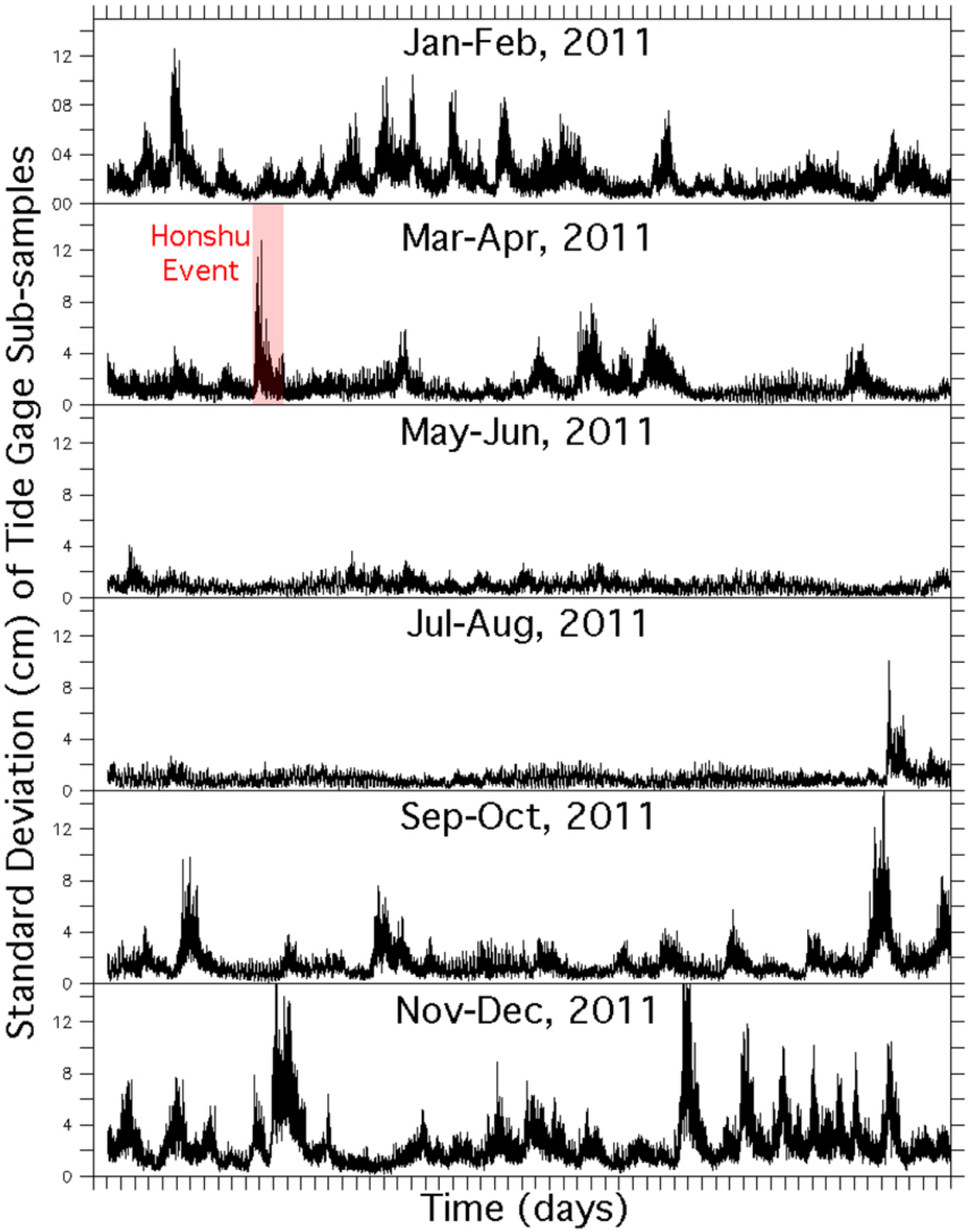

Figure 8. One year of the standard deviation measure of sub-sample noise that accompanies the 6-minute tide gage data from Elfin Cove (in two month strips with a common vertical scale.) Only one tsunami event (highlighted) of significance occurred during the year but noise "bursts" associated with winds and waves are common, particularly during winter months.

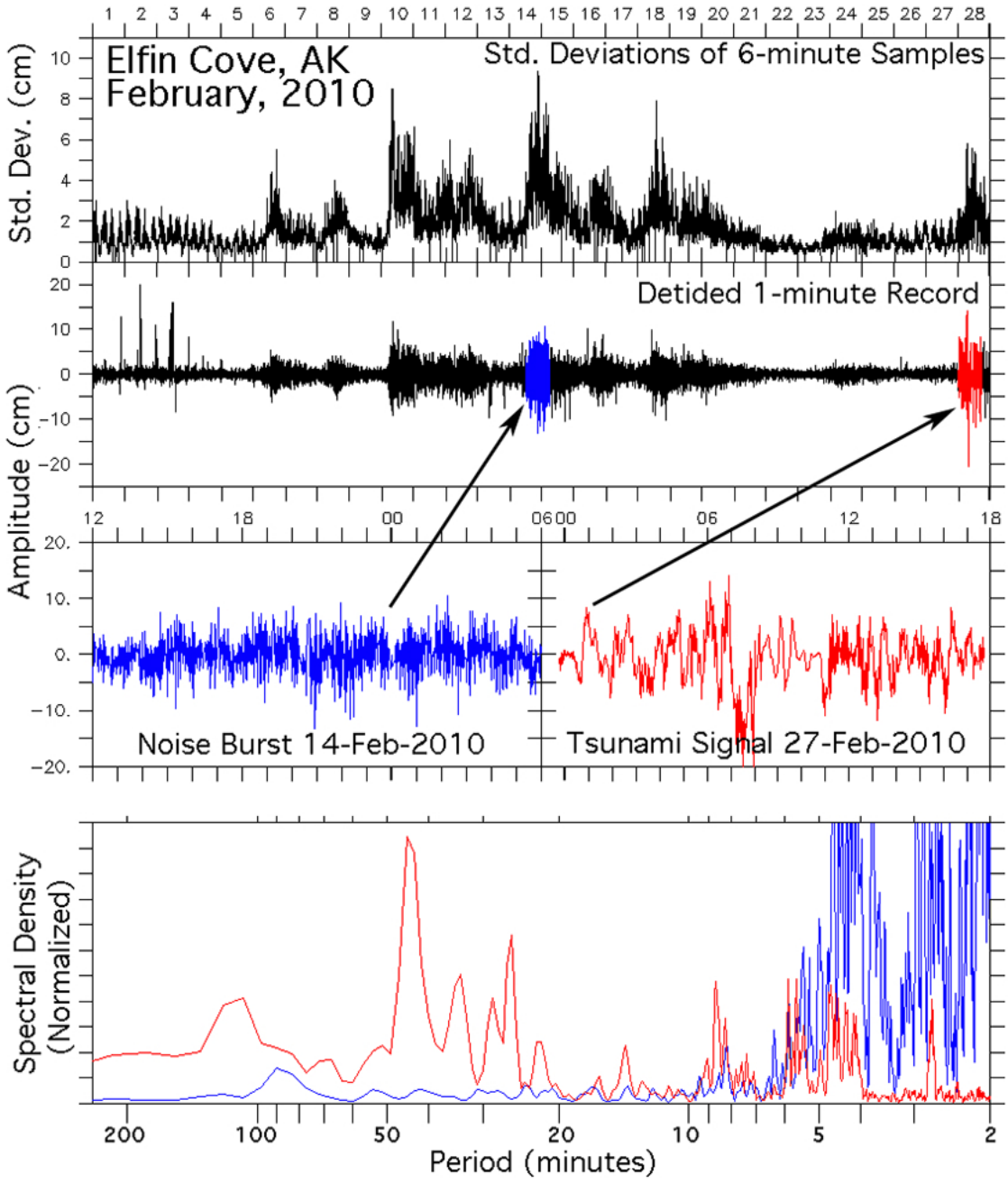

Figure 9. As in Figure 7, but for the Chile tsunami event of February 2010, whose impact in the Gulf of Alaska was comparable to that of Honshu-2011.

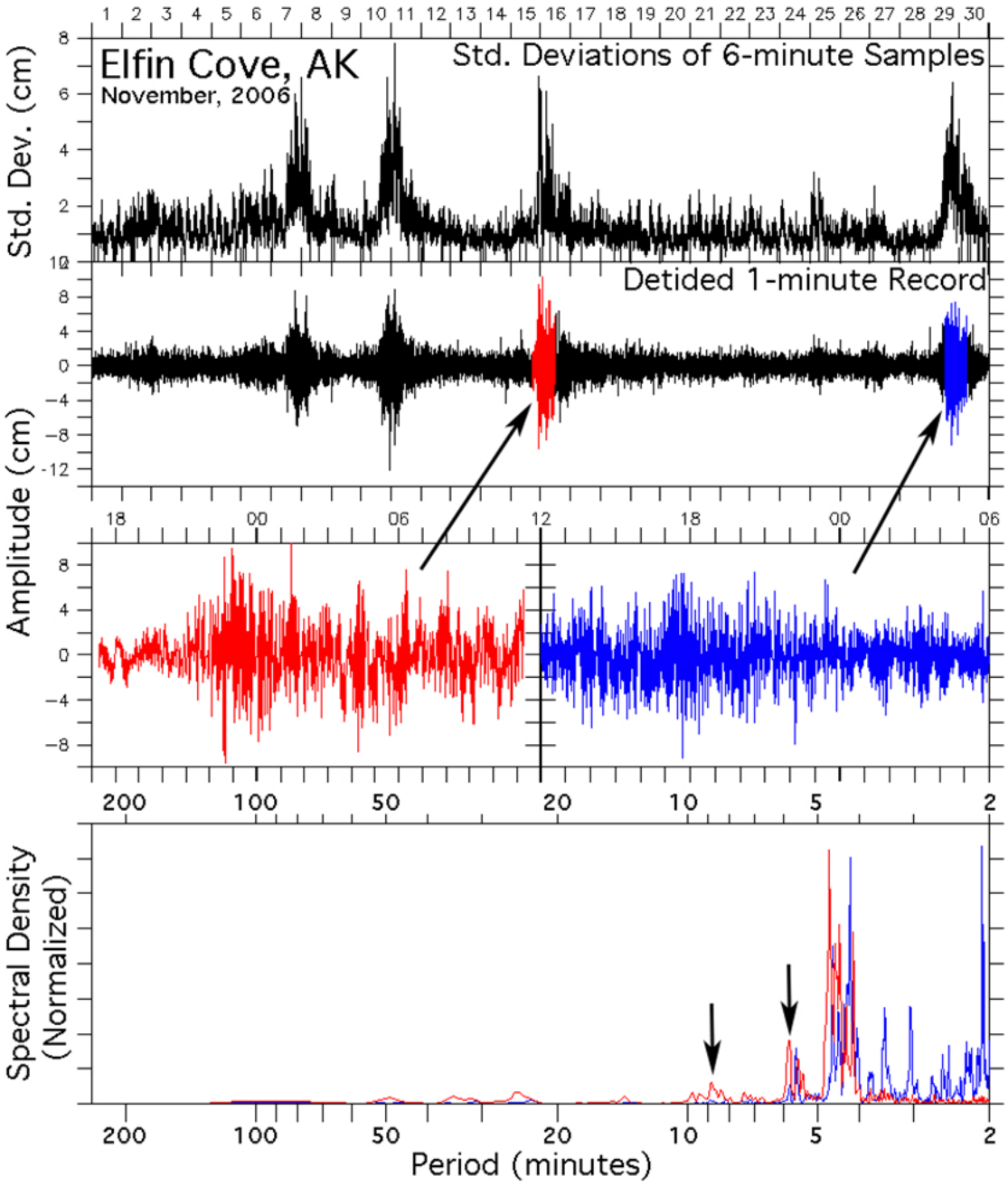

Figure 10. As in Figures 7 and 9, but illustrating the poor signal to noise ratio during the Kuril tsunami event of November 2006. A standard for validation of other Pacific basin forecast models, this event is of limited use for Elfin Cove, AK.

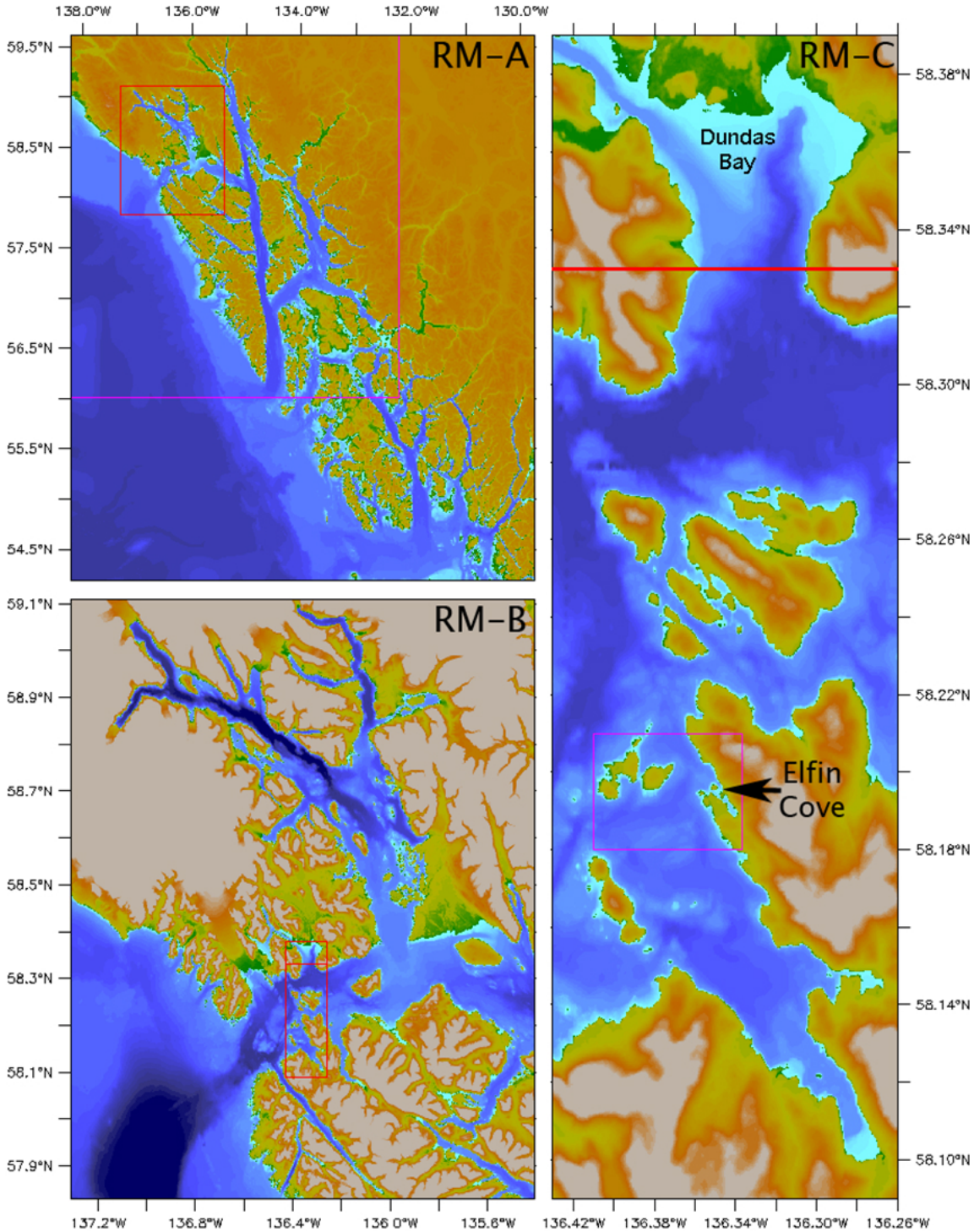

Figure 11. Nested grid representation employed in the Reference (RM) version of the Elfin Cove tsunami model, progressing counterclockwise from the coarsest resolution A-grid in the upper left, through the extensive, medium resolution B-grid which includes all of Glacier Bay, to the finely resolved C-grid that includes the Inian Passes (see Figure 4a.) Red rectangles are used to indicate the inner RM grids; magenta ones indicate the grids of the Forecast Model (FM.) See main text for a discussion of the upper section of Dundas Bay, excluded in the final version of the Reference Model C-grid.

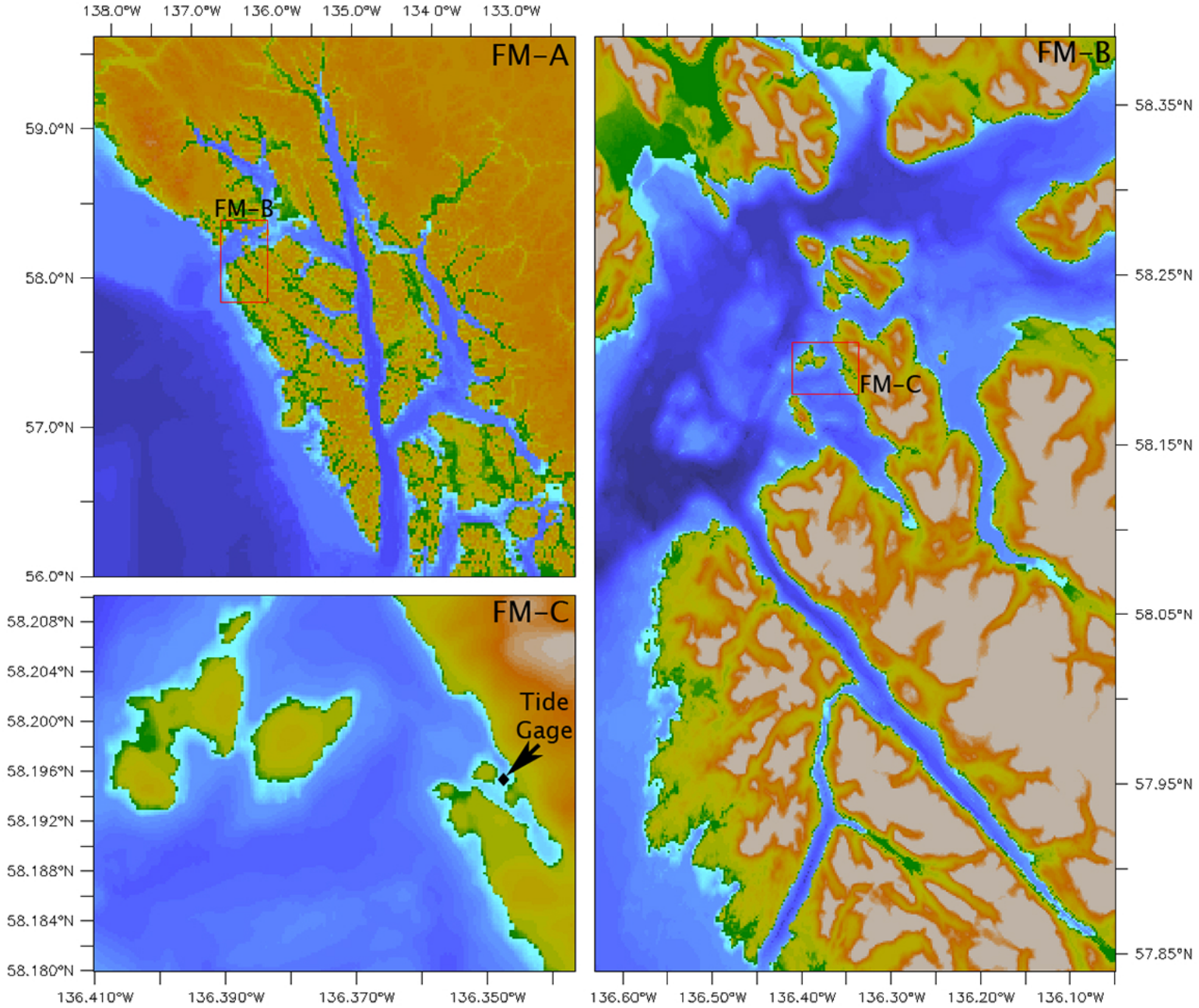

Figure 12. Nested grids of the Forecast (FM) version of the Elfin Cove tsunami model. The progression is clockwise with the innermost C-grid, which is much reduced in extent, appearing in the lower left panel. The Inian Passes are best represented in the B-grid, while Glacier Bay appears only coarsely in the A-grid.

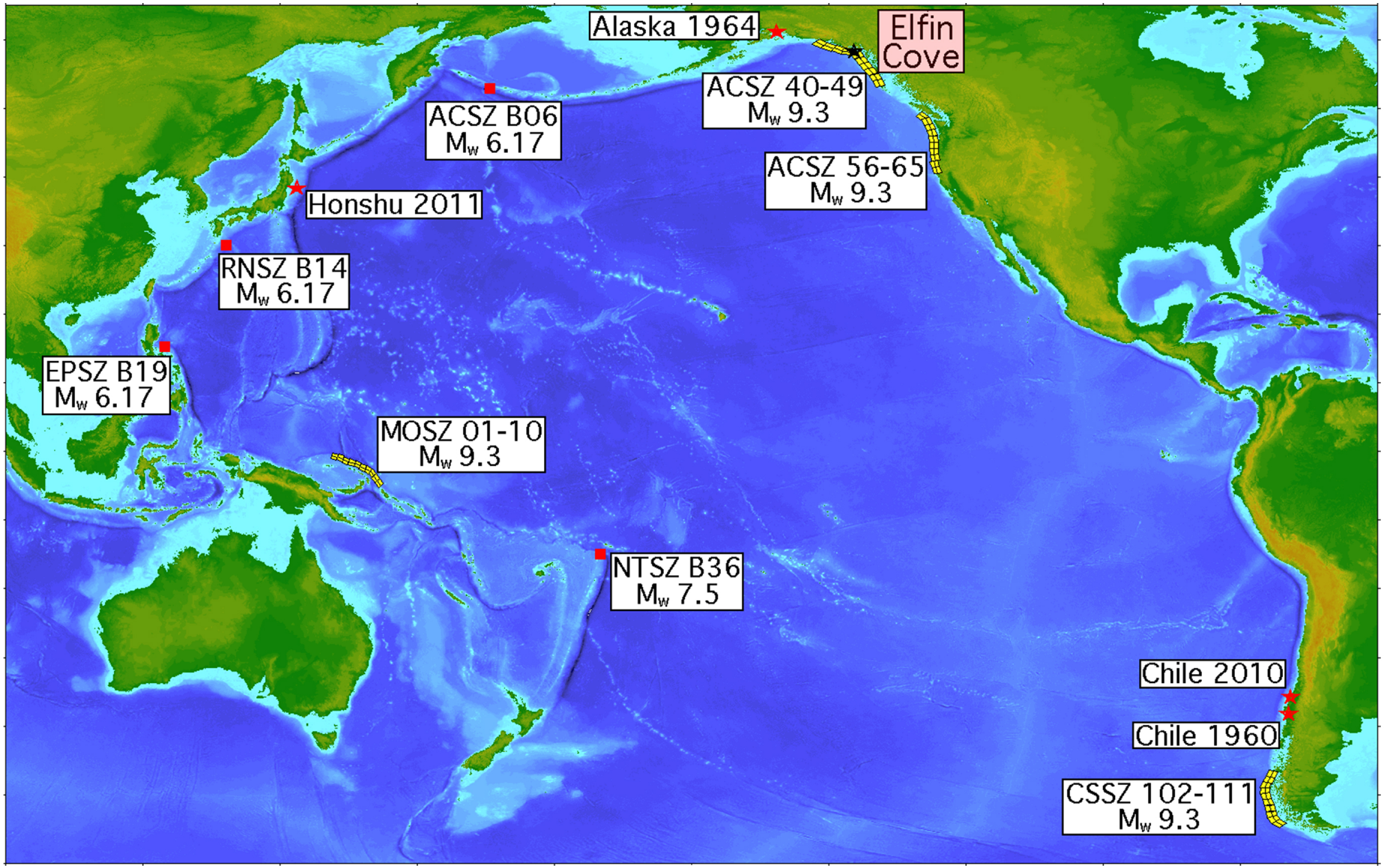

Figure 13. Synthetic and historic event scenarios employed in inter-comparison of the Reference and Forecast versions of Elfin Cove tsunami model. Evenly-distributed slip values, are applied in ten adjacent unit sources (yellow rectangles) of the propagation database to represent mega-tsunami events; single unit sources are used for the other synthetic events. For the historic cases, a linear combination of unit sources is employed as detailed in Table 6.

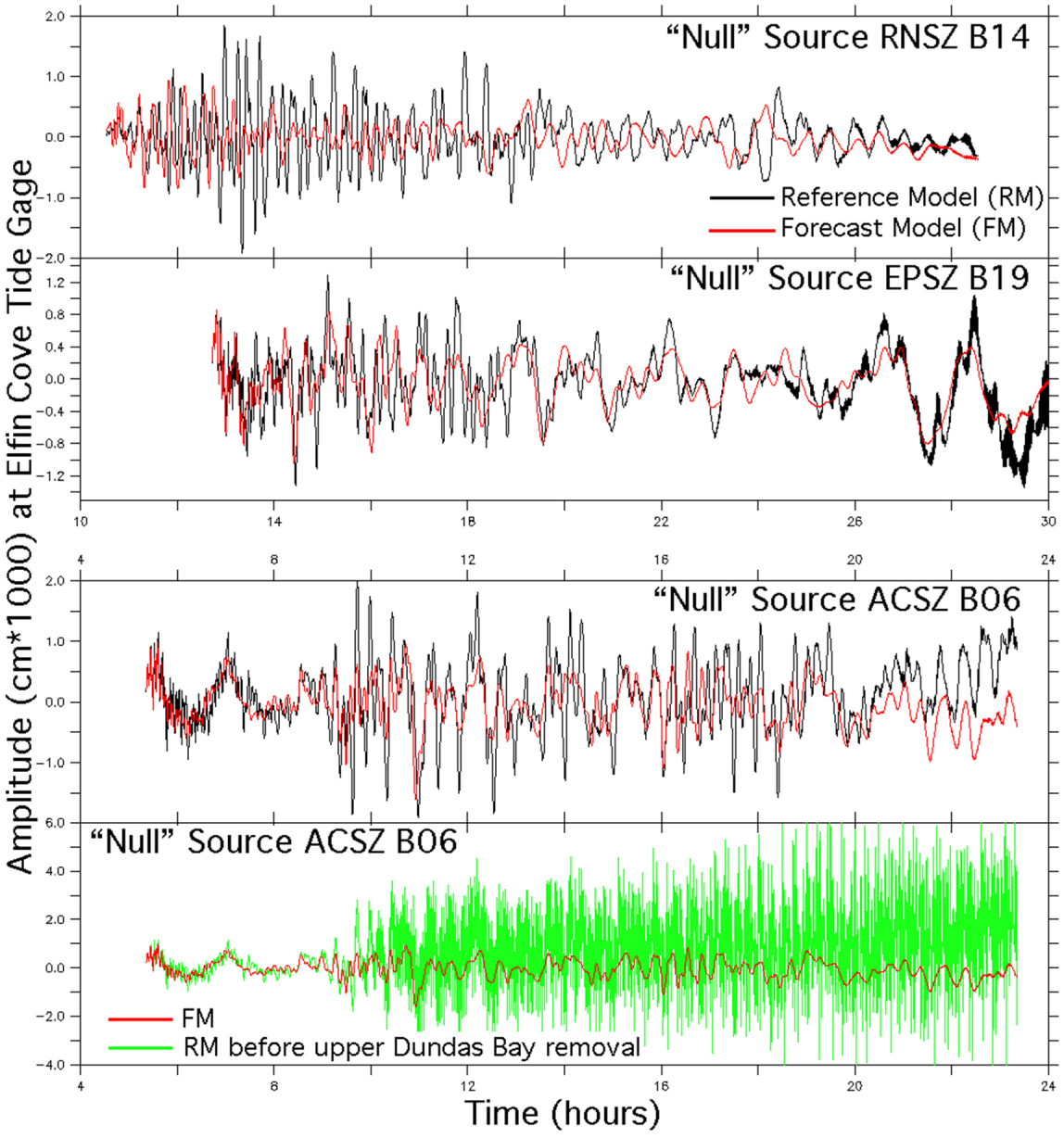

Figure 14. Comparison of Reference (RM) and Forecast Model (RM) predictions for the Elfin Cove tide gage site for three "null" (very low magnitude) sources. Such runs highlight low level model instabilities that might be missed in modeling larger events. The lower panel shows the Reference Model at an early stage of development; instabilities emanating from upper Dundas Bay (see Figure 11) proved difficult to eliminate while employing reasonable time and space steps. These instabilities are essentially eliminated in the final C-grid.

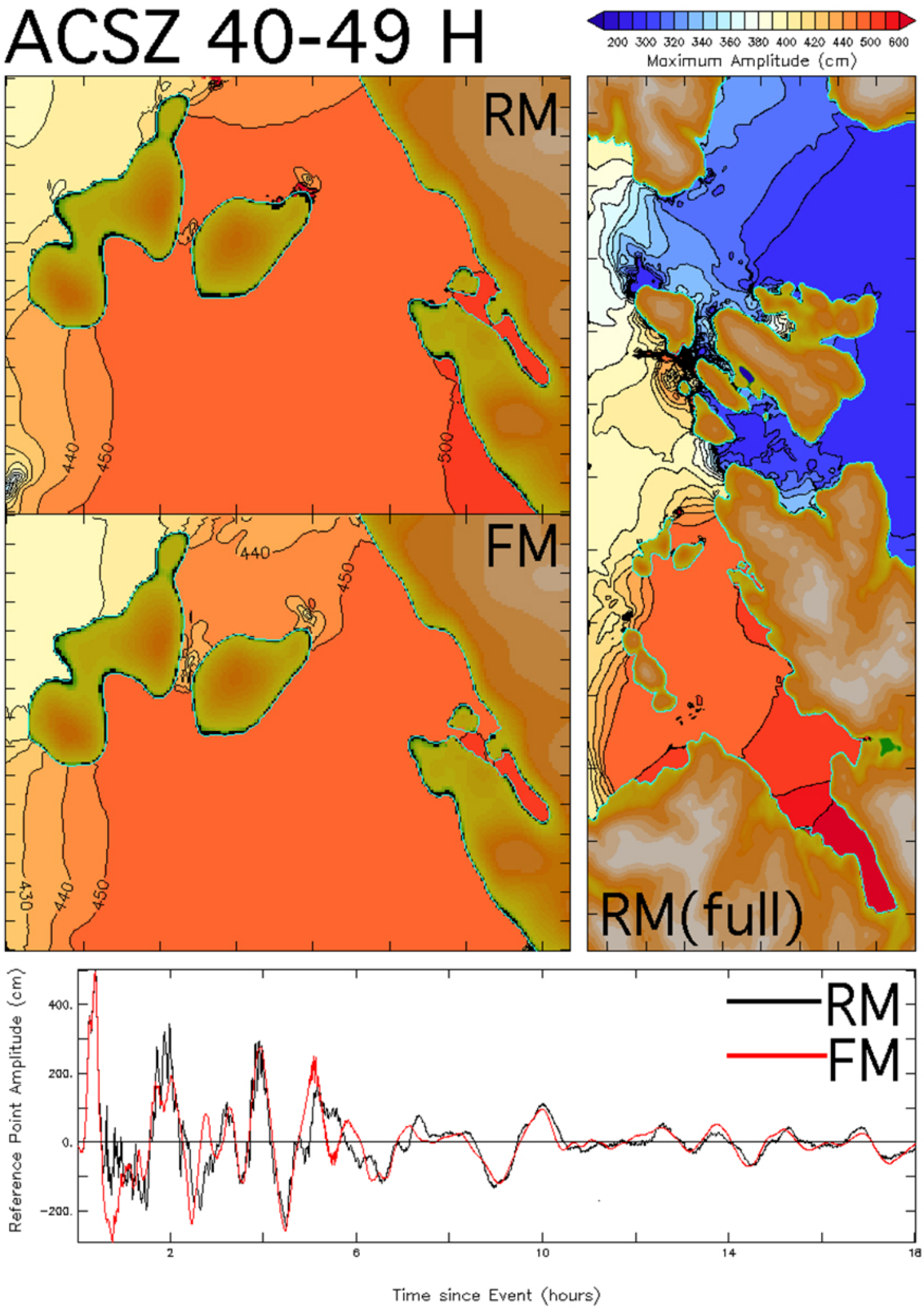

Figure 15. Comparison of Reference (RM) and Forecast (RM) results for the ACSZ 40-49 mega-tsunami scenario, which is local to Elfin Cove. The left hand panels are for the C-grid domain of the Forecast Model; the right hand panel shows the entirety of the Reference Model C-grid. The lower panel contrasts the Reference (black) and Forecast (red) versions of the time series at the Elfin Cove tide gage. a) distribution of maximum amplitude during the 18-hour simulation

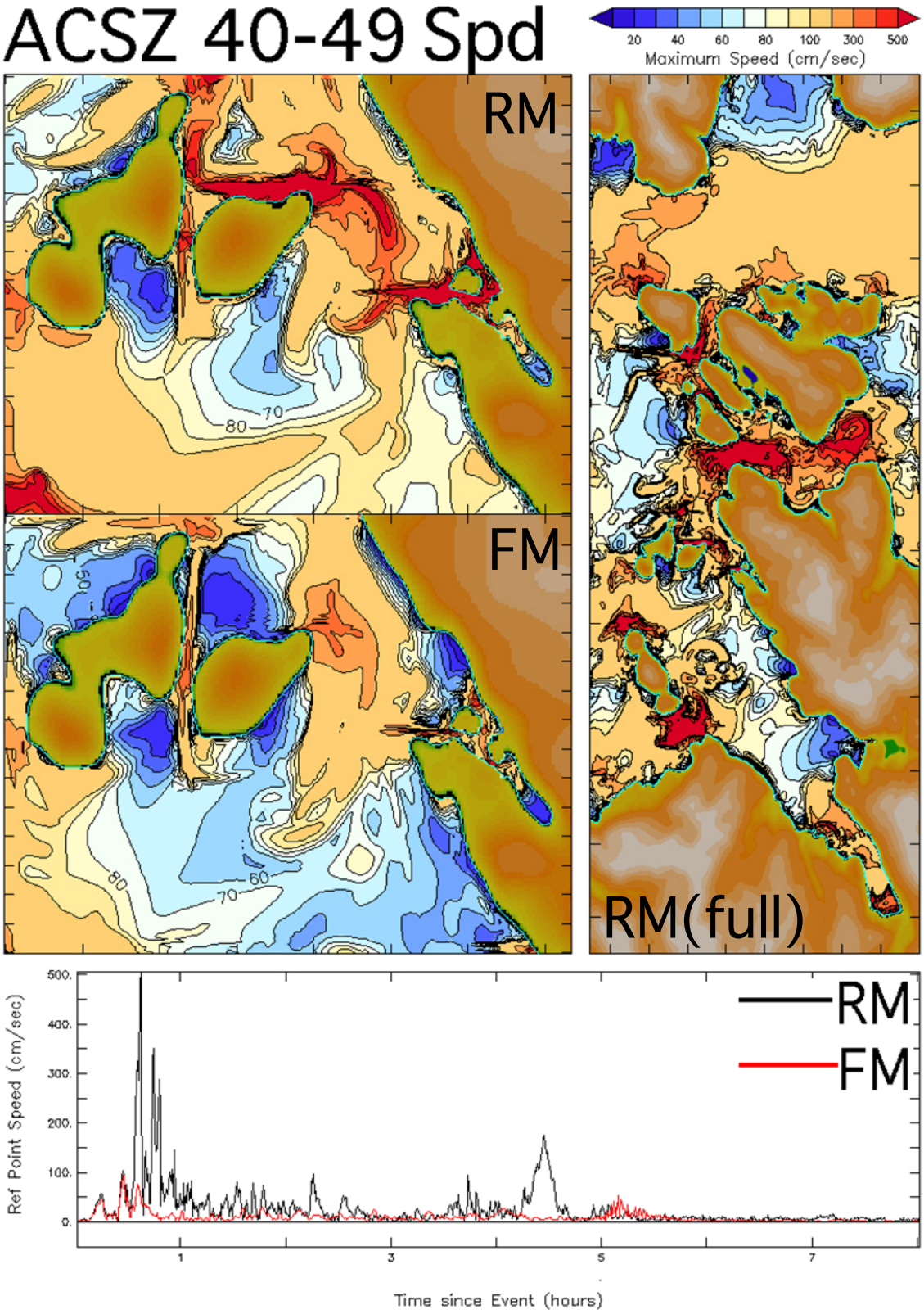

Figure 15 continued. b) distribution of maximum speed.

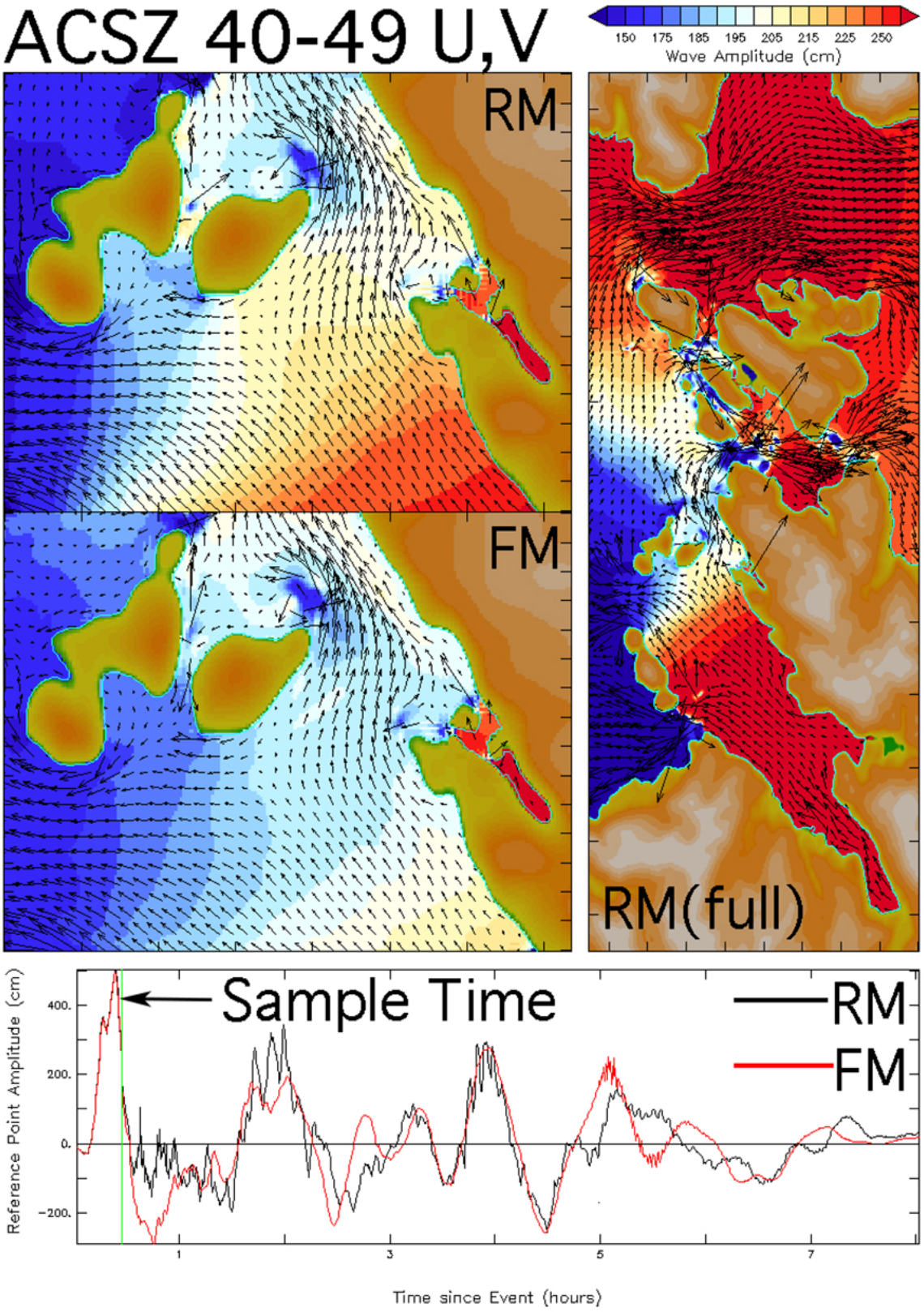

Figure 15 continued. c) a snapshot of the current field at the time indicated by the green line in the lower panel.

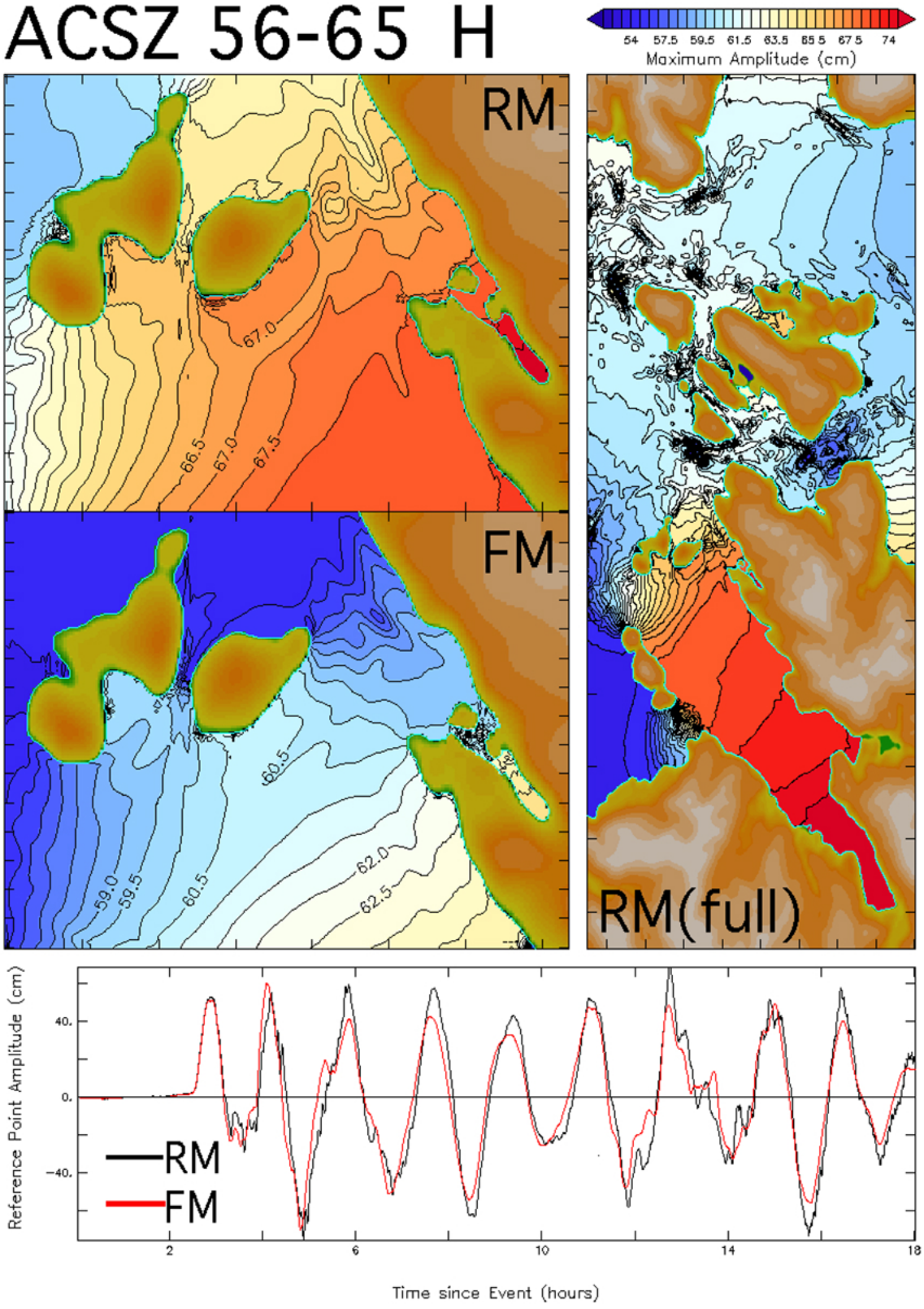

Figure 16. As in Figure 15, but for a synthetic mega-tsunami source, ACSZ 56-65, representative of the Cascadia Subduction Zone.
a) distribution of maximum amplitude during the 18-hour simulation.

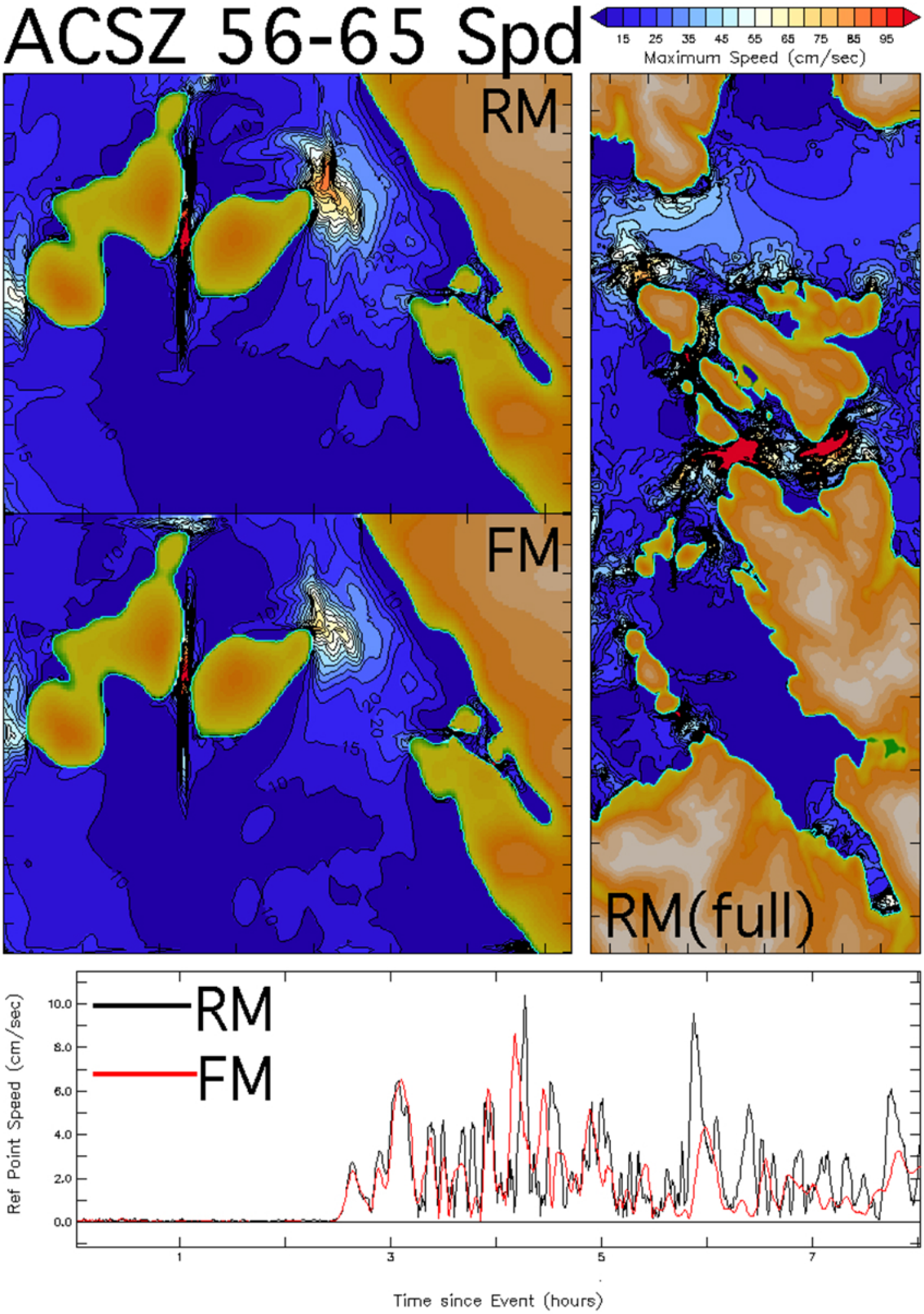

Figure 16 continued. As in Figure 15, but for a synthetic mega-tsunami source, ACSZ 56-65, representative of the Cascadia Subduction Zone. b) distribution of maximum speed.

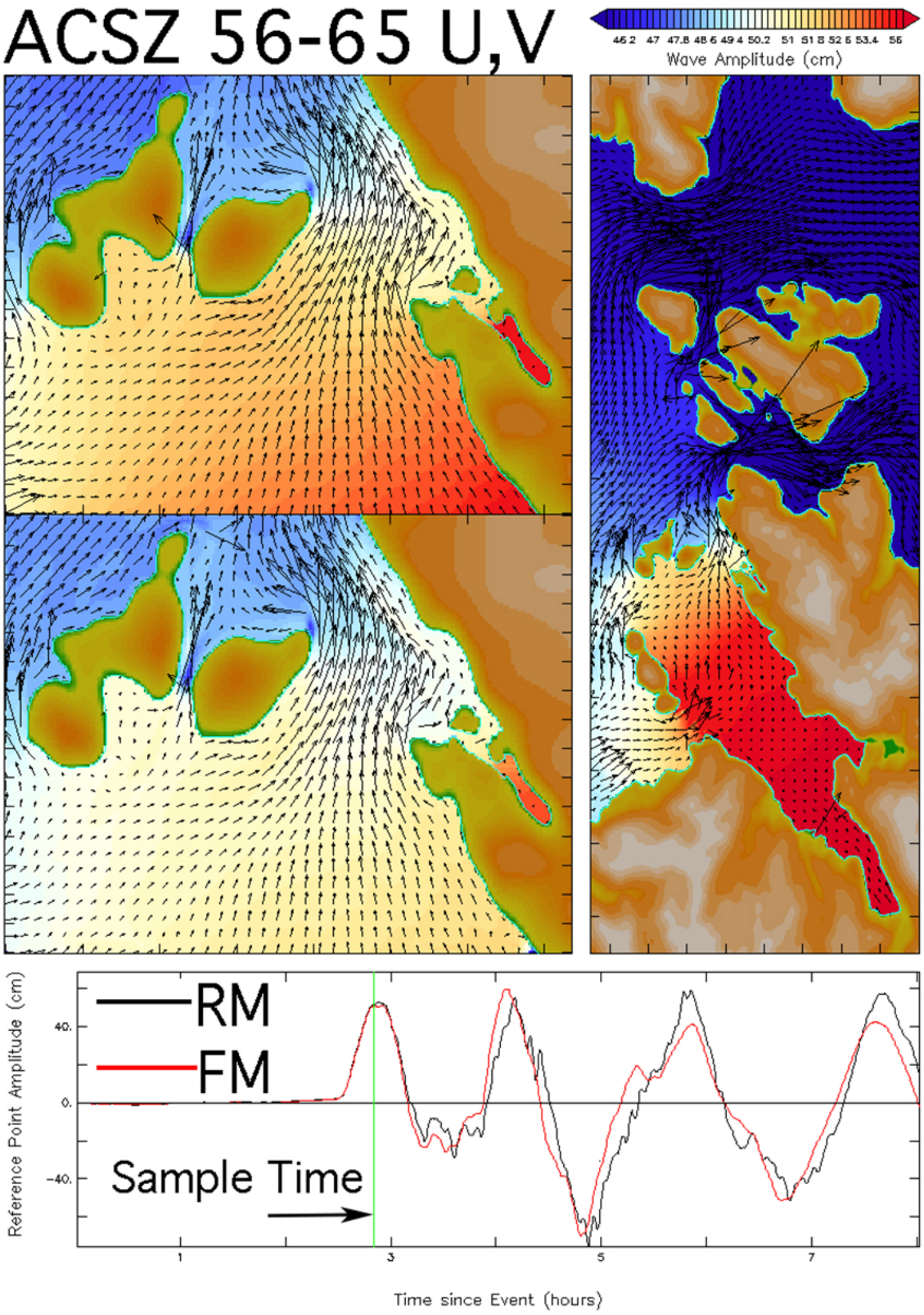

Figure 16 continued. As in Figure 15, but for a synthetic mega-tsunami source, ACSZ 56-65, representative of the Cascadia Subduction Zone.
c) a snapshot of the current field at the time indicated by the green line in the lower panel.

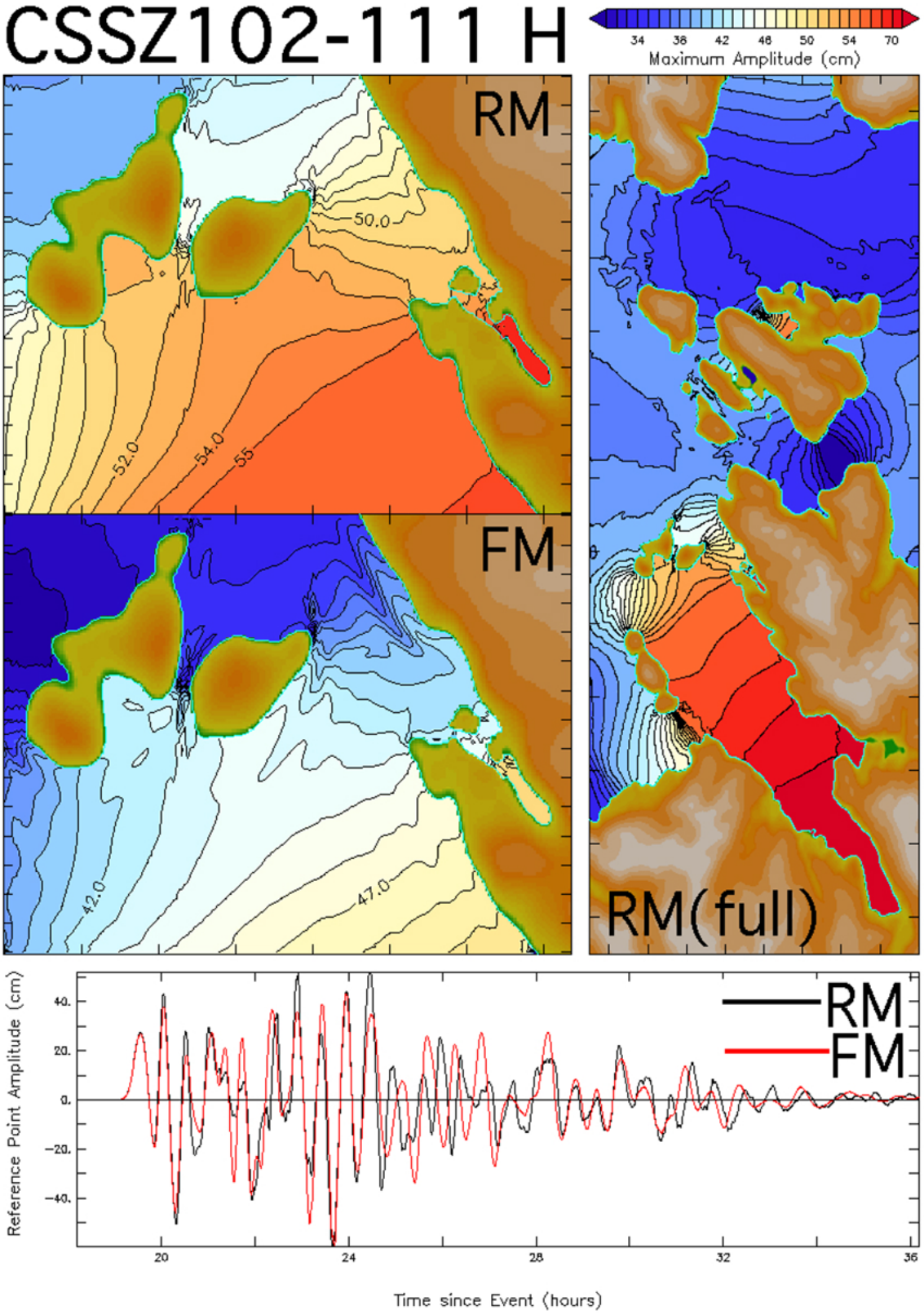

Figure 17. As in Figure 15, but for a synthetic mega-tsunami source, CSSZ 102-111, located in southern Chile.
a) distribution of maximum amplitude during the 18-hour simulation.

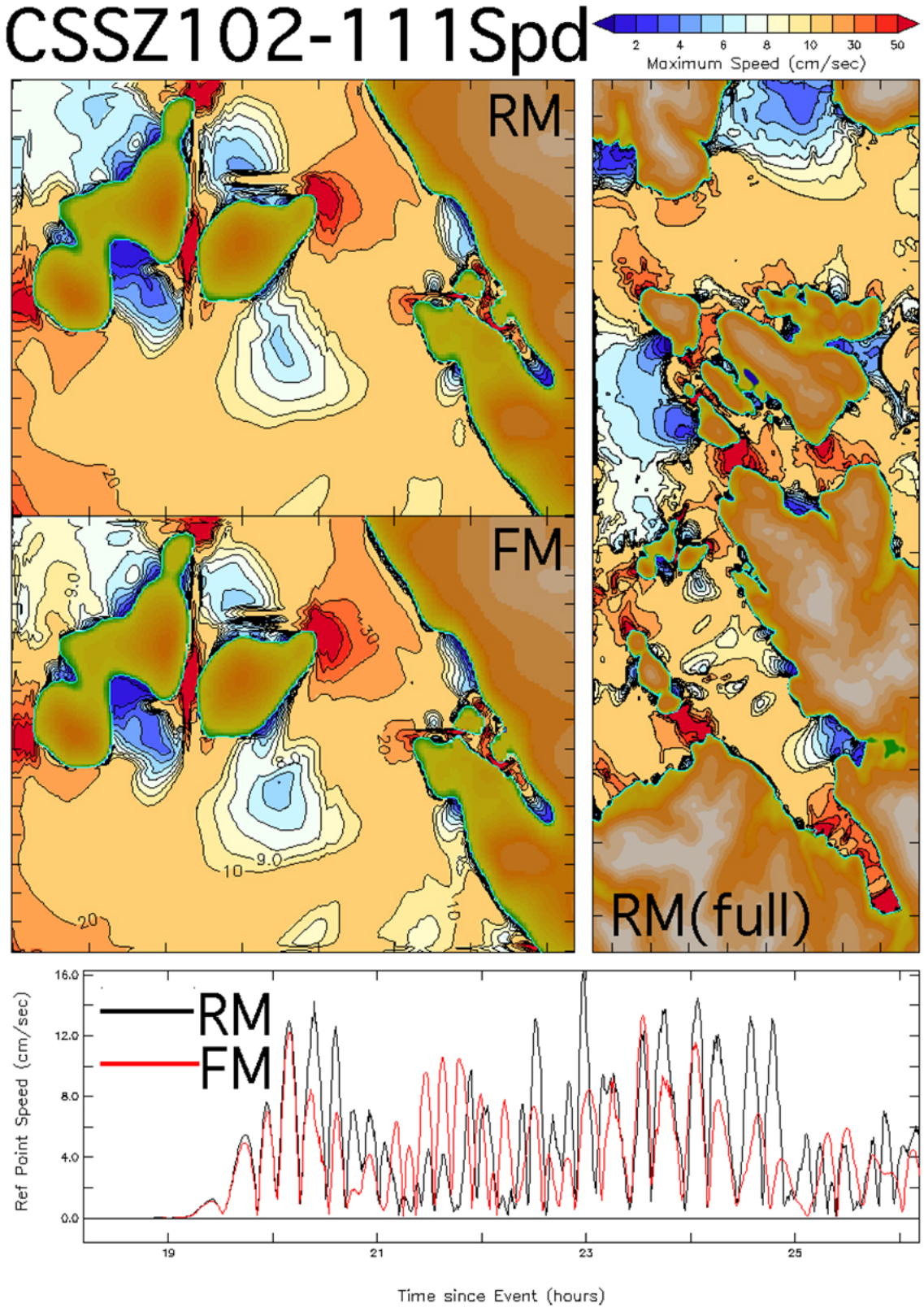

Figure 17 continued. As in Figure 15, but for a synthetic mega-tsunami source, CSSZ 102-111, located in southern Chile.
b) distribution of maximum speed.

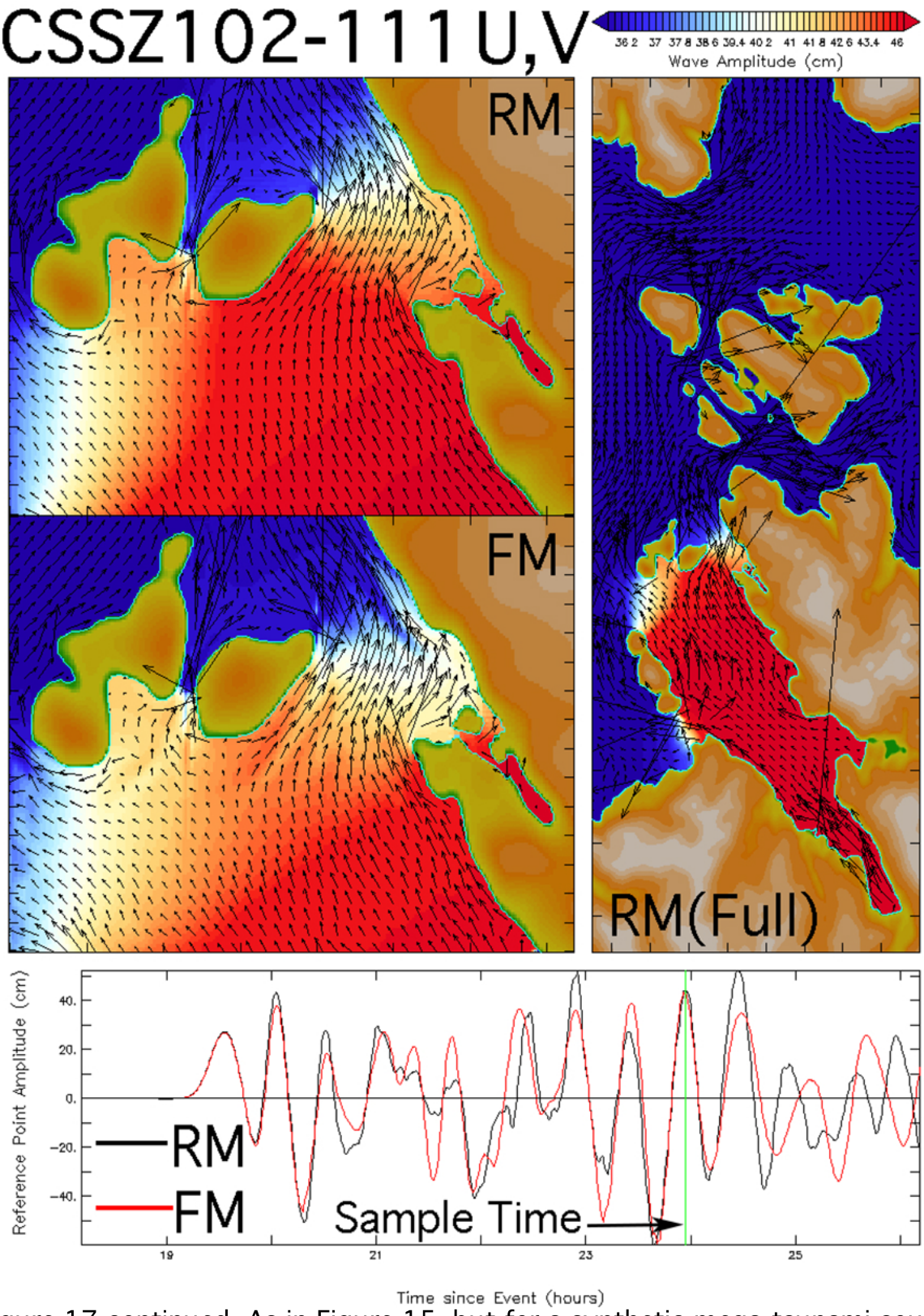

Figure 17 continued. As in Figure 15, but for a synthetic mega-tsunami source, CSSZ 102-111, located in southern Chile.
c) a snapshot of the current field at the time indicated by the green line in the lower panel.

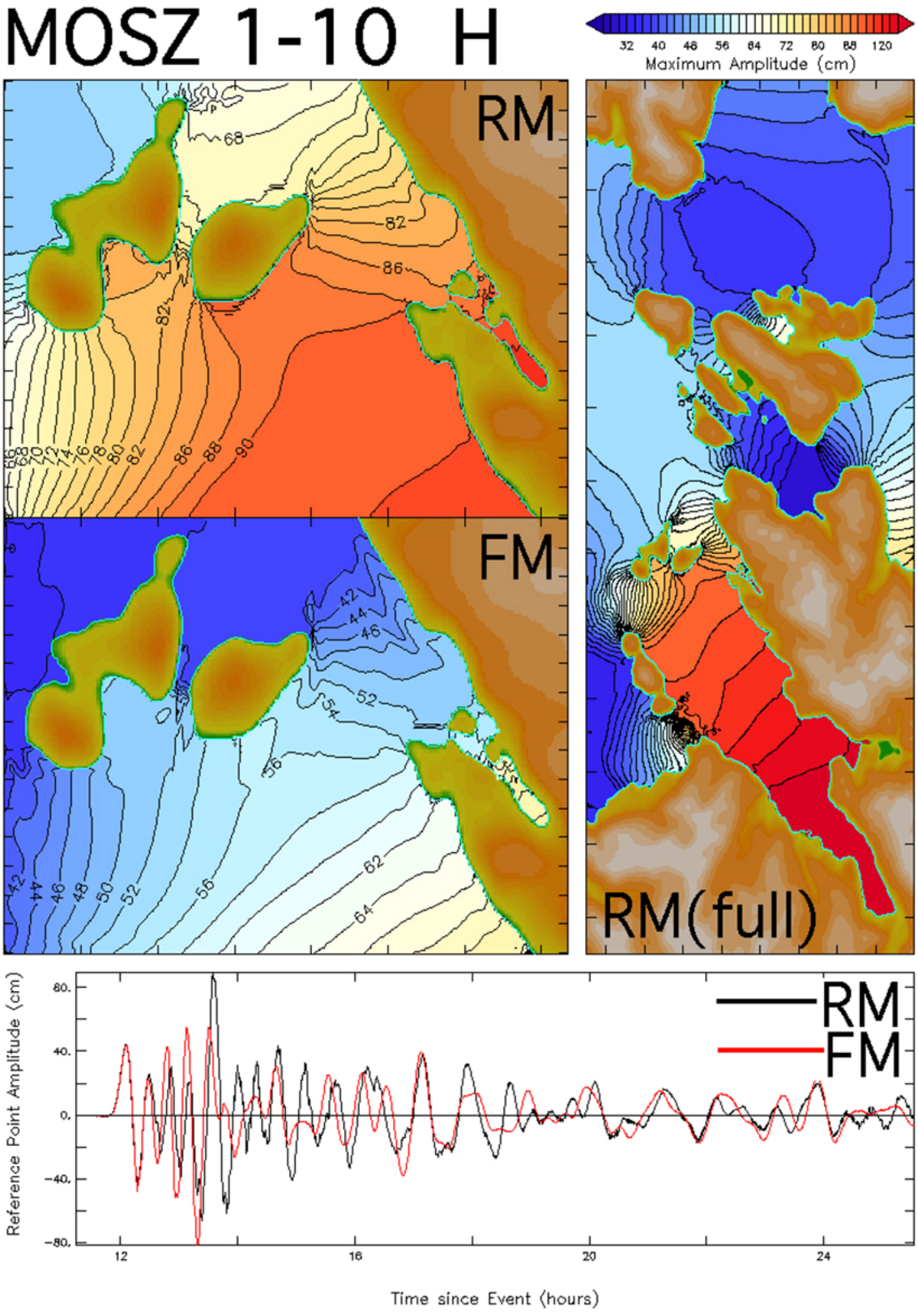

Figure 18. As in Figure 15, but for a synthetic mega-tsunami source, MOSZ 1-10, located in the western Pacific.
a) distribution of maximum amplitude during the 18-hour simulation.

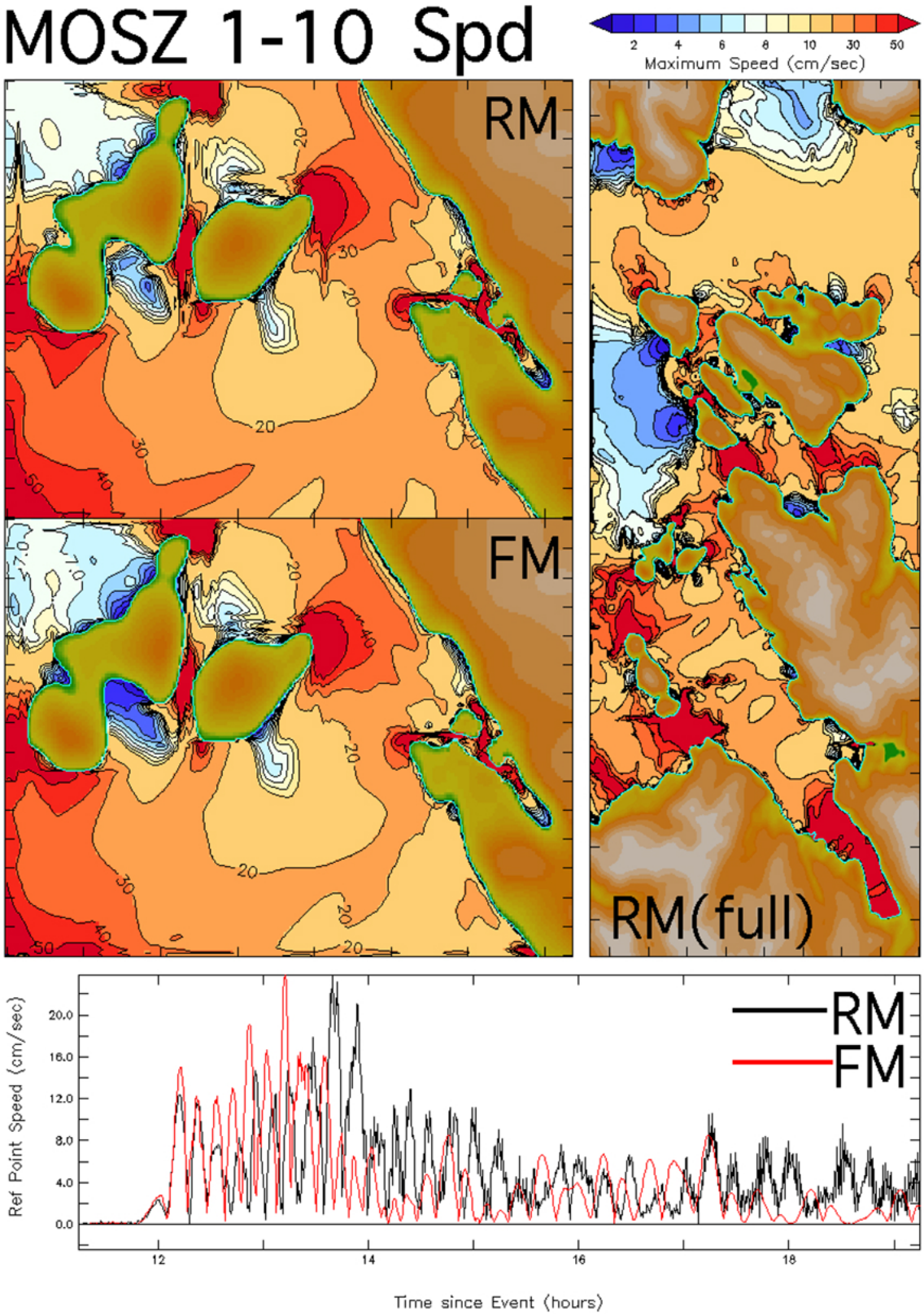

Figure 18 continued. As in Figure 15, but for a synthetic mega-tsunami source, MOSZ 1-10, located in the western Pacific.
b) distribution of maximum speed.

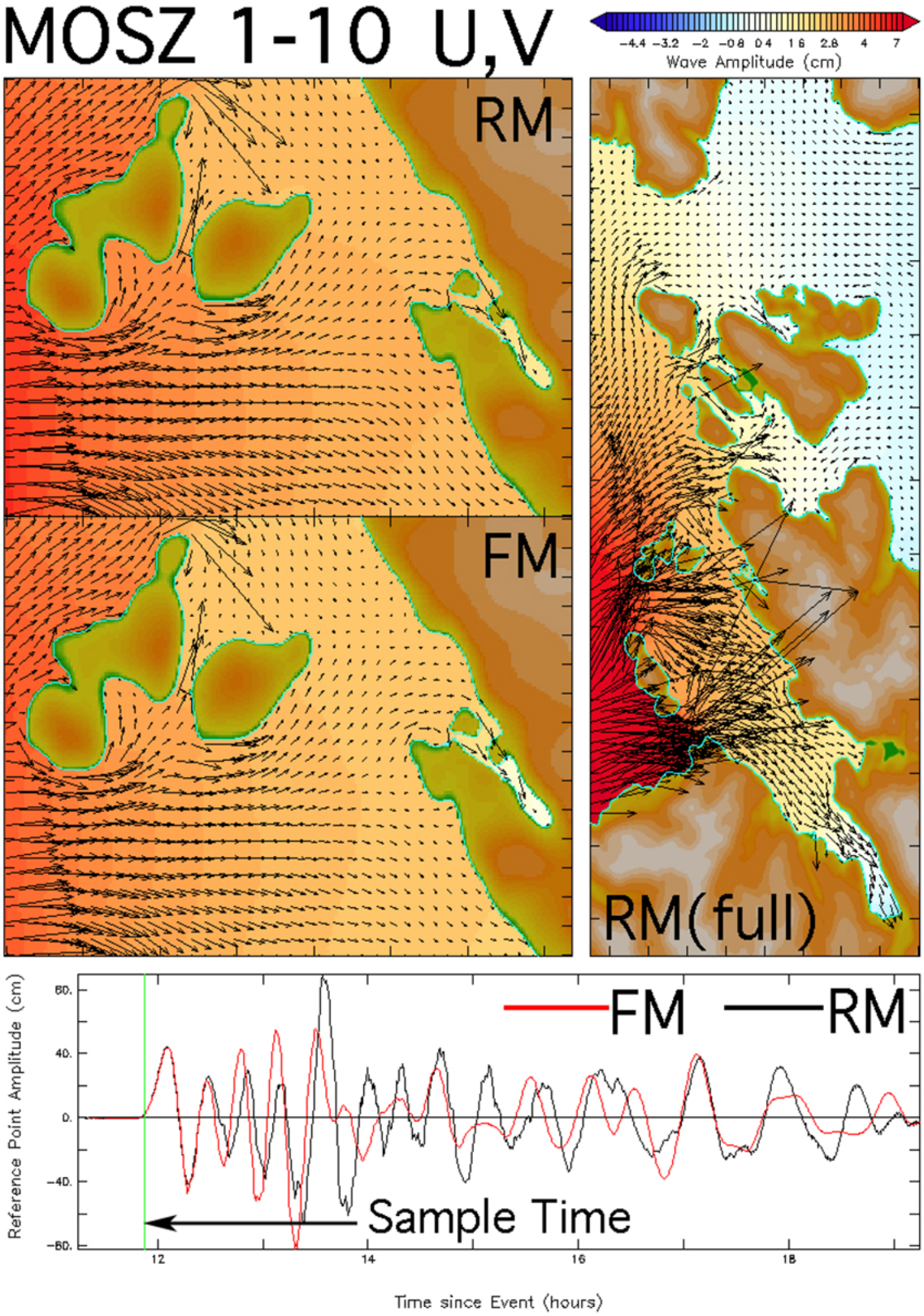

Figure 18 continued. As in Figure 15, but for a synthetic mega-tsunami source, MOSZ 1-10, located in the western Pacific.
c) a snapshot of the current field at the time indicated by the green line in the lower panel

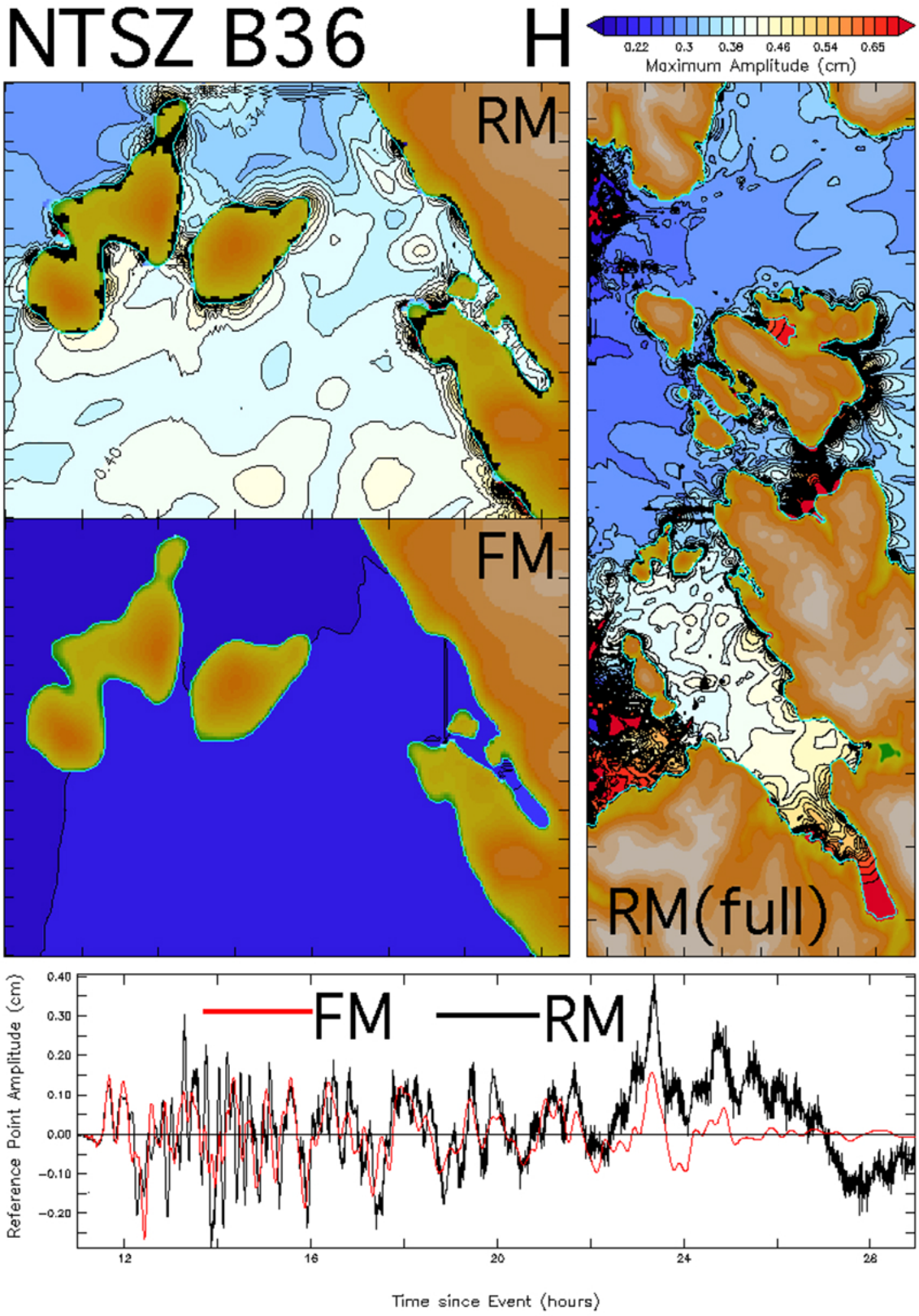

Figure 19. Comparison of Reference (RM) and Forecast Model (FM) solutions for a mild synthetic tsunami near Samoa (the single unit source NTSZ B36.) Though tracking well for 22 hours of the simulation, the time series at the tide gage diverge later and degrade the comparison of the maximum amplitude field.

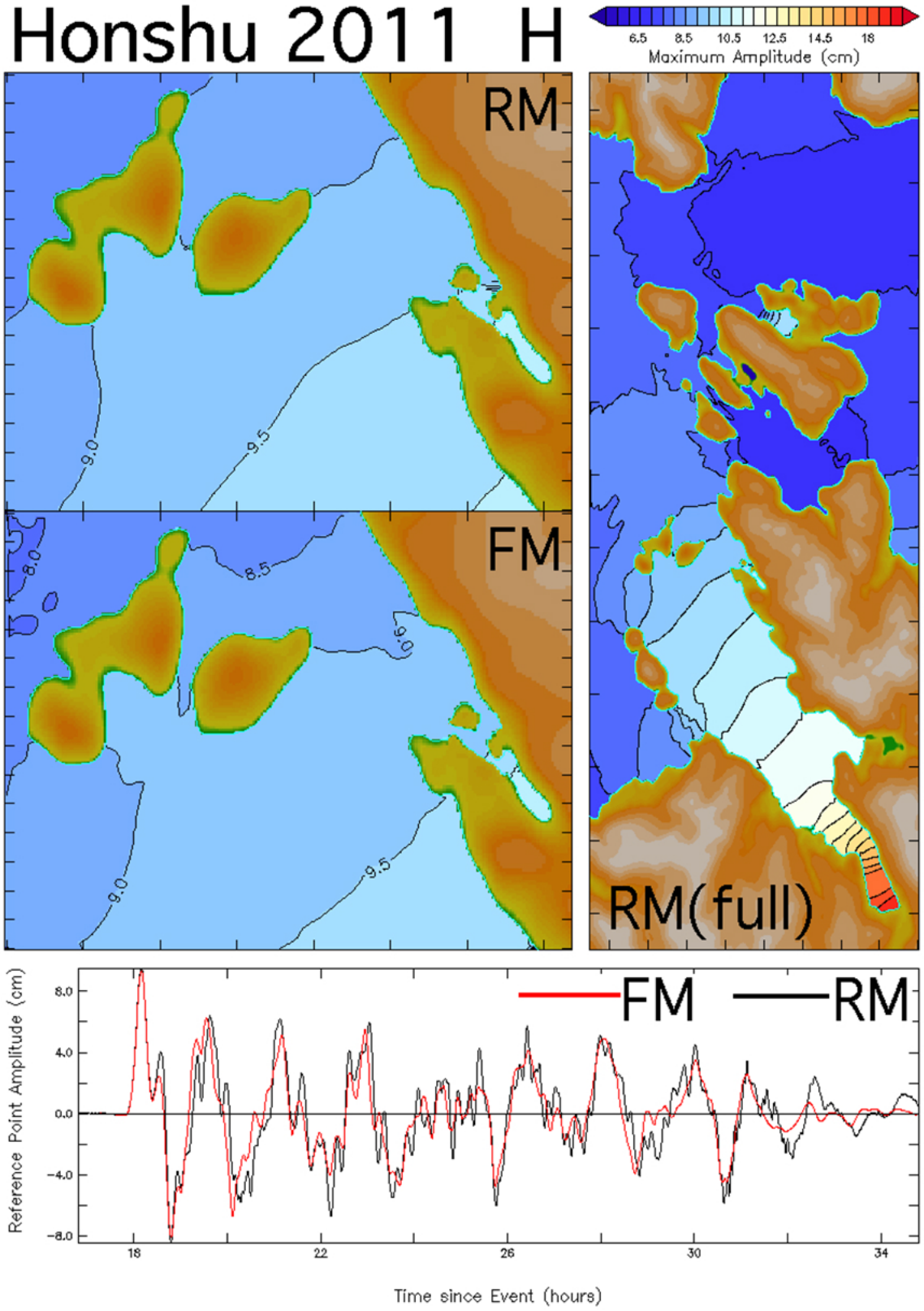

Figure 20. As for Figure 15 but for a hindcast of the Honshu-2011 historic event. The model is forced by a combination of unit sources and slip values selected in real time during the event (see Table 6) using DART® observations near the tsunami source. The Reference (RM) and Forecast Model (FM) predictions are in good agreement; validation results, using data from the Elfin Cove tide gage, are presented later. a) distribution of maximum amplitude during the 18-hour simulation.

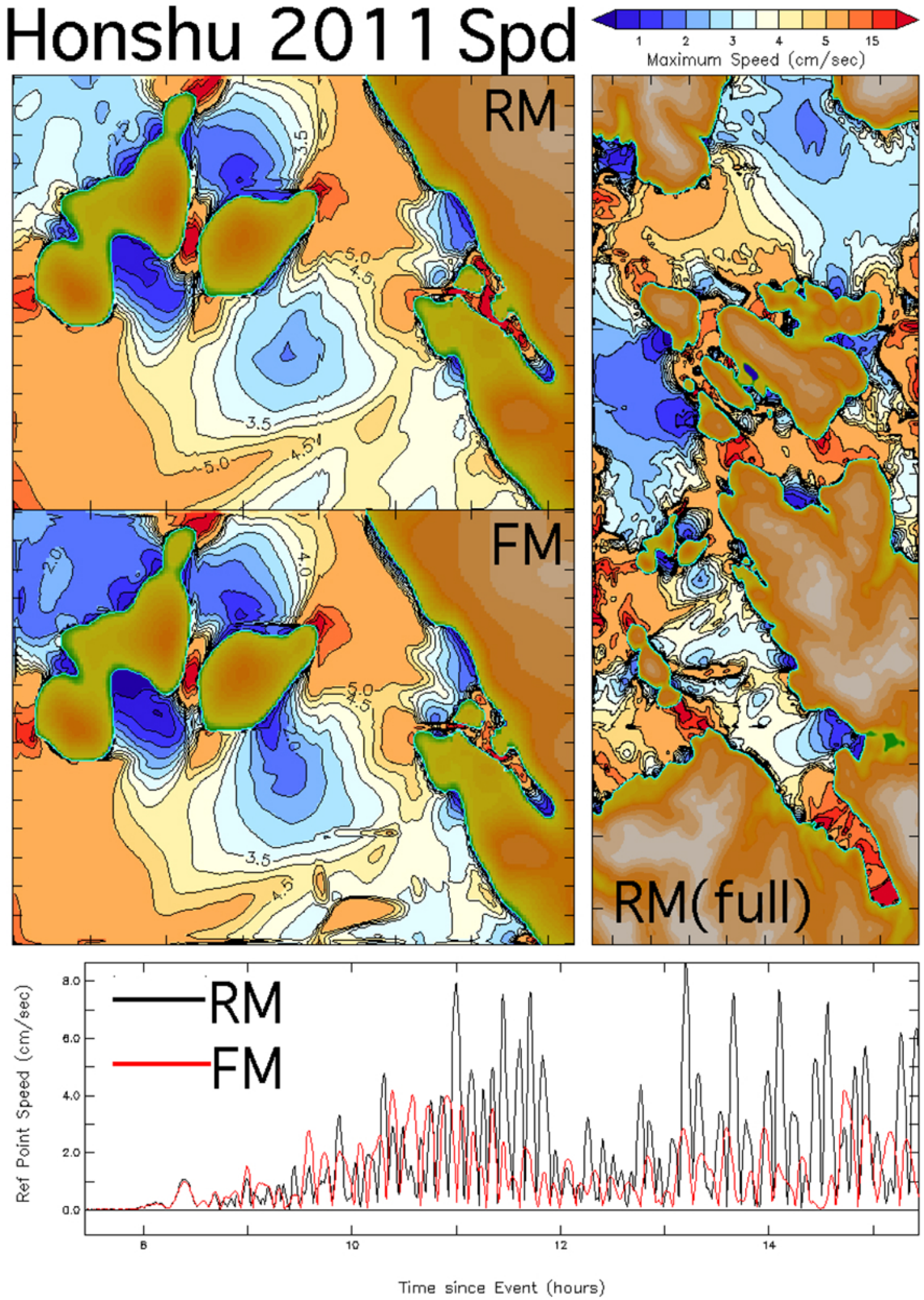

Figure 20 continued. As for Figure 15 but for a hindcast of the Honshu-2011 historic event. b) distribution of maximum speed.

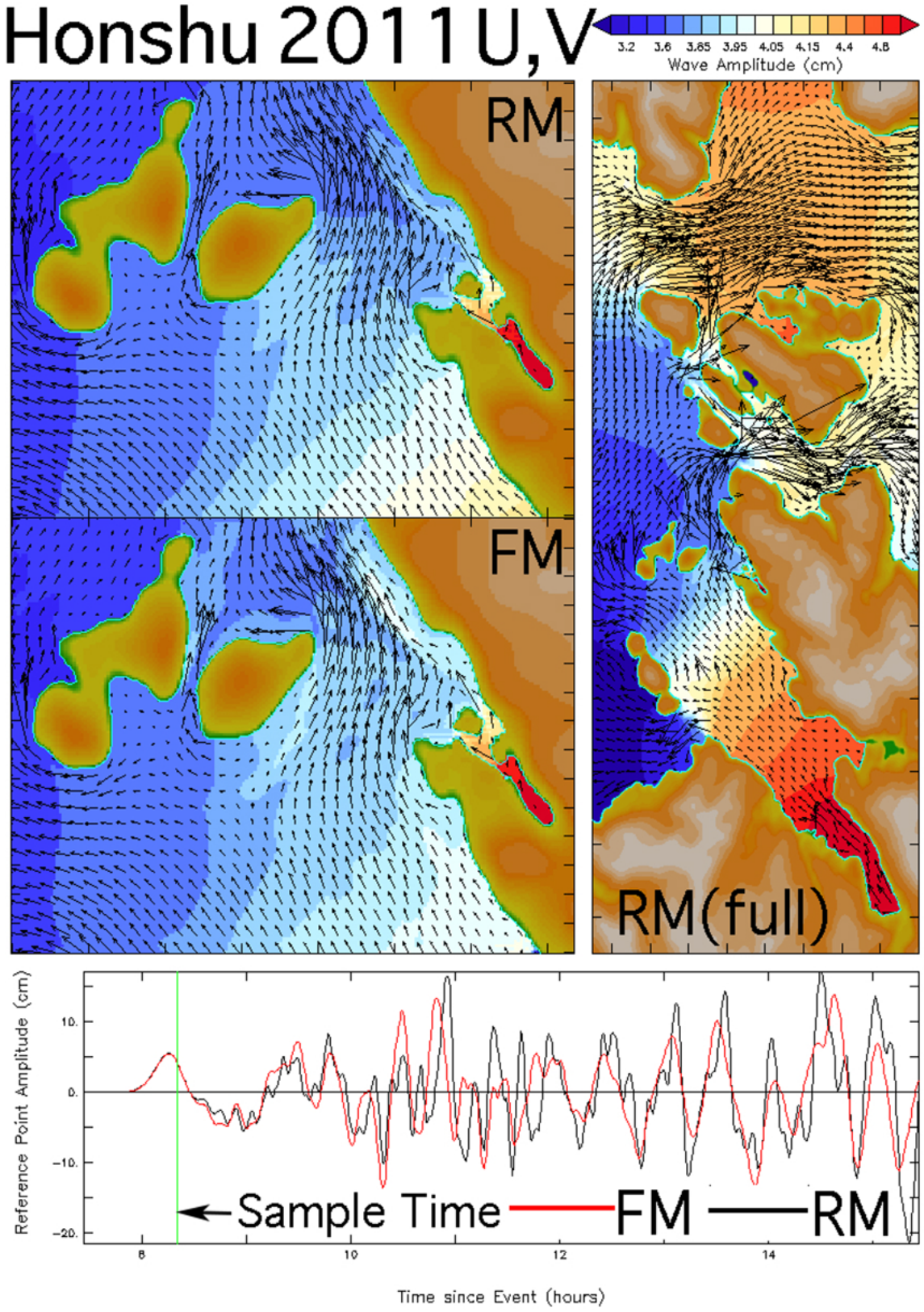

Figure 20 continued. As for Figure 15 but for a hindcast of the Honshu-2011 historic event.
c) snapshot of the current field at the time indicated by the green line in the lower panel.

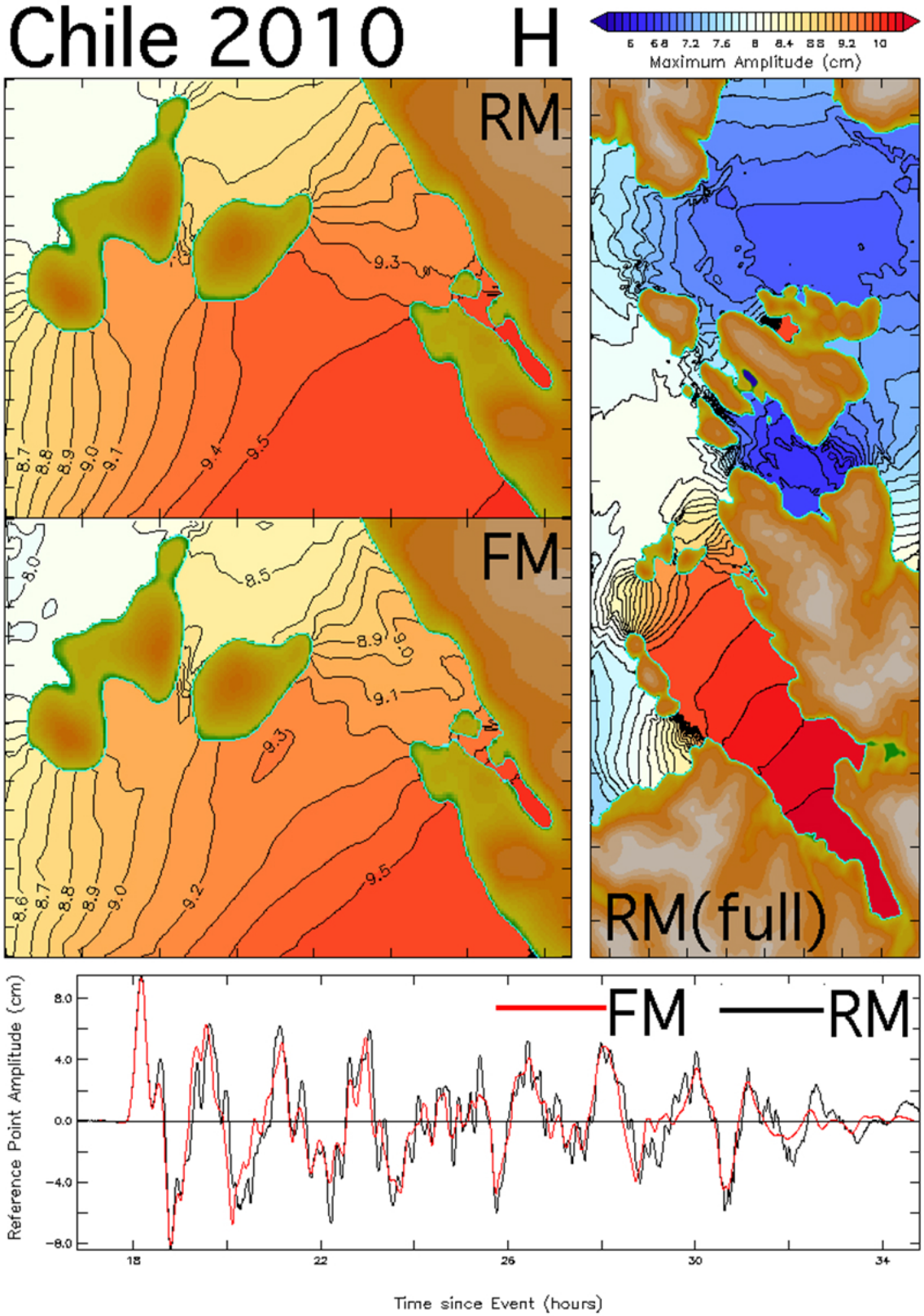

Figure 21. As for Figures 15 and 20, but for a hindcast of the Chile-2010 historic event. The model forcing is based on DART® data collected during the event, and validation results are presented later. a) distribution of maximum amplitude during the 18-hour simulation.

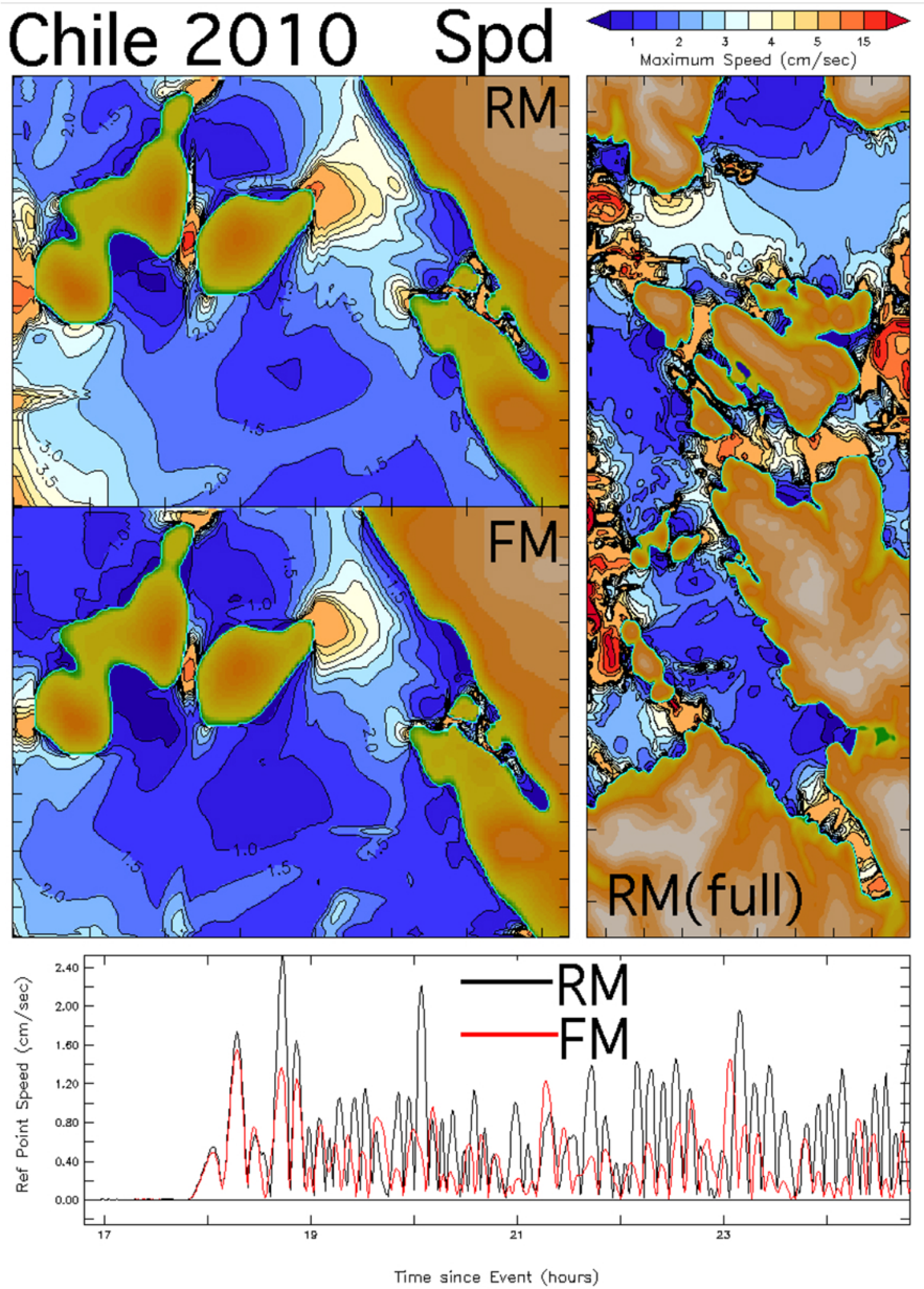

Figure 21continued. As for Figures 15 and 20, but for a hindcast of the Chile-2010 historic event. b) distribution of maximum speed.

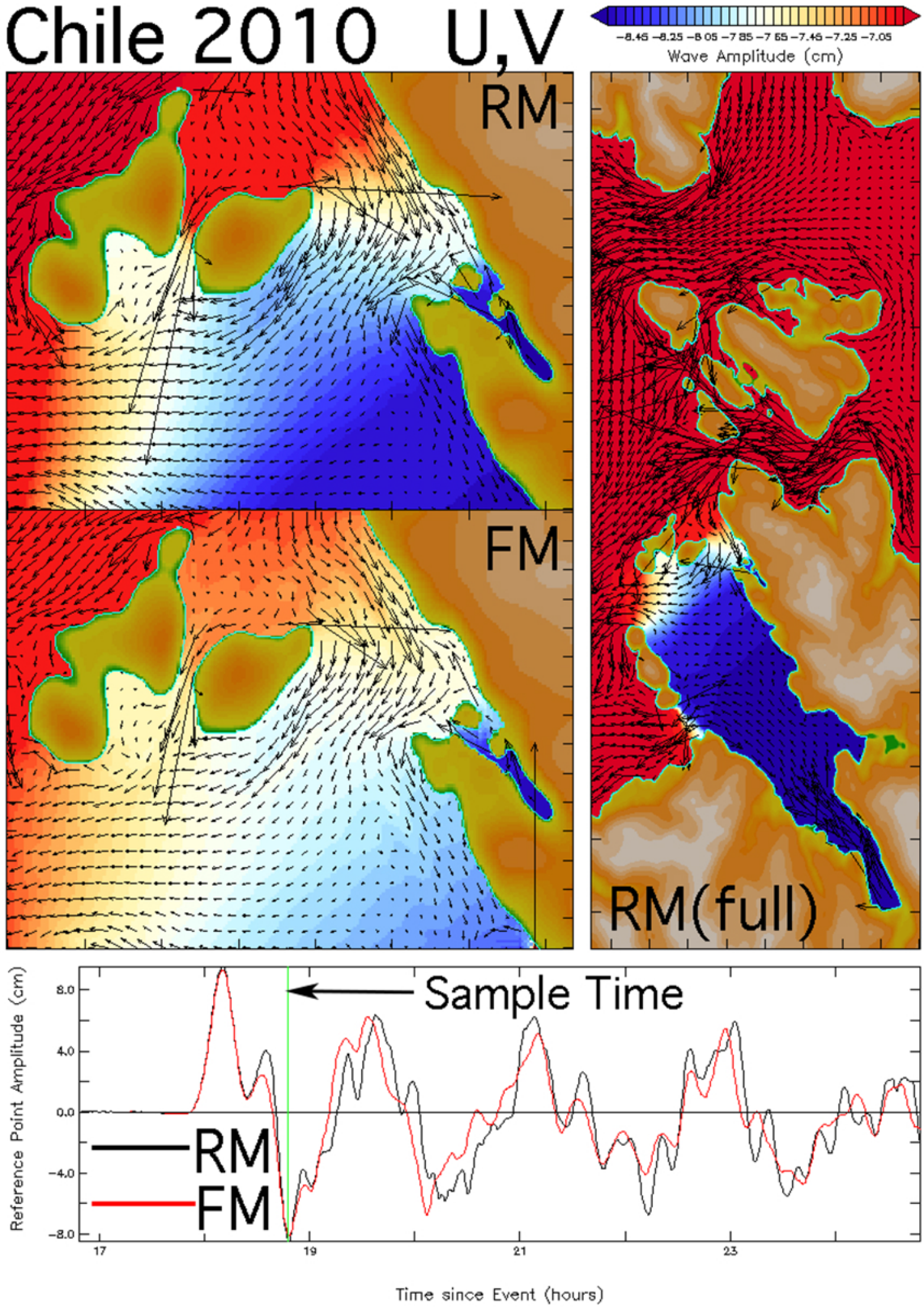

Figure 21 continued. As for Figures 15 and 20, but for a hindcast of the Chile-2010 historic event. c) a snapshot of the current field at the time indicated by the green line in the lower panel.

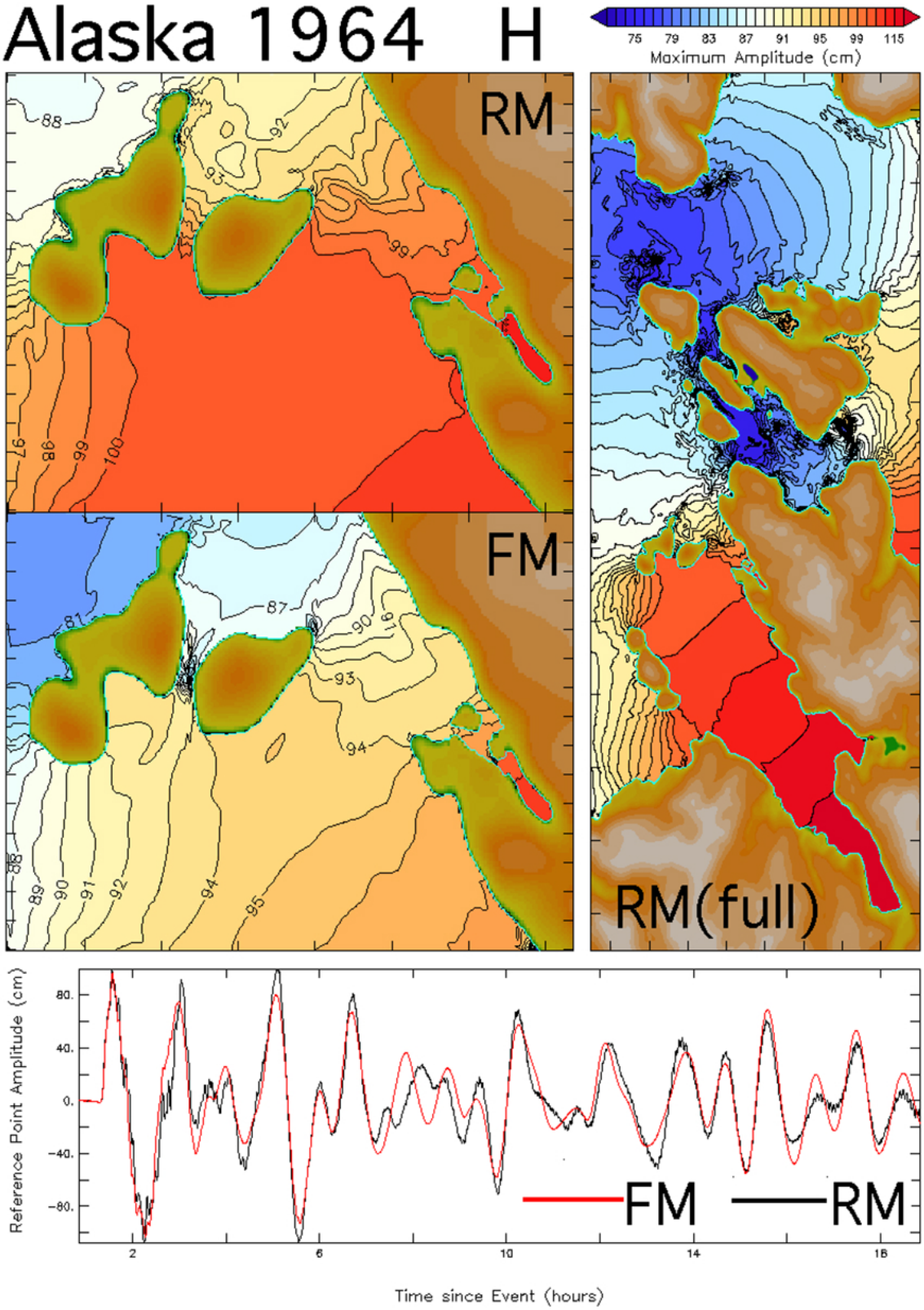

Figure 22. As for Figures 15 and 20 but for a hindcast of the Alaska-1964 tsunami, the largest event impacting Gulf of Alaska communities. The event pre-dated deep ocean tsunami detection capability so the representation of the source is based on post-event studies reported in the literature. a) distribution of maximum amplitude during the 18-hour simulation.

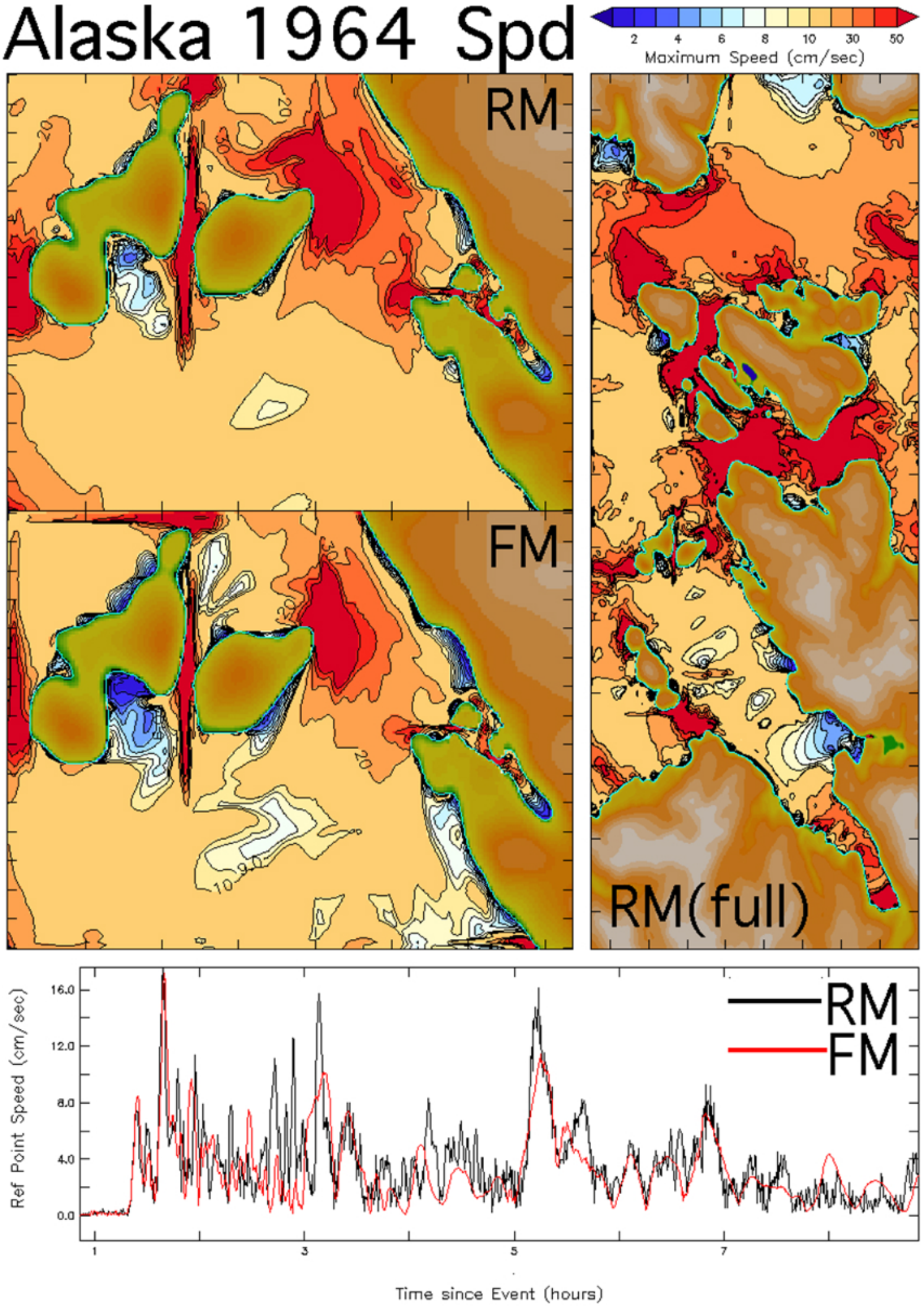

Figure 22 continued. As for Figures 15 and 20 but for a hindcast of the Alaska-1964 tsunami. b) distribution of maximum speed.

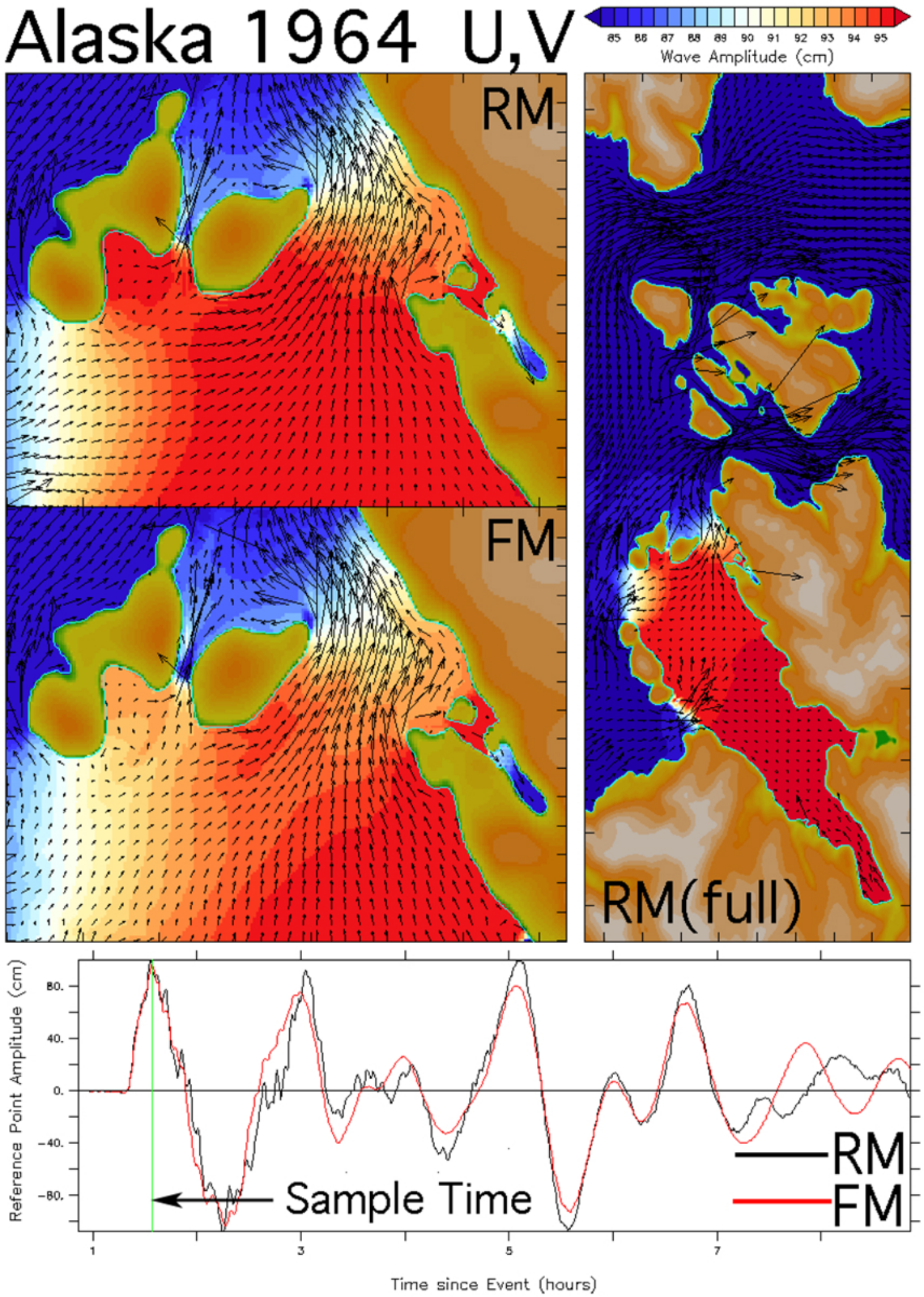

Figure 22 continued. As for Figures 15 and 20 but for a hindcast of the Alaska-1964 tsunami.
c) a snapshot of the current field at the time indicated by the green line in the lower panel.

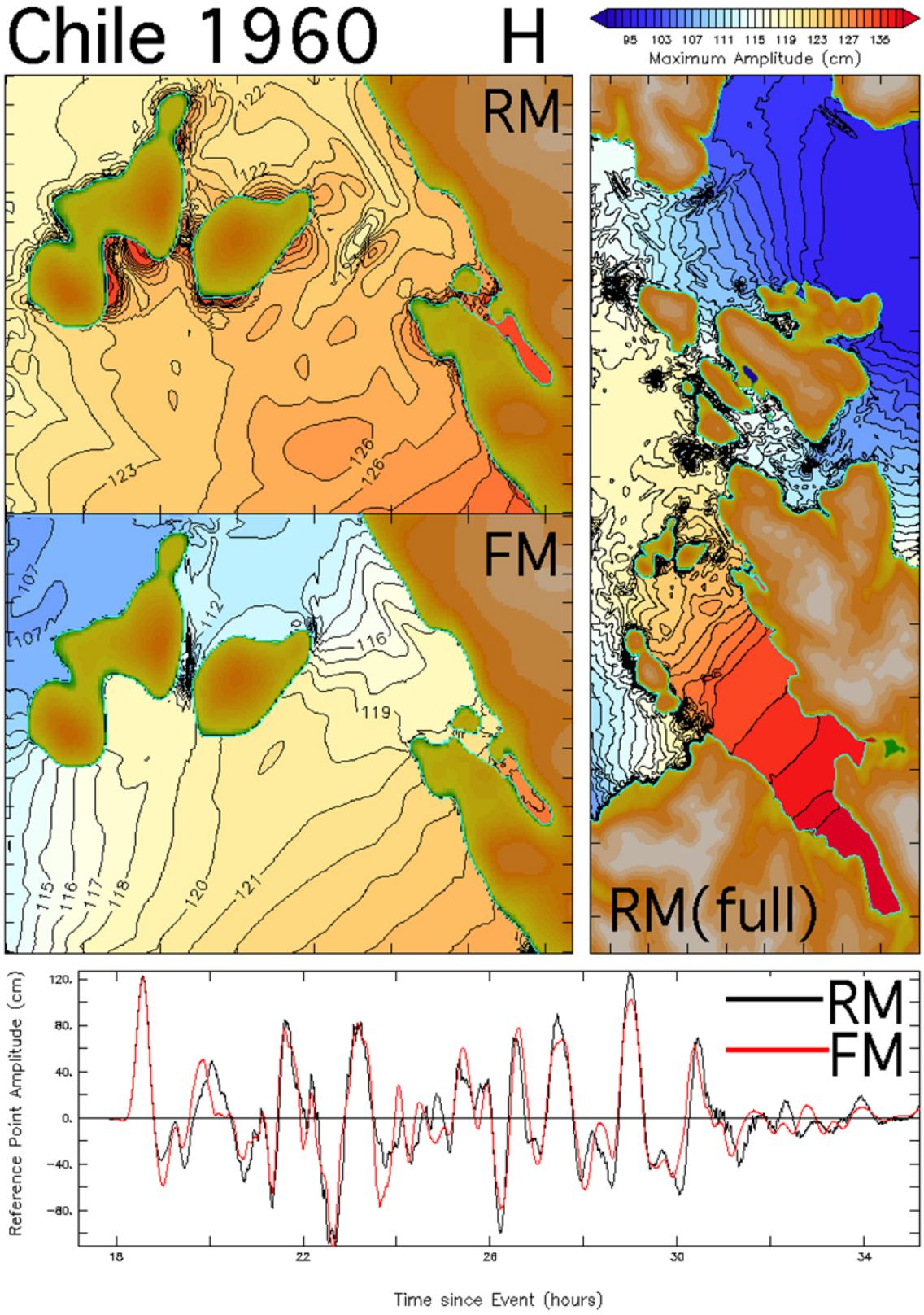

Figure 23. As for Figures 15 and 20 but for a hindcast of the Chile-1960 historic event that was widely felt through the Pacific basin. The source representation is shown later to be poor, but this does not invalidate its use for inter-comparison.
a) distribution of maximum amplitude during the 18-hour simulation.

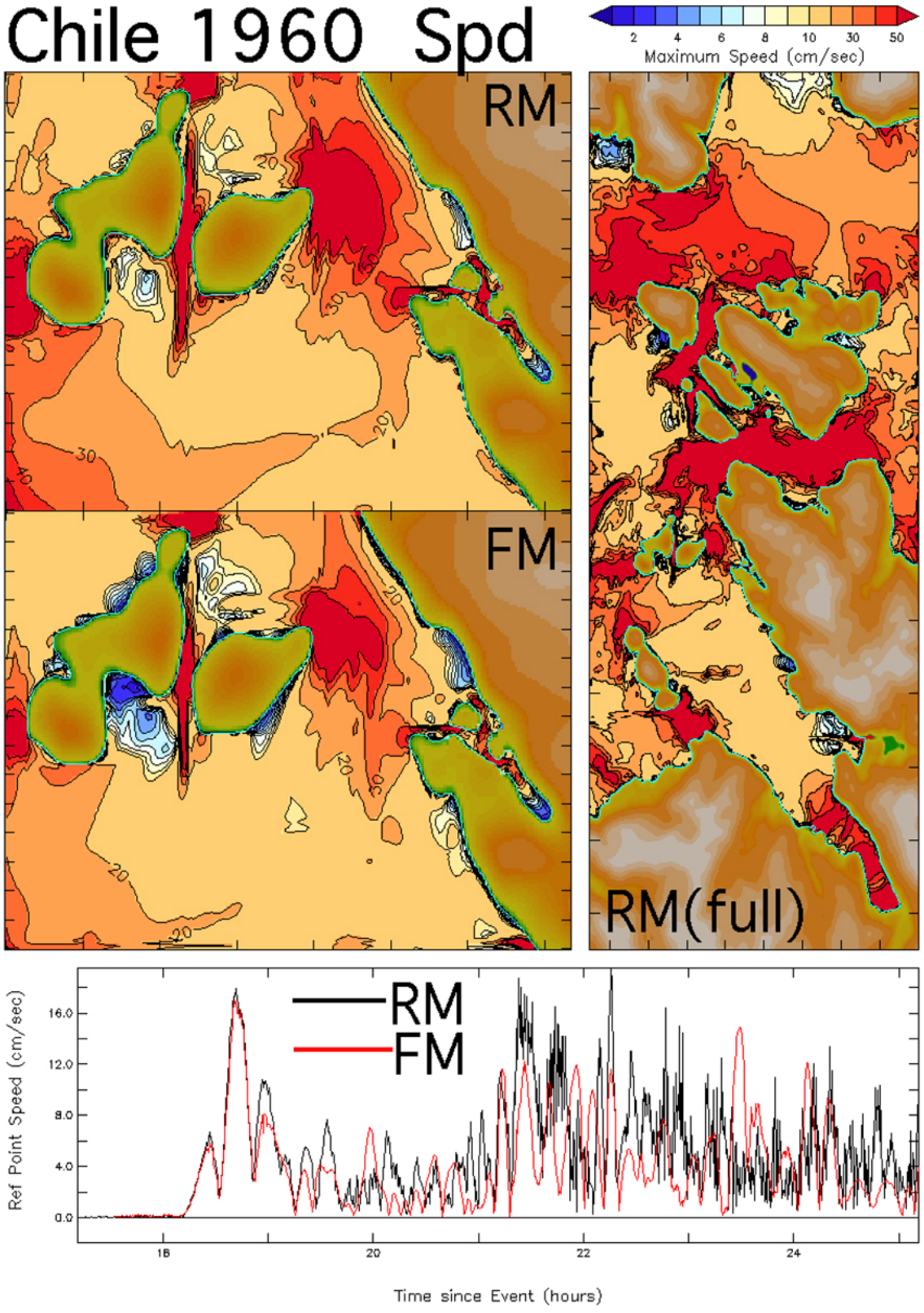

Figure 23 continued. As for Figures 15 and 20 but for a hindcast of the Chile-1960 historic event . b) distribution of maximum speed.

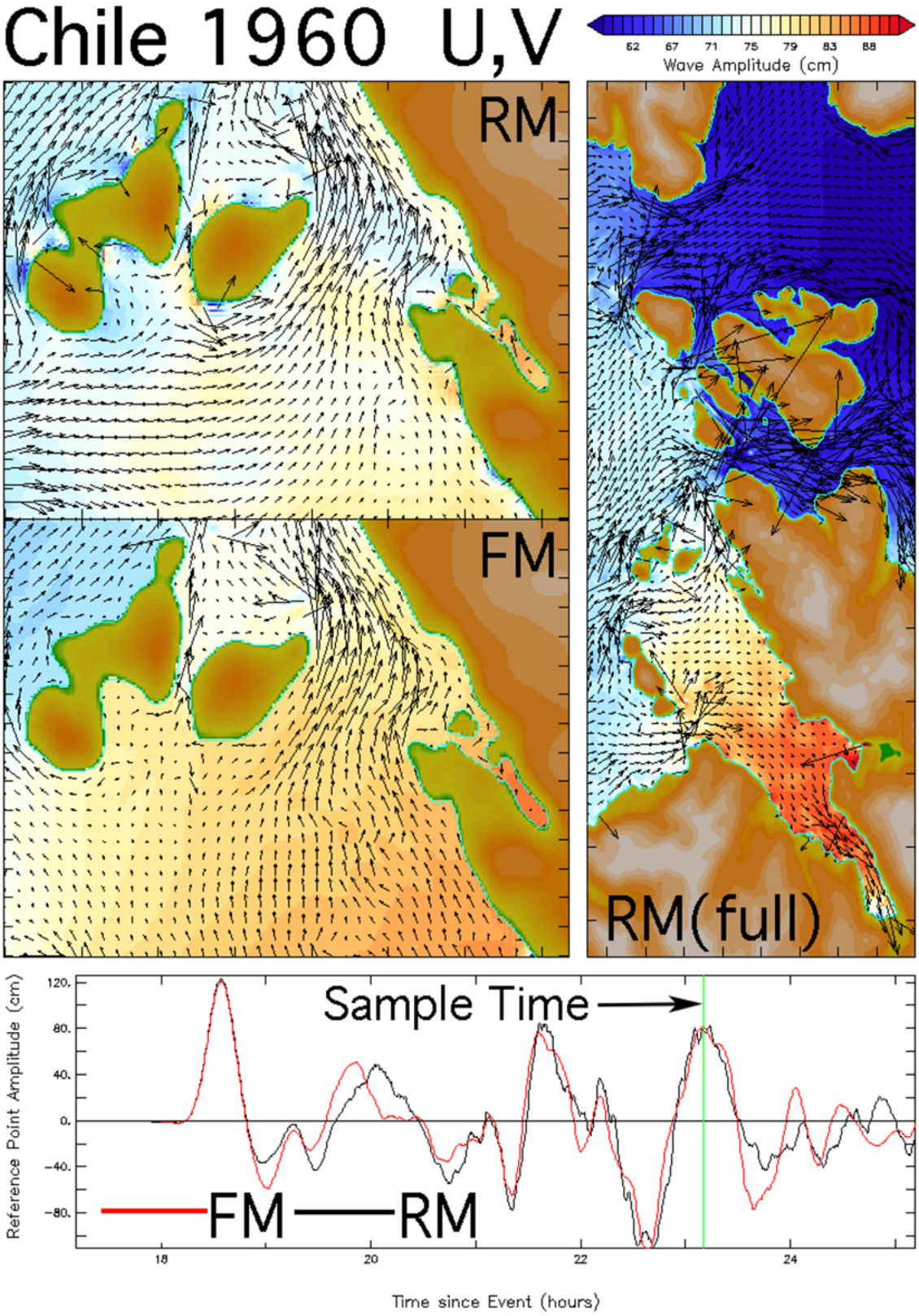

Figure 23 continued. As for Figures 15 and 20 but for a hindcast of the Chile-1960 historic event.
c) a snapshot of the current field at the time indicated by the green line in the lower panel.

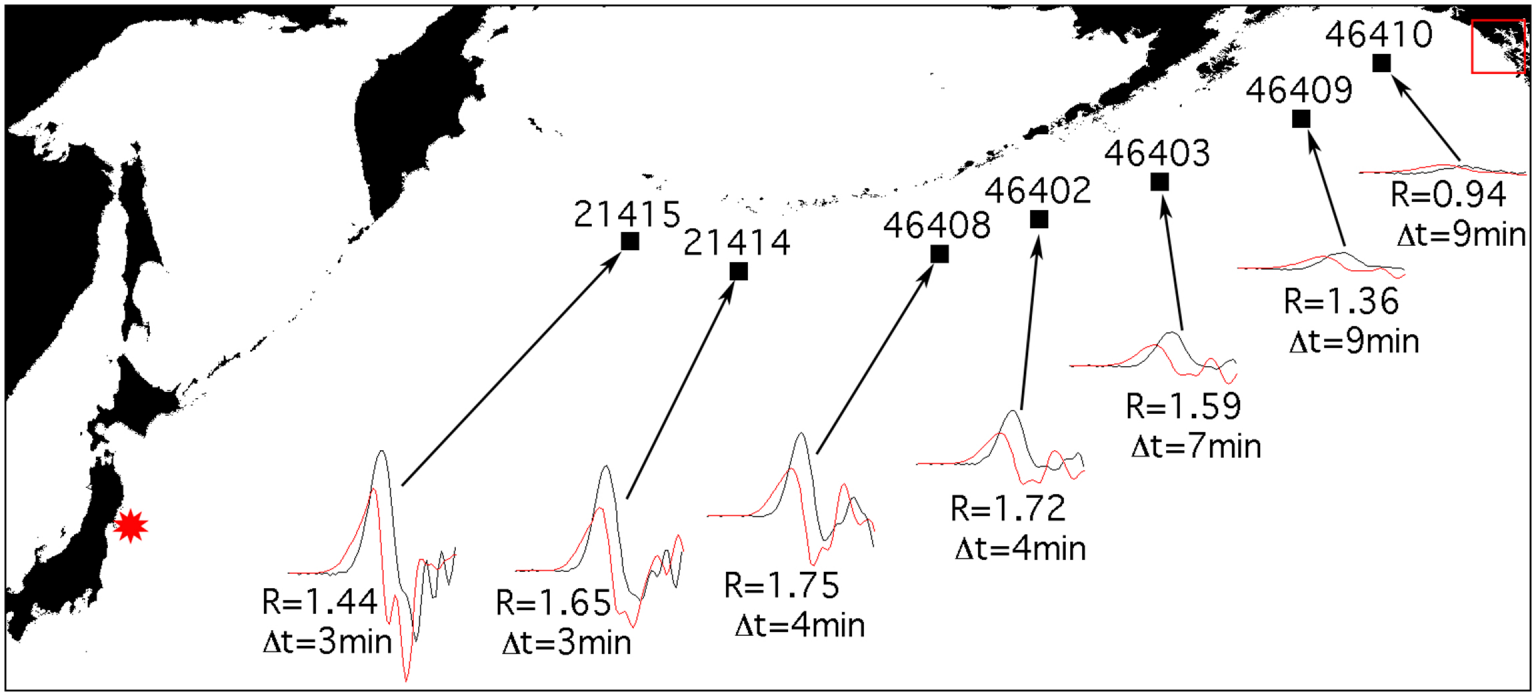

Figure 24. Propagation of the Honshu-2011 tsunami across the North Pacific from its epicenter (red star) to the Gulf of Alaska. DART® observations and model results from MOST use a common vertical and horizontal scale at all locations. The ratio of observed to model amplitude is denoted by R; Δt is the time lead of the model.

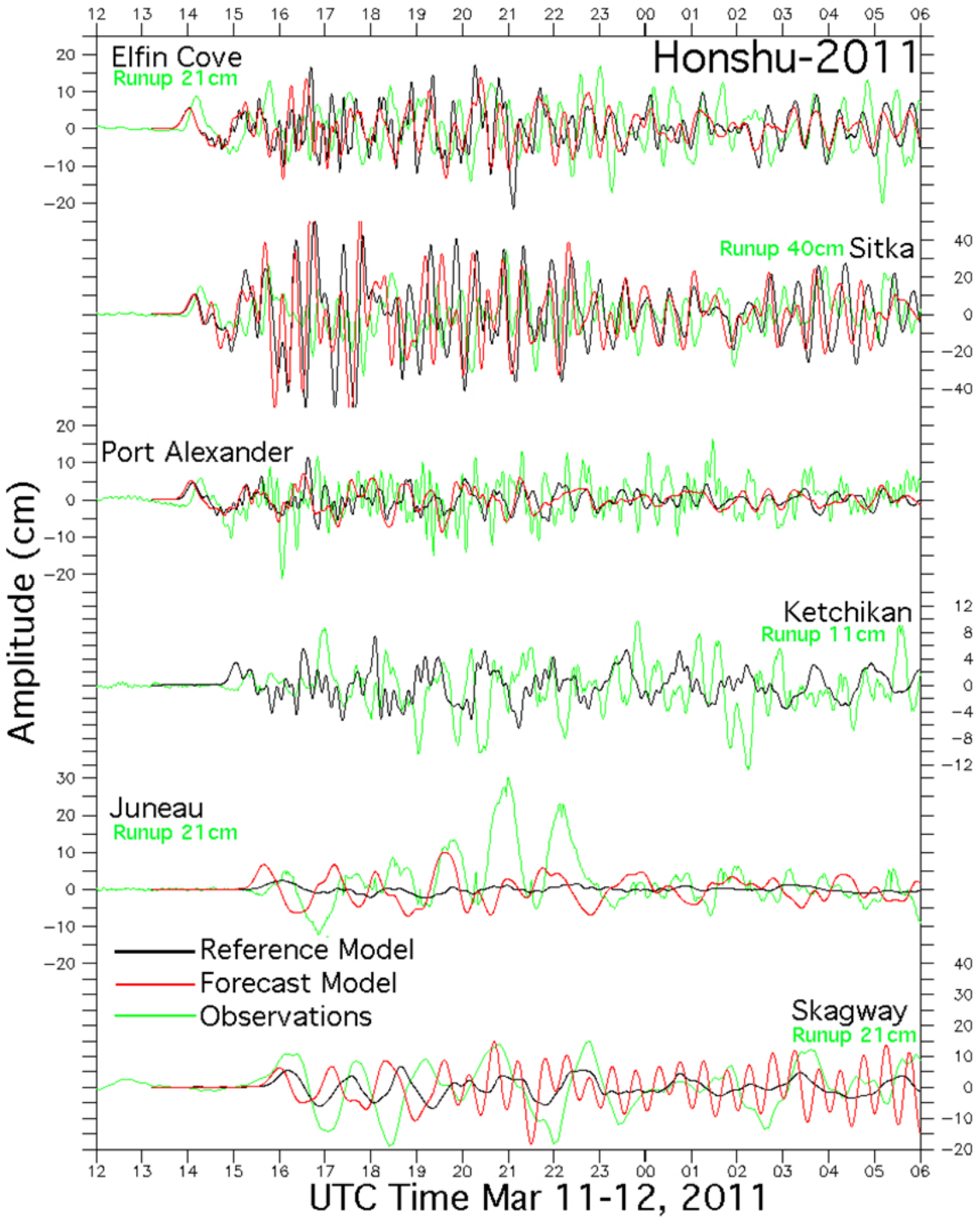

Figure 25. Model validation based on detided and low-passed observations (green) of the Honshu-2011 tsunami at locations within the Elfin Cove model grids. The Reference (RM) and Forecast Model (FM) hindcasts are shown in black and red respectively. Model time series lead the observations, as is common for tele-tsunami events. Agreement is best for Elfin Cove, in the model C-grid, Sitka, and Ketchikan (which is outside the FM grids.) The Port Alexander validation is unclear due to noise in the observations. At Juneau and Skagway, whose grid representation has low resolution, only an approximate match is found.

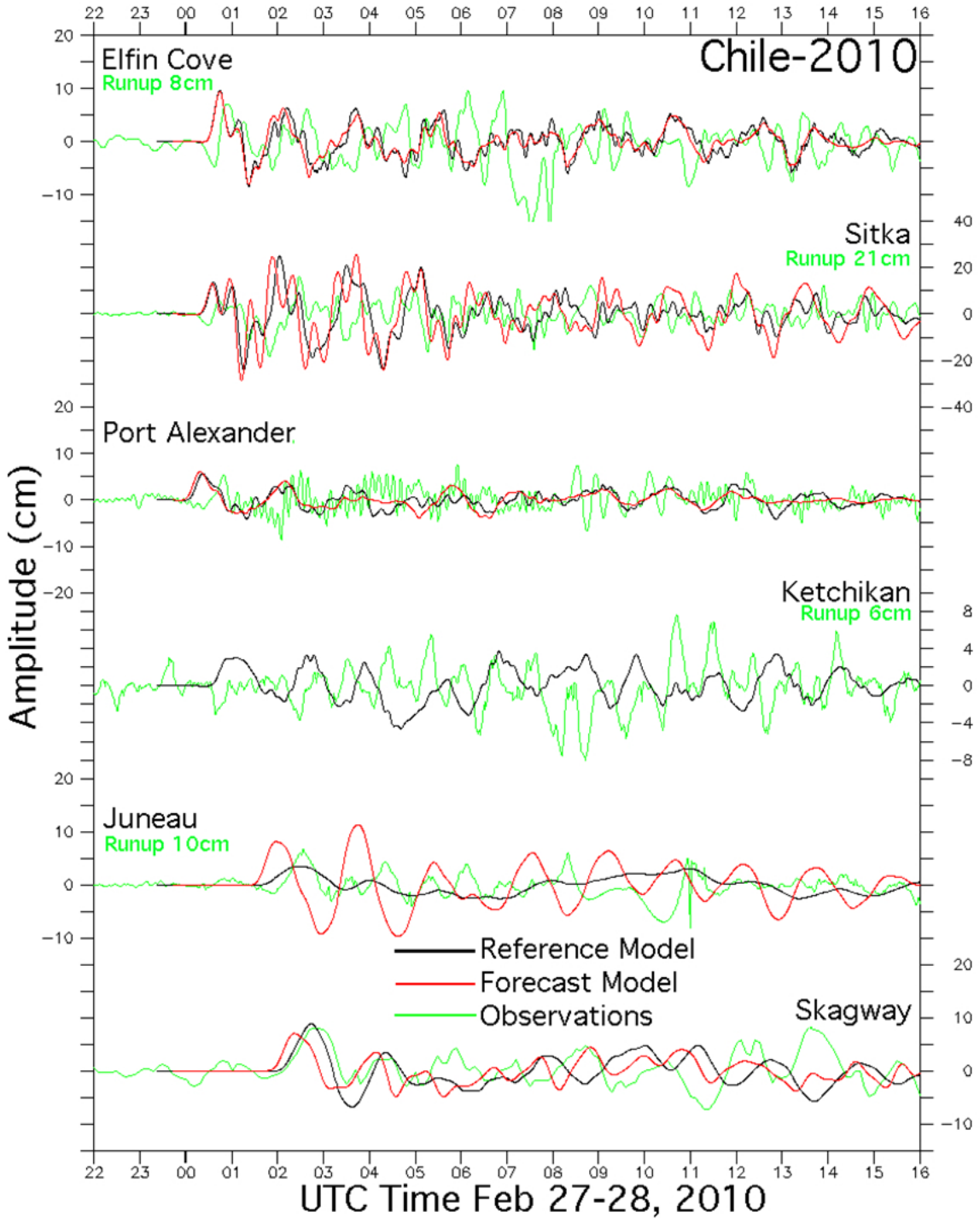

Figure 26. As in Figure 25 but for the Chile-2010 historic tsunami. The model results at the various sites are consistent for the upper three panels in overestimating the observed signal. For Juneau and Skagway the better resolution of the RM A-grid results in improved agreement with the data.

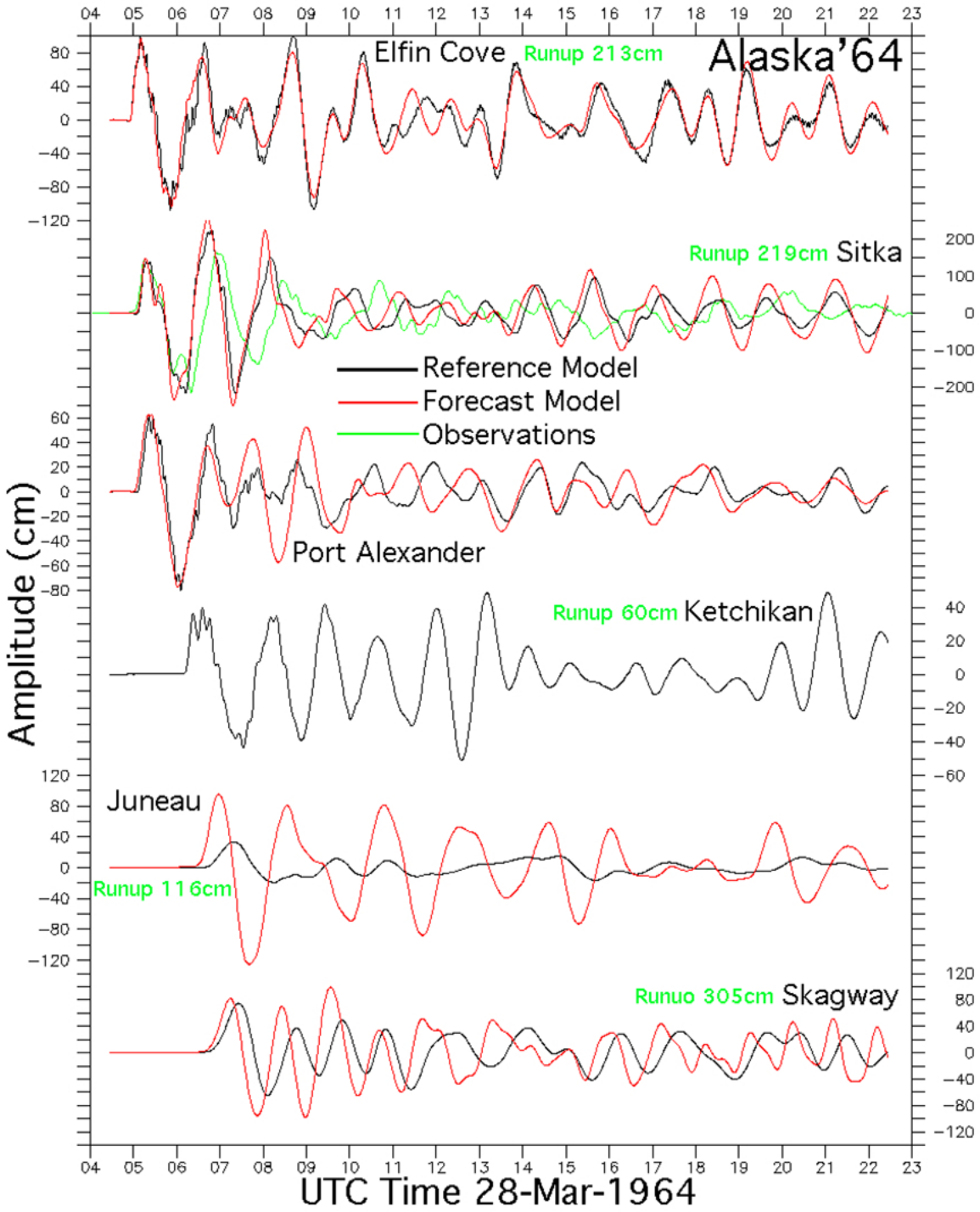

Figure 27. Model validation based on the Alaska-1964 historic tsunami. An observed time series is only available for Sitka, based on a digitized marigram in the WCATWC archives. At Elfin Cove, Port Alexander, and Skagway the agreement between the Reference (RM) and Forecast Model (FM) hindcasts is good, throughout the event. Juneau is less satisfactory but, consistent with the Honshu-2011 and Chile-2010 results, FM exceeds RM.

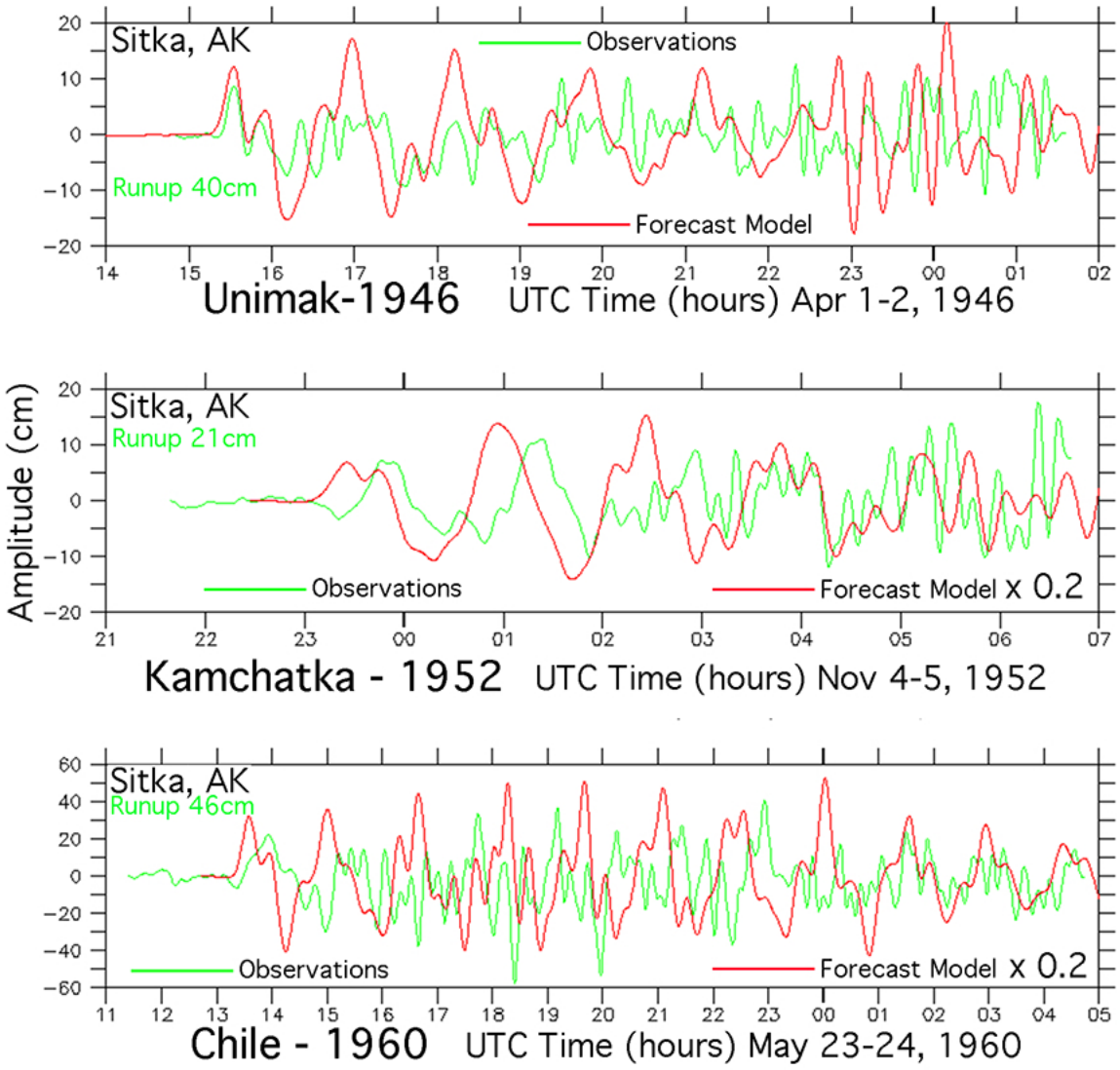

Figure 28. Attempted model validation based on digitized marigrams for Sitka associated with the Unimak-1946, Kamchatka-1952 and Chile-1960 tsunamis.

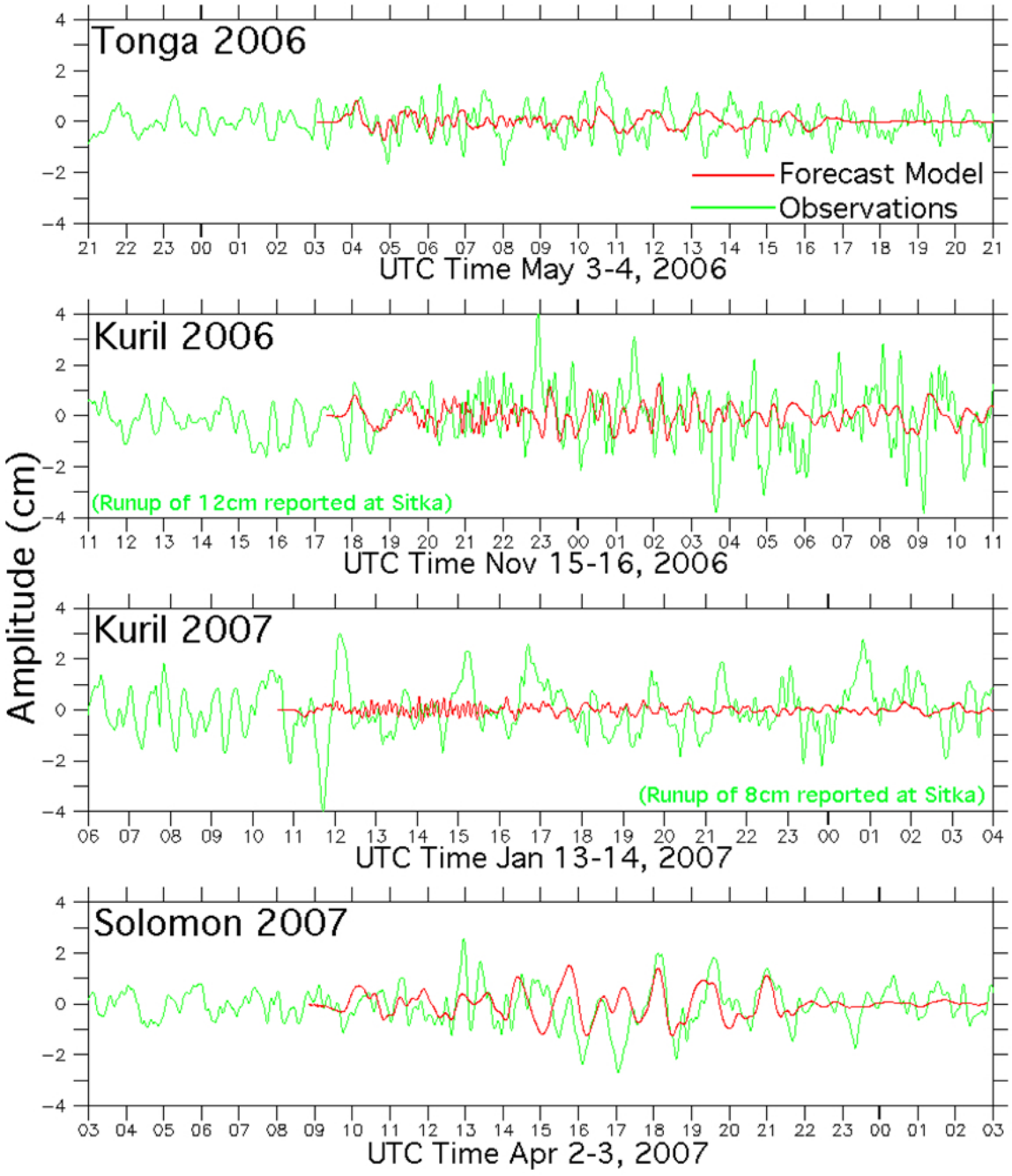

Figure 29. Comparison of Forecast Model (FM) hindcasts at the Elfin Cove tide gage with observations for selection of historic events since one-minute data became available. Owing to the weak response of the Gulf of Alaska region, and poor signal to noise ratios, none of these events were of use in model validation.

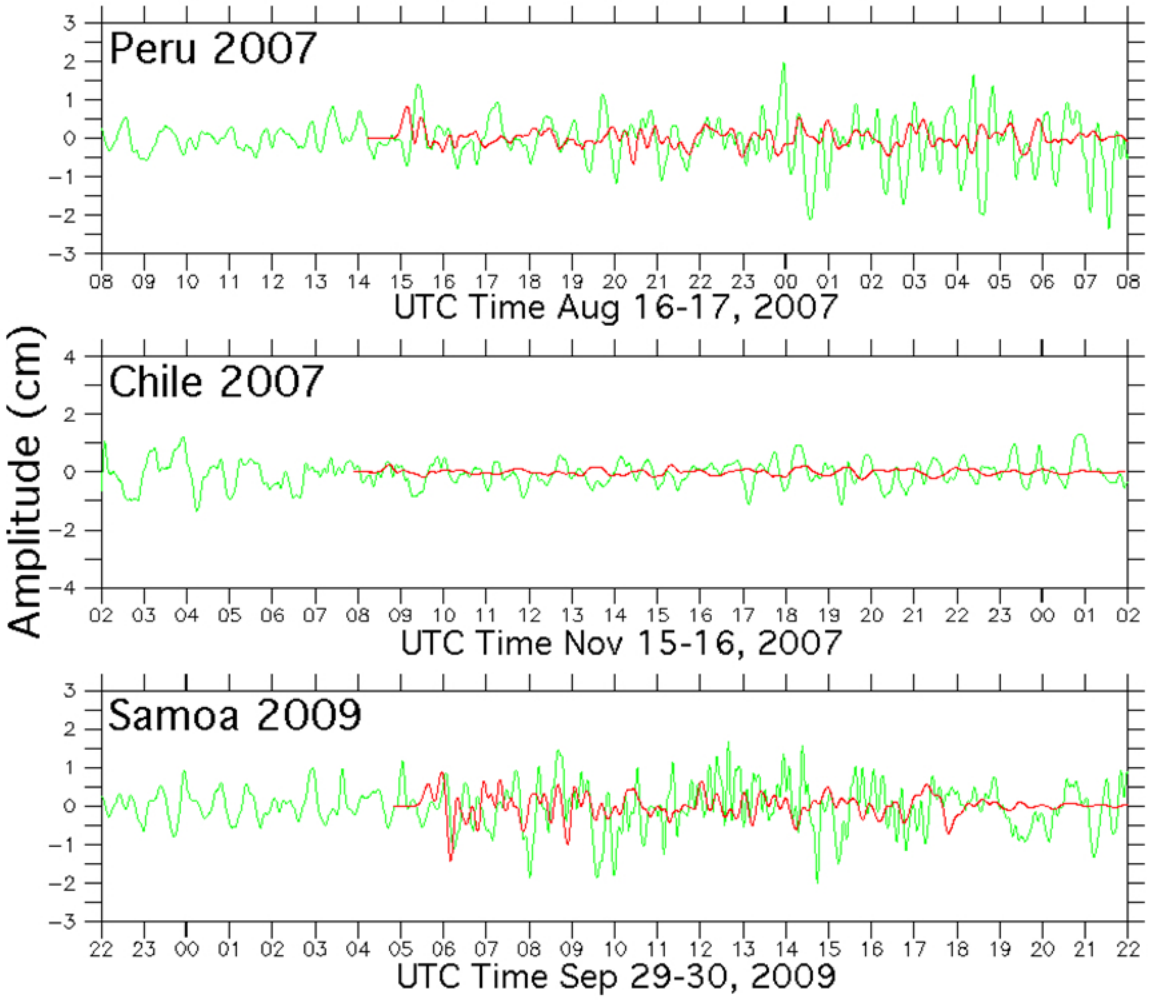

Figure 29 continued. Comparison of Forecast Model (FM) hindcasts at the Elfin Cove tide gage with observations for selection of historic events since one-minute data became available.

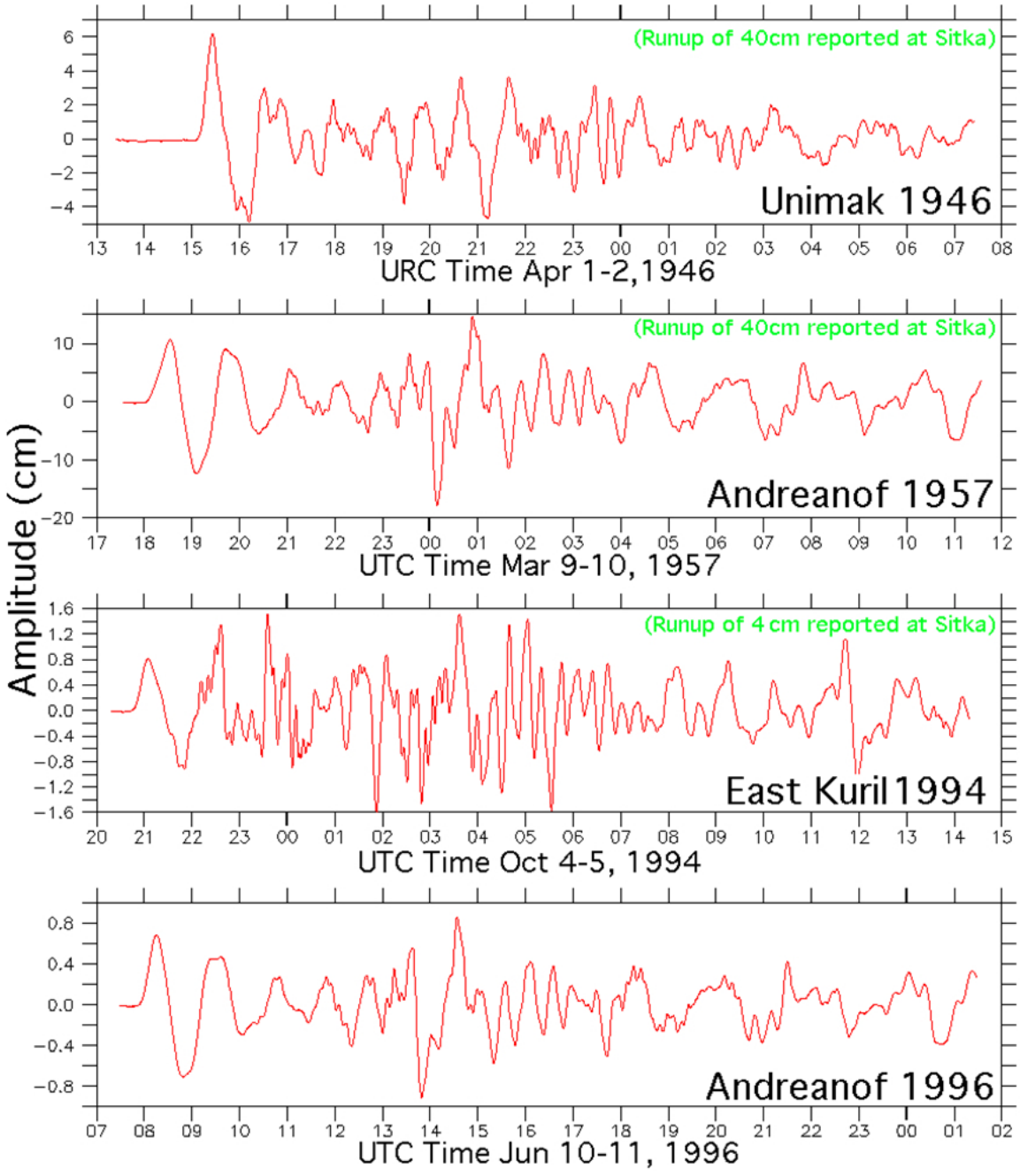

Figure 30. Forecast Model hindcasts for Elfin Cove during various earlier tsunamis for which tide gage records are unavailable. Some Sitka runup reports are indicated.

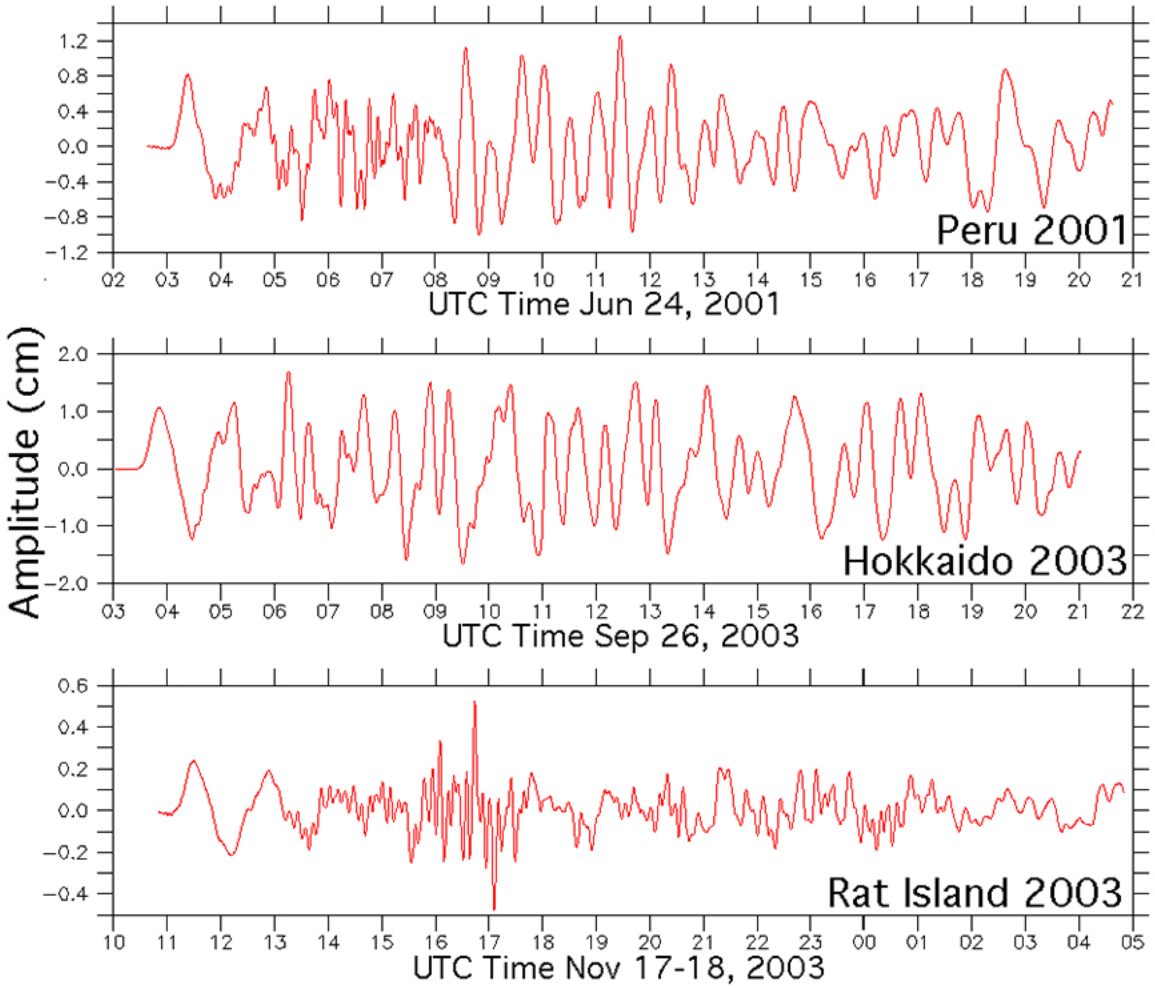

Figure 30 continued. Forecast Model hindcasts for Elfin Cove during various earlier tsunamis for which tide gage records are unavailable. Some Sitka runup reports are indicated.

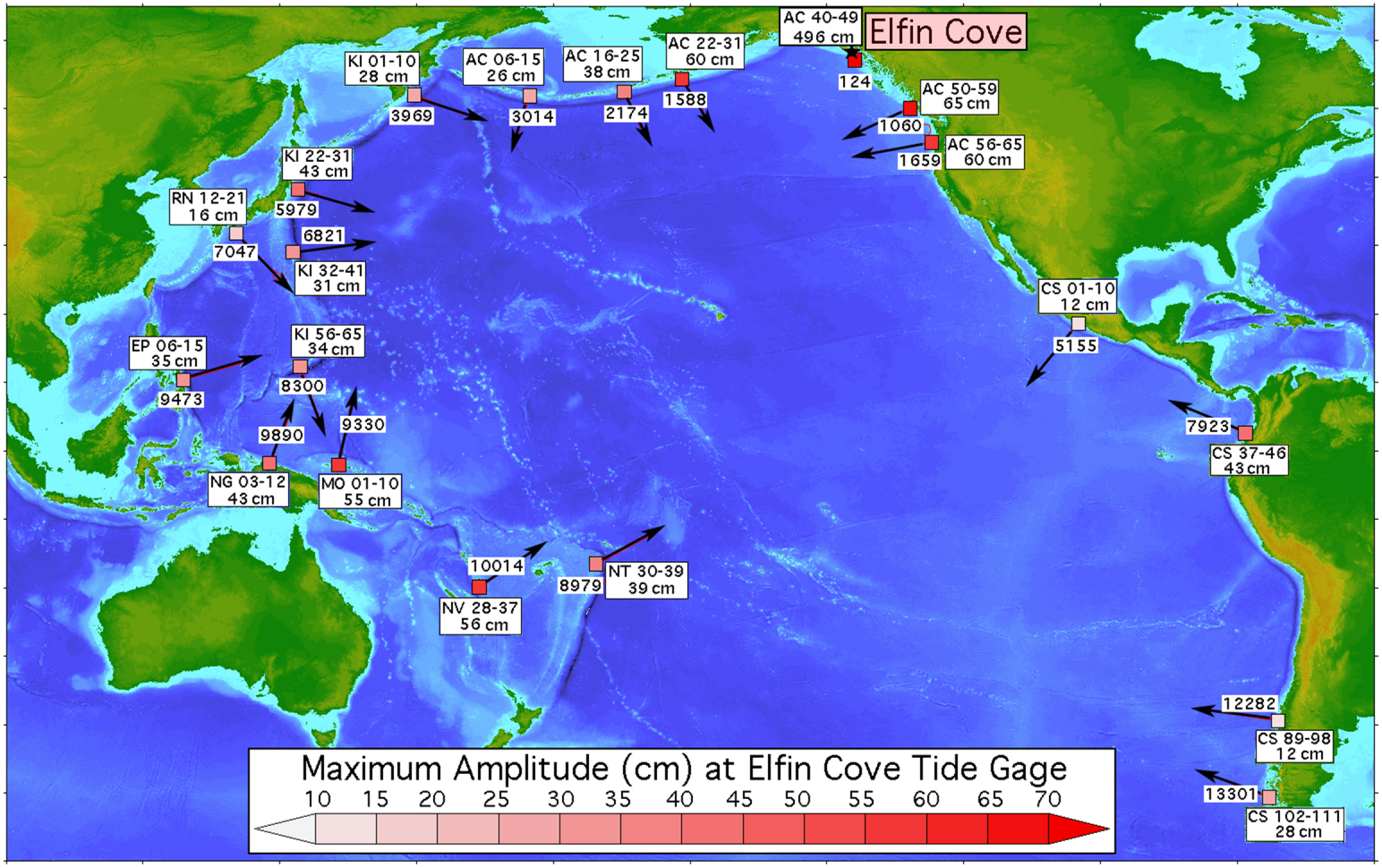

Figure 31. Chart summarizing predicted maximum amplitudes at the Elfin Cove tide gage associated with the full suite of mega-tsunami events listed in Table 5. Numerical values are shown on the chart, together with great circle distances to Elfin Cove as an indication of the likely main beam direction near the source.

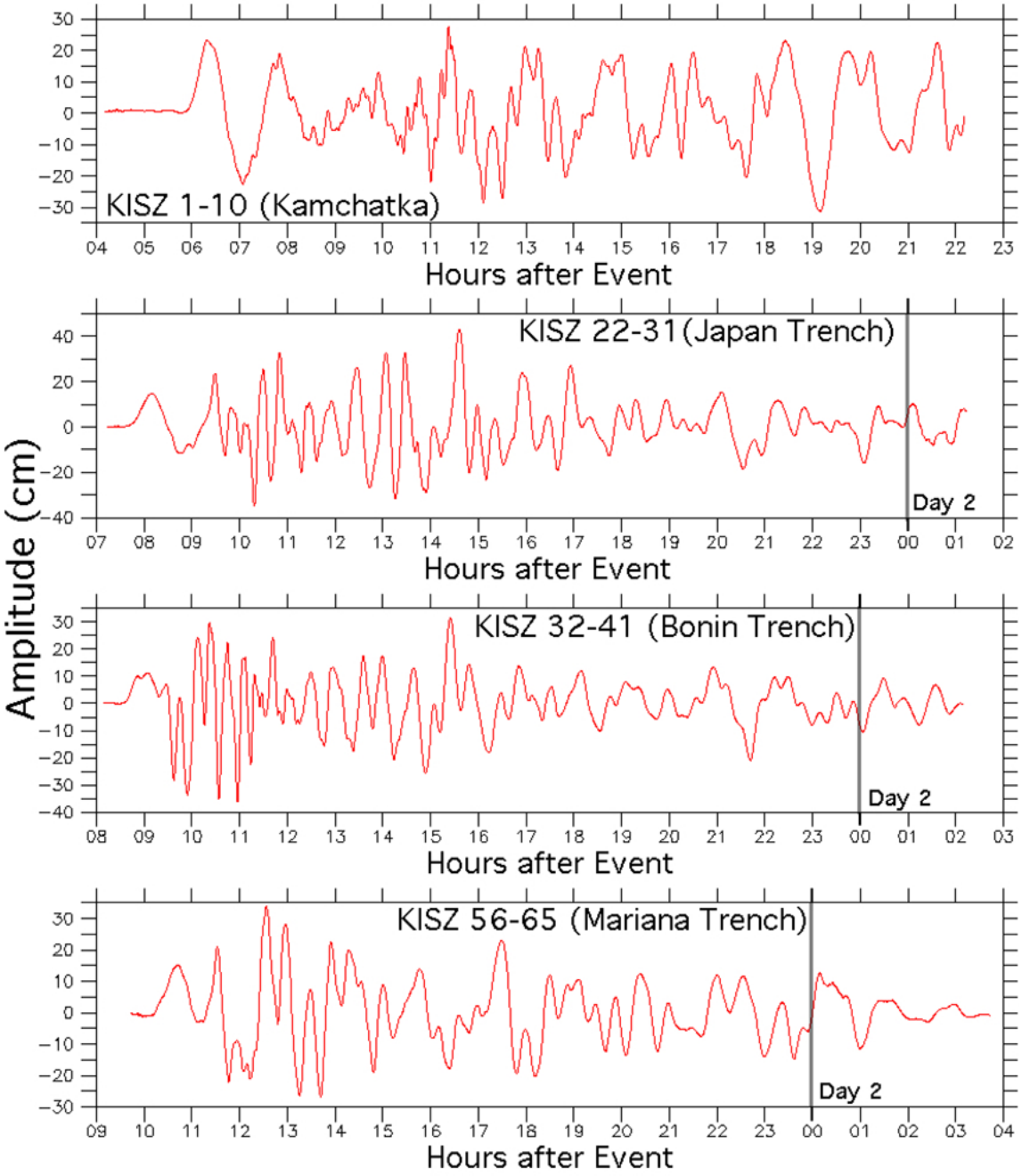

Figure 32. Complete time series of Forecast Model predictions at the Elfin Cove tide gage site for each of the mega-tsunami scenarios. Time is in hours from the event and, although each simulation is limited to 18 hours after the wave enters the model domain, some events extend into a second day after the event.

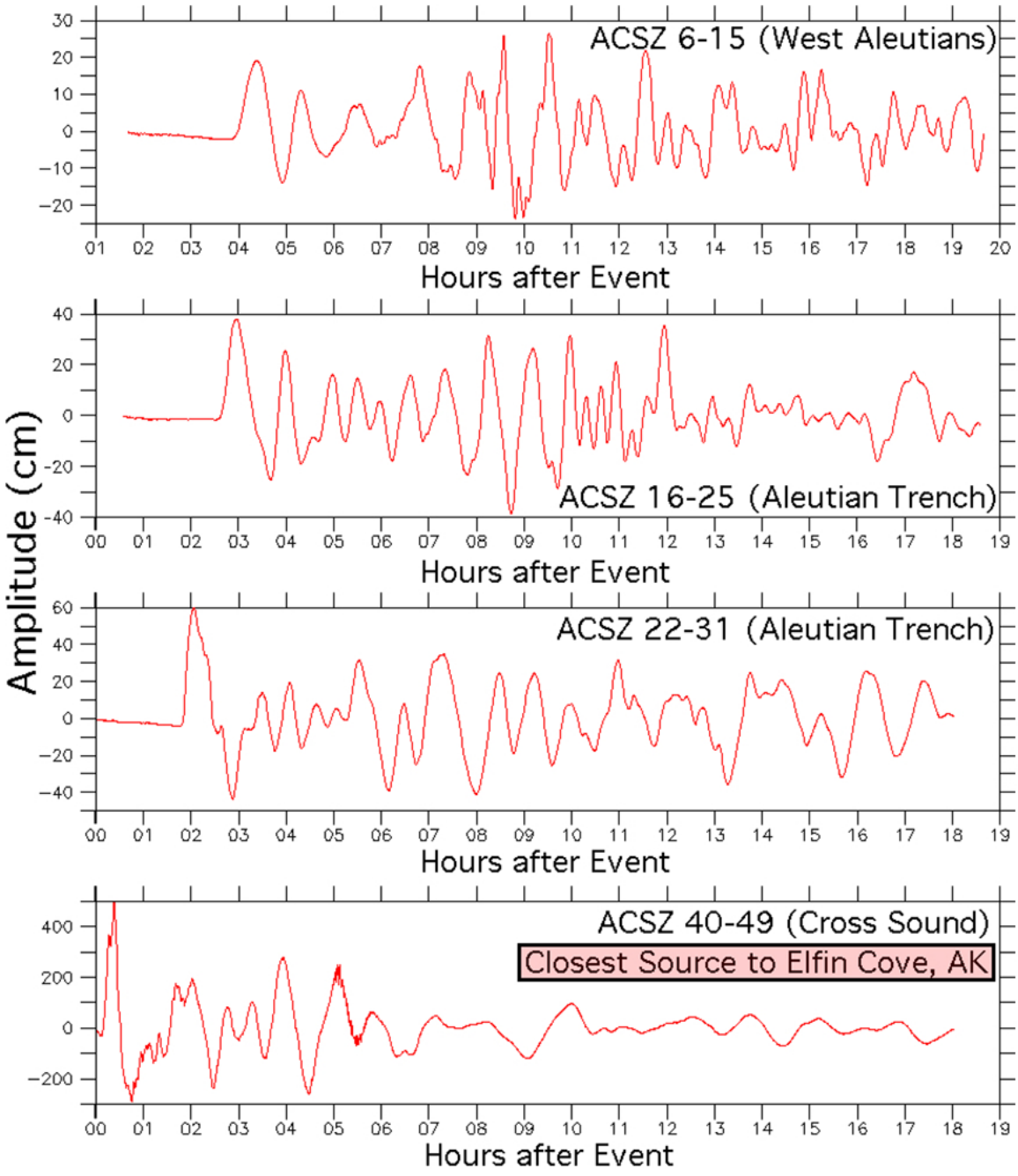

Figure 32 continued. Complete time series of Forecast Model predictions at the Elfin Cove tide gage site for each of the mega-tsunami scenarios.

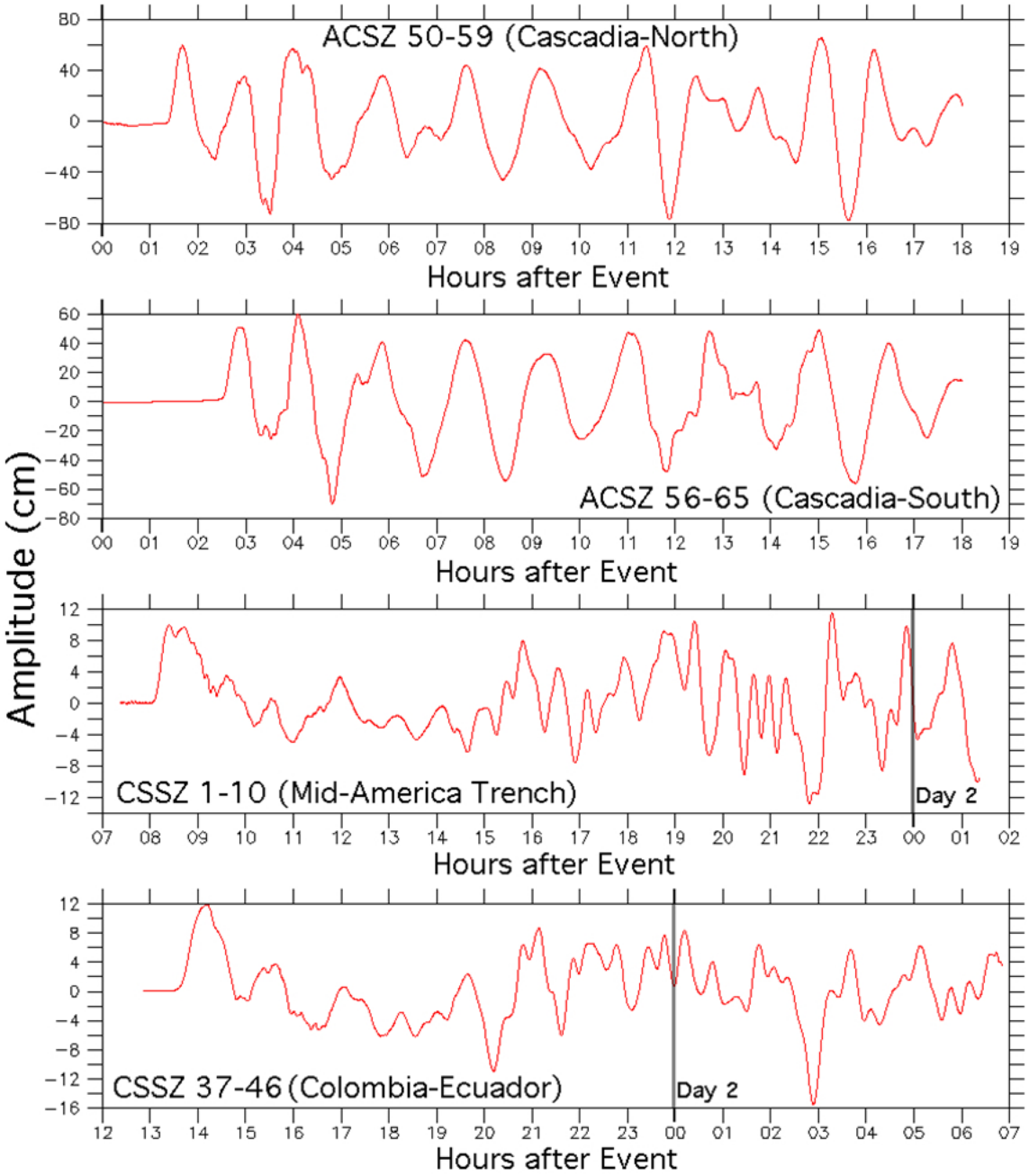

Figure 32 continued. Complete time series of Forecast Model predictions at the Elfin Cove tide gage site for each of the mega-tsunami scenarios.

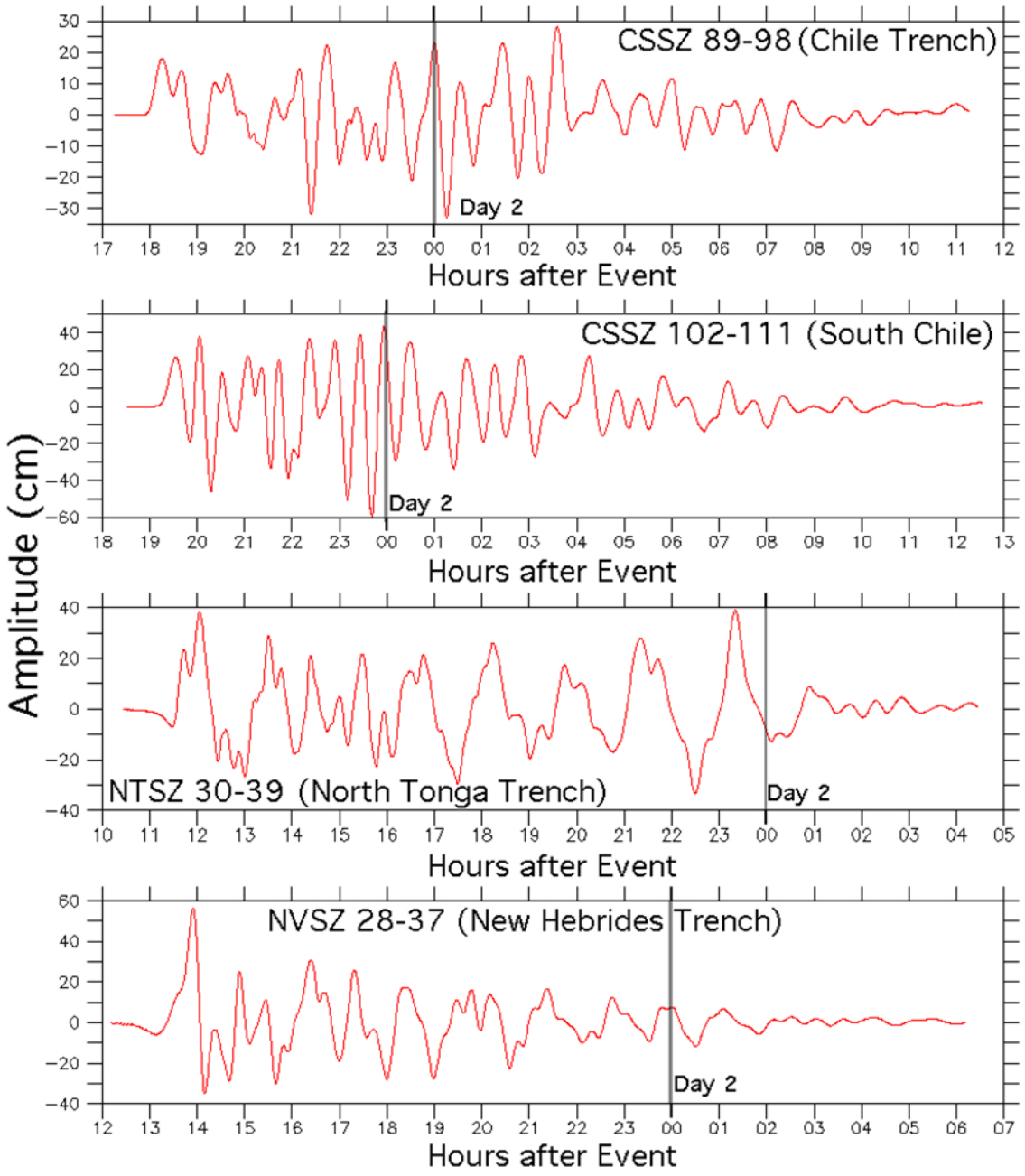

Figure 32 continued. Complete time series of Forecast Model predictions at the Elfin Cove tide gage site for each of the mega-tsunami scenarios.

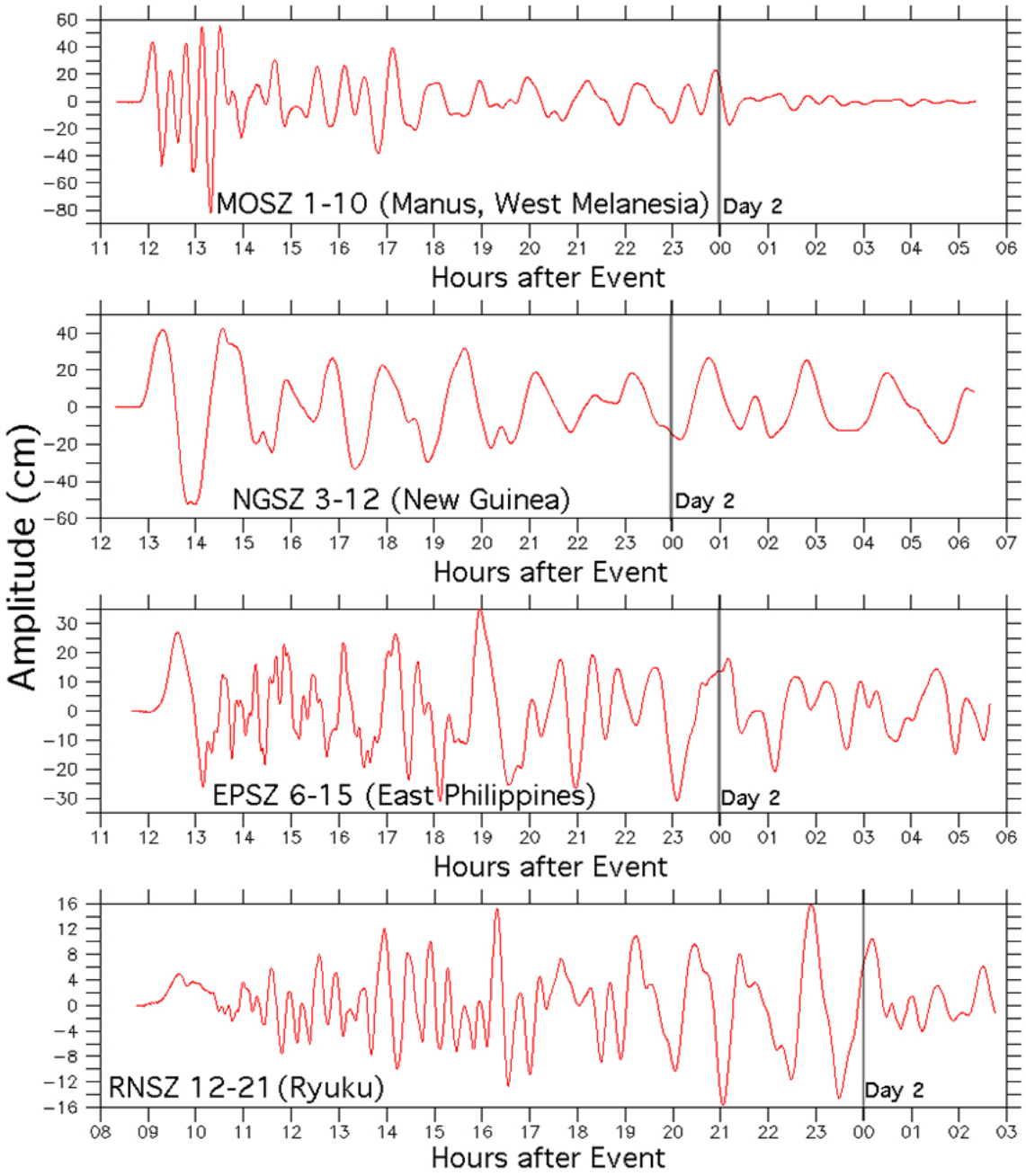

Figure 32 continued. Complete time series of Forecast Model predictions at the Elfin Cove tide gage site for each of the mega-tsunami scenarios.

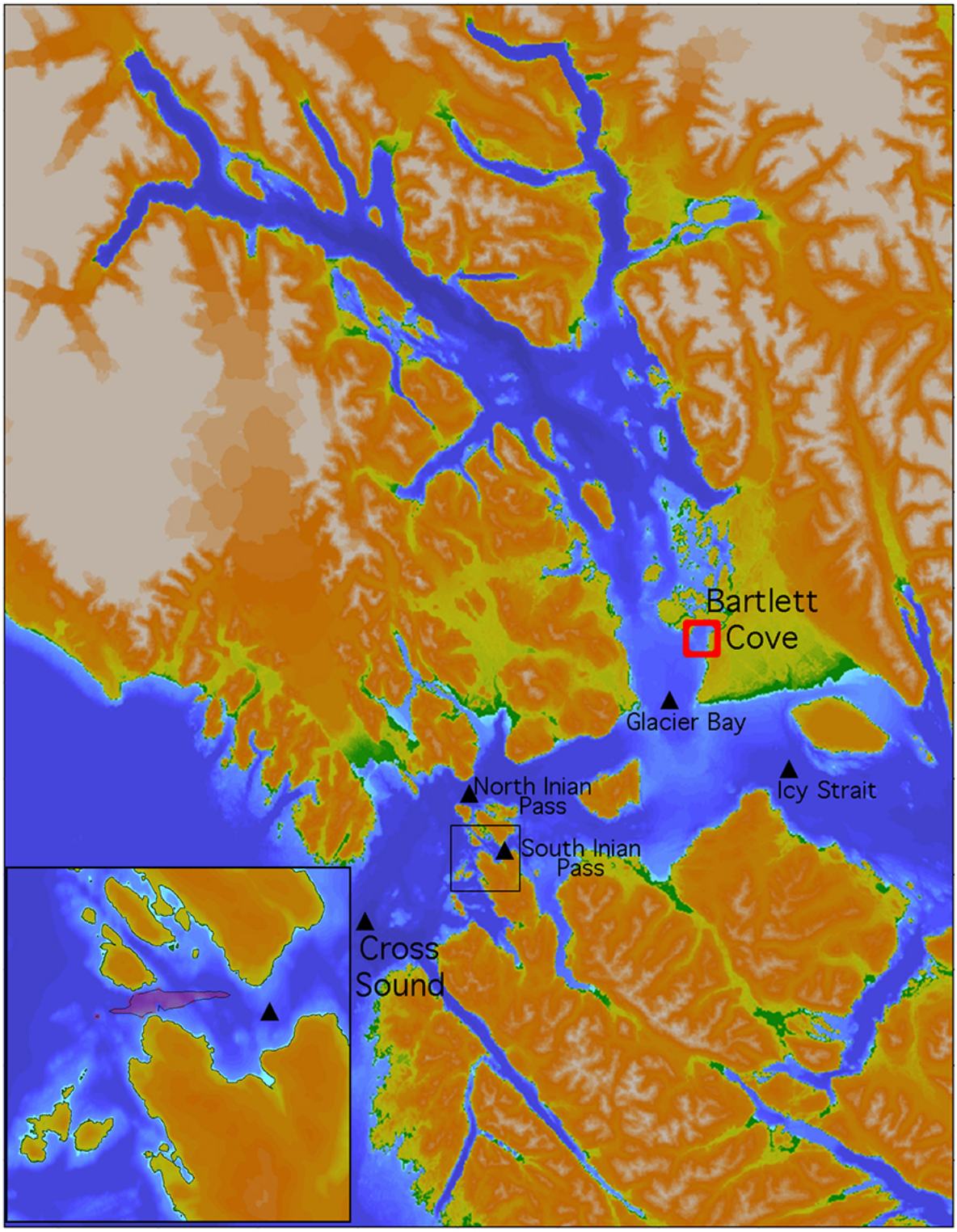

Figure 33. Current meter sites instrumented by NOAA's EcoFOCI Program (Stabeno, personal communication) for which mega-event speed maxima from the Elfin Cove model were extracted and listed in Table 10. The inset panel shows the 10 knot contour for the local (ACSZ 40-49) scenario which produces the strongest currents.

Appendix A

A1. Reference Model Input (*.in) File for Elfin Cove, AK

The following table contains the parameter and file choices used in the input file for the SIFT implementation (most3_facts_nc.in) of the reference model (RM) for Elfin Cove, AK. When run on an Intel® Xeon® E5670 2.93GHz processor the Elfin Cove, AK reference model simulates four hours in 6.77 CPU hours.

Parameter/File*	**Purpose**
0.0010	Minimum amp. of input offshore wave (m)
2.5	Minimum depth of offshore (m)
0.1	Dry land depth of inundation (m)
0.0009	Friction coefficient (n**2)
1	Let A-Grid and B-Grid run up
900.0	Max eta before blow-up (m)
0.25	Time step (sec)
115200	Total number of time steps in run
12	Time steps between A-Grid computations
4	Time steps between B-Grid computations
120	Time steps between output steps
0	Time steps before saving first output step
1	Save output every n-th grid point
ElfinCoveAK_RM_A.most	A-grid bathymetry file
ElfinCoveAK_RM_B.most	B-grid bathymetry file
ElfinCoveAK_RM_C.most	C-grid bathymetry file
./	Directory of source files
,/	Directory for output files

* The column headings are not part of most3_facts_nc.in

A2. Forecast Model Input (*.in) File for Elfin Cove, AK

The following table contains the parameter and file choices used in the input file for the SIFT implementation (most3_facts_nc.in) of the optimized forecast model (FM) for Elfin Cove, AK. When run on an Intel® Xeon® E5670 2.93GHz processor the Elfin Cove, AK forecast model simulates four hours in 13.57 minutes.

Parameter/File*	**Purpose**
0.0010	Minimum amp. of input offshore wave (m)
2.5	Minimum depth of offshore (m)
0.1	Dry land depth of inundation (m)
0.0009	Friction coefficient (n**2)
1	Let A-Grid and B-Grid run up
900.0	Max eta before blow-up (m)
0.4166666667	Time step (sec)
69120	Total number of time steps in run
12	Time steps between A-Grid computations
4	Time steps between B-Grid computations
72	Time steps between output steps
0	Time steps before saving first output step
1	Save output every n-th grid point
ElfinCoveAK_FM_A.most	A-grid bathymetry file
ElfinCoveAK_FM_B.most	B-grid bathymetry file
ElfinCoveAK_FM_C.most	C-grid bathymetry file
./	Directory of source files
,/	Directory for output files

* The column headings are not part of most3_facts_nc.in

Appendix B Propagation Database: Pacific Ocean Unit Sources